INTRASEASONAL VARIABILITY OF SUMMER CONVECTION OVER SOUTH AMERICA

A Thesis
Presented to
The Academic Faculty

by

Fernando Endo Hirata

In Partial Fulfillment
of the Requirements for the Degree
Doctor of Philosophy in the
School of Earth and Atmospheric Sciences

Georgia Institute of Technology

December 2013

INTRASEASONAL VARIABILITY OF SUMMER CONVECTION OVER SOUTH AMERICA

Approved by:

Dr. Peter J. Webster, Advisor
School of Earth and Atmospheric Sciences
Georgia Institute of Technology

Dr. Yi Deng
School of Earth and Atmospheric Sciences
Georgia Institute of Technology

Dr. Judith A. Curry
School of Earth and Atmospheric Sciences
Georgia Institute of Technology

Dr. Rosana Nieto-Ferreira
Department of Geography
East Carolina University

Dr. Robert X. Black
School of Earth and Atmospheric Sciences
Georgia Institute of Technology

Date Approved: September 27, 2013

This thesis is dedicated to those who have perished or lost family and friends in disasters caused by extreme weather events in Brazil.

"It's a cash and carry world. Sometimes you pay a little. Mostly it's a lot. Sometimes, it's everything you have".

Stephen King, *Storm of the Century: An Original Screenplay* [1999].

ACKNOWLEDGEMENTS

I wish to thank my family, friends, and the support from Dr. Peter J. Webster and past and present members of his research group at Georgia Tech. Special thanks to Dr. Violeta Toma, Dr. James Belanger, Dr. Hyemi Kim, Dr. Matthew Widlansky, Dr. Carlos Hoyos, Dr. Manuel Zuluaga, and the members of my comprehensive examination committee (Dr. Annalisa Bracco, Dr. Robert Black, Dr. Judith Curry, and Dr. Kurt Frankel) for invaluable comments and suggestions. I'm also obliged to the EAS administrative staff: Kathy Plummer, Laura Cederquist, Rosalyn Law-Darden, Angelica Remolina, and Mack Jenkins for their assistance and availability throughout the last five years. This research was partially funded by CAPES/Fulbright IIE grant number 15087700 and NOAA award NA10OAR4310161.

TABLE OF CONTENTS

		Page
ACKNOWLEDGEMENTS		iv
LIST OF TABLES		vii
LIST OF FIGURES		viii
LIST OF SYMBOLS AND ABBREVIATIONS		xiv
SUMMARY		xvi
CHAPTER		
1	Introduction	1
	Thesis Outline	2
2	Monsoons and Intraseasonal Variability	4
	Tropical Intraseasonal Variability	6
	Extratropical Activity Associated with the MJO	13
	The South American Summer Monsoon and its Variability	16
3	Austral Summer Tropical Intraseasonal Oscillations	23
	Definition of Intraseasonal Events	24
	Intraseasonal Life Cycles of Convection	31
	EOF3 and ENSO Dependence	37
	Conclusion	39
4	Intraseasonal Dependence, Wave Accumulation and Intense SACZ events	43
	Definition of the SACZ	47
	SACZ Correlation with Tropical Intraseasonal Events	48
	Independent SACZ	47
	SACZ preceding the MJO	53

MJO preceding the SACZ 57

Negative Zonal Stretching Deformation and Synoptic Disturbances 60

Conclusions 67

5 Summertime Long-Term Rainfall Variations and the SACZ 72

Precipitation Trends from 1979 to 1999 over South America 74

Precipitation Trends after 1999 over South America 78

Submonthly Variability 79

Conclusions 81

6 Conclusion 87

REFERENCES 94

VITA 107

LIST OF TABLES

Page

Table 3.1: Categories of EOF-based intraseasonal events 26

Table 4.1: Lead-lag relationship between SACZ events and intraseasonal events identified in chapter 2 50

Table 4.2: Number of high-frequency (3-6-day) disturbances identified by OLR minima below -1 standard deviation at 25^{o}S, 45^{o}W. The lag refers to the number of days the high-frequency synoptic disturbance was observed before the SACZ (SACZ lags the high-frequency). 63

LIST OF FIGURES

Page

Figure 2.1: Schematic of the annual cycle of the Indian Ocean monsoon system for boreal summer (June-September) and winter (December-February). Black arrows denote surface winds, gray dashed arrows denote Ekman transport, and the vertical gray arrows indicate the direction of the net ocean heat transport (from Webster et al. [2002]). 6

Figure 2.2: Composite time-longitude diagram of band-passed (20-90 days) SLP (shadings in Pa) and OLR anomalies (contours, green and magenta indicate positive and negative anomalies, respectively) relative to maximum intraseasonal convection over the Indian Ocean (composite day 0). Black lines (1 and 2) represent approximate eastward propagation of two radiating, fast Kelvin waves in SLP. Yellow line represent the eastward propagation of the convective center (forced Kelvin wave). When maximum convection approaches 120^{o}E, strong positive OLR anomalies develop to the west. To the east, surface easterlies associated with the radiating Kelvin wave promote convergence, pulling the convective packet to the east. 10

Figure 2.3: (a) PSA1 (EOF2) and (b) PSA2 (EOF3) of 500 hPa mean height anomalies. Positive values are shaded. PSA1 explains 13 % and PSA2, 11% of the total variance. (c) PSA1 (EOF3) and (d) PSA2 (EOF4) of 200 hPa streamfunction anomalies (mean zonal winds removed). PSA1 explains 8.2% and PSA2, 7.6% of the total variance (from Mo and Nogués-Paegle [2001]). 15

Figure 2.4: Global Precipitation Climatology Project (GPCP) 1979-2010 monthly rainfall average over A) northern Amazon; B) southern Amazon; C) central eastern Brazil. 17

Figure 2.5: ERA-Interim SON (left) and DJF (right) 200 hPa average geopotential height illustrating the seasonal formation of the upper-level Bolivian High. 18

Figure 2.6: October-March OLR unfiltered variance (upper panel); band-passed intraseasonal (20-90 days) variance (middle panel); Percentage of intraseasonal relative to unfiltered variance (lower panel). 19

Figure 2.7: A) Oct-Mar intraseasonal (20-90 days) OLR variance; B) Global wavelet spectrum of area-averaged OLR anomalies taken from the box displayed on A; C) Wavelet power spectrum for the same OLR time series. The annual cycle was removed prior to the analysis. Red noise spectrum in B (dashed black line) was calculated using the time series lag-1 autocorrelation value of 0.7. 20

Figure 2.8: Sign of linear trends for 12 rainfall indices from Haylock et al. [2006]. An increase is shown by a plus sign, a deacrese is shown by a circle. Trends significant at 0.05 levels are indicate by bold signs. PRCPTOT is the annual total precipitation during wet days, SDII is the average precipitation during wet days, CDD is the maximum number of consecutive dry days, CWD is the maximum number of consecutive wet days, R10mm is the number of days with rainfall rate RR $\geq$ 10 mm, R20mm is the number of days with RR $\geq$ 20 mm, R95p is the total annual precipitation when RR > 95th percentile (1961-1990), R99p is the total annual precipitation when RR > 99th percentile (1961-1990), RX1day is the annual maximum 1-day precipitation amount, RX5day is the annual maximum 5-day precipitation amount, R95pTOT is the percentage of annual total precipitation from days with RR $\geq$ 95th percentile (1961-1990), and R99pTOT is the percentage of annual total precipitation from days with RR $\geq$ 99th percentile (1961-1990). A wet day means RR $\geq$ 1mm and a dry day means RR < 1 mm. 22

Figure 3.1: a) Austral summer EOF modes of averaged (5^{o}N to 5^{o}S) intraseasonal OLR. b) Ratio of intraseasonal variance as a function of longitude for each EOF mode. c) Composite day 0 for PC1 events with minimum below -1 standard deviation. d) Composite day 0 for PC2 events with minimum below -1 standard deviation. e) Composite day 0 for PC3 events above +1 standard deviation, representing strengthened convection over the Indian and West Pacific oceans. 25

Figure 3.2: Lag-correlation among PC1, PC2, and PC3. Negative lags indicate that, for each pair of PCs identified by the legend, the first leads the second. 26

Figure 3.3: Band-passed SST composites for canonical MJO events (days -14, -7, 0, and +7). Right-hand side: OI AVHRR-only; left-hand side: TMI. Pink contours indicate significant SST anomalies at 95% confidence level. 29

Figure 3.4: Band-passed SST composites for eastward decaying events (days -14, -7, 0, and +7). Right-hand side: OI AVHRR-only; left-hand side: TMI. Pink contours indicate significant SST anomalies at 95% level. 30

Figure 3.5: Band-passed SST composites for EI events (days -14, -7, 0, and +7). Right-hand side: OI AVHRR-only; left-hand side: TMI. Pink contours indicate significant SST anomalies at 95% level. 31

Figure 3.6: a) Longitude-time diagrams of composite life cycles for the canonical MJO, b) ED, and c) EI events. Shading (contours) represent band-passed SST (OLR) anomalies averaged between 5^{o}N and 10^{o}S to highlight stronger SST anomalies south of the equator in the surroundings of the MC (Figure 3.7). 32

Figure 3.7: Composites for the canonical MJO (a-d) and ED events (e-h). Right-hand side: shading represents significant SST anomalies and black (magenta) contours represent significant positive (negative) OLR anomalies (5 W m^{-2} intervals). Left-hand side: shading represents significant surface pressure anomalies and vectors represent 850 hPa winds with significant speed (90% significance level; maximum wind anomalies of -4.5 m s^{-1} on panel d). 33

Figure 3.8: Composites for EI events. Right-hand side: shading represents significant SST anomalies and black (pink) contours represent significant positive (negative) OLR anomalies (5 W m^{-2} intervals). Left-hand side: shading represents significant surface pressure anomalies and vectors represent 850 hPa winds with significant wind speed (90% significance level; maximum wind anomalies of 5.1 m s^{-1} on panel g). 36

Figure 3.9: EI composite day -14: a) Vectors represent the zonal component of the wind field (m s^{-1}) and omega (Pa s^{-1}) along the equator. Only vectors with significant magnitude at 90% level are plotted. Shading denotes streamfunction anomalies. b) Band-passed 200 hPa geopotential anomalies from ERA-Interim Reanalysis. Pink contours indicate significant anomalies at 90% level. 37

Figure 3.10: Zero-lag correlations between Southern Hemisphere summer seasonal averages of PC1 and PC3. Horizontal black lines indicate ±1 standard deviation. 39

Figure 3.11: Schematic diagram for: a) Convective breaks before canonical MJO. b) Convective phase for canonical MJO. c) Break phase before EI events. d) Convective phase during EI events. Horizontal dashed lines represent the equator at 850 hPa (above SST anomalies). Dashed arrows represent upward/downward motions between 850 and 200 hPa. Black arrows represent the direction of wind anomalies. Red arrows along the equator indicate 850 hPa winds associated with Kelvin waves (easterlies for a wave associated with convection). L (H) indicates low-level negative (positive) pressure anomalies within cyclonic (anticyclonic) anomalies. Both (a) and (b) also depict ED life cycle, but the amplitude of the anomalies is smaller and less significant when compared to canonical MJO events. 40

Figure 4.1: (a) First intraseasonal EOF calculated from daily filtered OLR data. Magenta contour outlines the 245 W m^{-2} October-March mean OLR. Boxes indicate the areas used to calculate the spectra in d-f. (b) SACZ composite day 0 for CPC rainfall (shading) and ERA-Interim 850 hPa winds (vectors) and negative 500 hPa omega(black contours at -5 and -2.5 x 10^{-2} Pa s^{-1}. (c) Mean October-March Era-Interim 200 hPa winds, geopotential (green), and negative zonal stretching deformation (red). (d-f) Global wavelet spectra [Torrence and Compo, 1998] of unfiltered area-averaged OLR taken from the boxes in (a). Dashed lines indicate significance level based on 95% autocorrelation. 44

Figure 4.2: Lagged cross-correlations between each PC of the tropical modes of intraseasonal oscillations (Figure 3.1) and the PC associated with the SACZ mode (Figure 4.1a) for Oct-Mar, 1979 to 2012. Horizontal lines indicate the 0.05 significance level assessed by a two-sided t-test assuming 4 degrees of freedom per season. 49

Figure 4.3: OLR (contours) and surface pressure (shadings) composite cycle for independent SACZ events. Black (magenta) contours represent positive (negative) OLR anomalies from at 5 W m^{-2} intervals. Zero contour is omitted. Only values significant at 95% confidence levels are displayed. 51

Figure 4.4: 200hPa geopotential composites. (a-e) -10, -5, 0, +5, and +10 composite days for the average SACZ cycle. Contour indicates 95% significance. (f-j) Same, but for independent SACZ. (k-o) Same, but for SACZ preceding MJO events. (p-t) Same, but for MJO preceding SACZ events. 53

Figure 4.5: Same as Figure 4.3 but for SACZ events preceding the MJO. 54

Figure 4.6: Hsu et al. [1990] 11-day means of 250 hPa streamfunction anomaly centered at 24 December 1985. The contour interval is 5 x 10^{-6} m^2 s^{-1}. The thick contour is indicates zero values and shading indicates values smaller than -5 x 10^{-6} m^2 s^{-1}. 56

Figure 4.7: Berbery and Nógues-Paegle [1993] streamfunction anomalies at (a) pentad 73 of 1985, (b) pentad 1 of 1986, and (c) pentad 2 of 1986. Contour interval is 5 x 10^{-6} m^2 s^{-1}. Negative values are dashed and zero line is omitted. 57

Figure 4.8: Same as Figure 4.3 but for MJO events preceding the SACZ. 59

Figure 4.9: Intraseasonal OLR anomalies (contours) and zonal stretching deformation (shading) for composite day 0 of (a) all identified SACZ events; (b) MJO-independent SACZ; (c) SACZ events preceding the MJO; and (d) MJO preceding the SACZ. OLR contours are plotted at 5 W m^{-2} intervals (zero contour omitted). Only values significant at 95% are shown. 61

Figure 4.10: High-frequency 3-6-day composite cycle relative to minima OLR below -1 standard deviation at 25ºS, 45ºW. Thin black (magenta) lines represent positive (negative) OLR anomalies at 5 W m^{-2} intervals. Thick magenta lines indicate October-March mean -245 W m^{-2} and it is used as a reference for the climatological SACZ position. No significance test applied. 62

Figure 4.11: Same as Figure 3.8 but for composite days 0, +2, and +4 of high-frequency disturbances concurrent with MJO-independent SACZ events (Table 4.2). Here, only significant anomalies at 90% are shown. 64

Figure 4.12: Same as Figure 3.9 but for SACZ events preceding the MJO (Table 4.2). 65

Figure 4.13: Time-longitude composite cycle at 25ºS for synoptic disturbances associated with MJO-independent SACZ events. Magenta contours indicate negative OLR anomalies at 5 W m^{-2} intervals. 65

Figure 4.14: Same as Figure 4.12 but for synoptic disturbances associated with SACZ events preceding the MJO. 66

Figure 5.1: Linear trends from 1979 to 1999. (a) GPCP monthly precipitation. (b) ERA-Interim mean sea level pressure. (c) ERA-Interim 200 hPa geopotential. (d) NOAA ERSST. Think black contours in (a), (c), and (d) indicate values significant at 0.05. Contours in (b) represent climatological values of JFM mean sea level pressure. Only values significant at 95% are display in (b). 76

Figure 5.2: Average January to March PDO index obtained from the Joint institute for the Study of the Atmosphere and Ocean, University of Washington, calculated as standardized values of the leading PC of monthly SST anomalies in the Pacific Ocean north of 20^{o}S [Mantua et al., 1997]. 78

Figure 5.3: Linear trends from 1999 to 2011. (a) GPCP monthly precipitation. (b) ERA-Interim mean sea level pressure. (c) ERA-Interim 200 hPa geopotential. (d) NOAA ERSST. Think black contours in (a), (c), and (d) indicate values significant at 0.05. Contours in (b) represent climatological values of JFM mean sea level pressure. Only values significant at 95% are displayed in (b). 79

Figure 5.4: Average summer (October-March) SACZ principal component time series variance-preserving spectra for three distinct periods. Note that a 90-day cycle is sampled twice a year. 81

Figure 5.5: Top panel displays climatological values of summer (October to March) negative zonal stretching deformation at 1 x 10^{-6} s^{-1}. Middle panel shows summertime zonal stretching deformation anomalies during El Niño years (1982/83, 1987/88, 1991/92, 1993/94, 1994/95, 1997/98, 2002/03, 2006/07 and 2009/10). Bottom panels shows summertime anomalies during La Niña years (1988/89, 1998/99, 1999/00, 2000/01, 2007/08, 2008/2009, 2010/11). 82

Figure 6.1: Composite time-longitude diagrams averaged at the between 5^{o}N and 5^{o}S relative to independent SACZ events identified on chapter 3. The left hand side plot displays the same pressure shadings with green (magenta) contours representing positive (negative) OLR anomalies at 5 W m^{-2} intervals (zero contour is omitted). The right hand side plot displays band-passed (20-90 days) sea level pressure anomalies (shadings in Pa) and thick (thin) contours indicate positive (negative 200 hPa geopotential anomalies at 15 m^2 s^2 (zero contour is omitted). Dashed vertical lines indicate the mean longitude of the East African Highlands and the Andes. 88

Figure 6.2: Same as Figure 6.1 but for SACZ preceding MJO events. 88

Figure 6.3: Same as Figure 6.1 but for MJO preceding SACZ events. 90

LIST OF SYMBOLS AND ABBREVIATIONS

ξ	Wave energy density
k	Zonal wavenumber
$\bar{U}$	Background zonal winds
AMSR	Advanced Microwave Scanning Radiometer
AVHRR	Advanced Very High Resolution Radar
CPC	Climate Prediction Center
ED	Eastward Decaying
EI	Eastward Intensifying
ENSO	El Niño-Southern Oscillation
EOF	Empirical Orthogonal Function
ERA	European Center for Medium Range Weather Forecast Reanalysis
GPCP	Global Precipitation Climatology Project
ITCZ	Intertropical Convergence Zone
JFM	January, February and March
MJO	Madden Julian Oscillation
NOAA	National Oceanic and Atmospheric Agency
OI	Optimum Interpolated
OLR	Outgoing Long-wave Radiation
PC	Principal Component
PDO	Pacific Decadal Oscillation
PNA	Pacific-North American Pattern
PSA	Pacific-South American Pattern
RMM	Real-time Multivariate MJO index

SACZ	South Atlantic Convergence Zone
SASM	South American Summer Monsoon
SLP	Sea Level Pressure
SPCZ	South Pacific Convergence Zone
SST	Sea Surface Temperature
TMI	TRMM Microwave Imager
TRMM	Tropical Rainfall Measurement Mission

SUMMARY

In other regions of the world, intraseasonal variations of precipitation have been used to extend the range of weather and hydrological forecasts especially during the rainy monsoon season. This intraseasonal variability is usually strongly tied to the Madden Julian Oscillation (MJO). The MJO influences South American precipitation through signals propagating eastward in the tropics and the extratropics of the Southern Hemisphere. First, the focus is on variations of the MJO as it propagates eastward. Three main categories are described. One is the canonical MJO, which propagates almost continuously from the Indian Ocean to the West Pacific. The other categories encompass intraseasonal convection that fails to reach the West Pacific and intraseasonal convection that begins closer to the Maritime Continent and intensifies while propagating eastward. The categories of intraseasonal convection are linked to intraseasonal variations of South American rainfall and it is demonstrated that the SACZ is influenced by the MJO both through the tropics and extratropics, but these influences are not always the same. There are evidences that accumulation of wave energy is an important process both to organize extratropical waves propagating from the Pacific to South America and to promote convection in the South Atlantic Convergence Zone (SACZ). Intraseasonal convection in the SACZ occurs even when tropical signals are not significant east of the Andes, suggesting that extratropical disturbances and wave accumulation are fundamental in the formation of the SACZ. In the long-term, variations of the SACZ are related to climate regimes in the Pacific Ocean, highlighting the fact that there is a shift of spectral energy in SACZ convection from intraseasonal to higher frequencies, indicating again the importance of extratropical waves for SACZ convection. Last, the main findings of this project are discussed, as well as their applicability to enhance precipitation predictability over South America.

CHAPTER 1

INTRODUCTION

During the last few years, heavily populated areas in Brazil have experienced severe weather and climate conditions especially during the wet summer monsoon season (October to March). Particularly, there has been a general increase in daily rainfall extremes and total annual rainfall over South America since the last half of the twentieth century [Marengo et al., 2010]. Positive trends in precipitation are more pronounced from January to March over south and eastern Brazil [Liebmann et al., 2004; Haylock et al., 2006]. Rainfall events exceeding 80 mm day^{-1} (3.15 in day^{-1}) were observed 9 times during the first decade of the current century while the average before 1970 was one event every 10 years [Silva Dias et al., 2013]. In addition to this seeming climatic shift, Brazilian metropolitan areas (i.e., Rio de Janeiro, São Paulo) are especially vulnerable to extreme precipitation events due to inadequate infrastructure and urban land-use caused by population growth [Torres et al., 2012]. The result is recurring floods, landslides, economic, and human losses. In 2008, the national gross domestic product estimated loss was approximately US$300,000,000 from floods in São Paulo metropolitan area alone [Haddad and Teixeira, 2013].

Traditional indices tracking the state of the Pacific Ocean surface waters or the atmospheric circulation over the North Atlantic seem to account for nearly 70% of the apparent rainfall increase over São Paulo [Silva Dias et al., 2013]. This high percentage of explained variance associated with large-scale climate phenomena suggests these variations may be predictable. Daily precipitation amounts over South America are also

strongly modulated by shorter period climate modes but the mechanisms controlling these modulations are not completely clear [e.g. Carvalho et al., 2002]. The main goal of this thesis is to describe how large-scale climate variations on different time scales interact to drive South American summer monsoon variability and to examine, based on these interactions, the potential predictability of summer conditions beyond the synoptic range.

The hypothesis behind this approach is that variations of austral summer rainfall over a vast region of the South American continent exhibits useful predictability beyond a few days in advance due to the impact of the dominant mode of tropical variability on intraseasonal timescales: the Madden-Julian Oscillation (MJO) [Madden and Julian, 1971; 1972]. Persistent circulation patterns tied to tropical intraseasonal variability also impact the Asian monsoon, extending skillful predictability up to 30 days [Webster and Hoyos, 2004]. Although South America is distant from the Indian and West Pacific oceans, where intraseasonal variability is stronger throughout the year, atmospheric wave propagation from the Eastern Hemisphere tropics can result in enhanced signal-to-noise ratio and potential predictability over Brazil. The behavior of these waves changes as lower frequency phenomena slowly evolves from one phase to the other and, therefore, the connections between the MJO and South American precipitation may also vary.

Thesis Outline

The thesis is organized in four chapters. On the basis that extended predictability depends on the periodic character of the predictand [Lorenz, 1963], the main sources of periodic variations of South American summer rainfall on timescales longer than that of weather are reviewed on Chapter 2. The review begins with a brief description of basic

features of monsoonal climates and intraseasonal variability (with special focus on the Asian monsoon), followed by highlights of similarities and distinctions observed during the South American wet season. An inspection of these basic features intends to identify predictors of South American summer intraseasonal variability as well as existent knowledge gaps that need to be addressed in order to design a skillful prediction scheme. Chapter 3 defines the structure and life cycle of austral summer tropical intraseasonal oscillations observed over the tropical Indian and Pacific Oceans and it is published in the Geophysical Research Letters [Hirata et al., 2013]. The categorization of these intraseasonal oscillations is instrumental for Chapter 4, where the formation of intense South Atlantic Convergence Zone (SACZ) events is linked to the MJO cycle, which comprises only a fraction of all tropical intraseasonal variability in the Eastern Hemisphere. This work is in final preparation to be submitted to the Journal of Climate. Finally, Chapter 5 examines long-term variations of rainfall in the surroundings of the SACZ, followed by concluding remarks (Chapter 6).

CHAPTER 2

MONSOONS AND INTRASEASONAL VARIABILITY

Monsoonal circulations and their variability affect most of the tropics and its inhabitants. Droughts and floods resulting from variations of the monsoons may be catastrophic for national economies and disastrous for the people, especially the poorest. In spite of more traditional and strict constrains about the definition of a monsoon, it is the spatial and temporal distribution of rainfall during the wet season that exert more profound impacts on food and energy production, water use, communications, trade, and housing. From a societal point of view, the most important characteristic of a monsoonal climate is the existence of well-defined dry winters and wet summers observed over large and highly populated regions of world [Webster et al., 1998]. This sharp seasonality is a consequence of the annual cycle and geography [Webster and Fasullo, 2003].

The annual solar cycle imposes the dominant period of the monsoons. Geography determines the monsoon's intensity and associated atmospheric and oceanic circulation features related to its variability. For a monsoon to exist, a large-scale atmospheric temperature gradient must be created so that winds carry moisture from the colder to warmer areas. In the summer hemisphere, solar heating rapidly increases temperature over continental land masses due to the smaller heat capacity and conductivity of soils compared to those of oceanic waters. Summer solar heating over elevated terrain strengthens gradients due to the high temperature generated over land versus the atmosphere at the same height.

During winter, continents lose heat as fast as it was gained during the beginning of the warm season. In the case of two large land masses located approximately on the

same longitudinal band (i.e. Asia and Australia), with one in the Northern and the other in the Southern Hemisphere, the temperature gradient in the atmosphere and consequent circulation are enhanced during the solstices. The existence of an ocean between these large continental land masses adds moisture to the lower atmosphere. Surface monsoonal winds then transport this humid air towards the summer hemisphere. Once over the heated continent, latent heat release further enhances the atmospheric temperature gradient in the middle and upper levels of the atmosphere.

An ocean-atmosphere feedback controls the amplitude of the annual monsoonal cycle and modulates its interannual variability [Webster et al., 2002]. The mean annual solar radiation into the North Indian Ocean is estimated to be around 180 W m^{-2} with a net surface heat flux of +50 W m^{-2} [Hastenrath and Greischar, 1993; Webster et al., 1998]. This warming is balanced by oceanic transport of heat from the summer to the winter hemisphere driven by Ekman dynamics [Loschnigg and Webster, 2000] (Figure 2.1). In boreal summer, monsoonal winds are southeasterlies over the South Indian basin and southwesterlies north of the equator. The net Ekman ocean transport in both hemispheres is southward. During boreal winter, winds are northeasterlies over the North Indian Ocean and northwesterlies south of the Equator. Thus, the resulting net Ekman transport is northward. Monsoonal winds, therefore, act to constrain the storage of heat in the upper Indian Ocean and promote a striking biennial variation of the South Asian monsoon. Years of more intense atmospheric circulation and rainfall tend to be intertwined by years of reduced vertical wind shear and deficient precipitation [Webster and Yang, 1992].

There is statistical evidence that El Niño (La Niña) events are usually associated with anomalously low (high) rainfall over India [Torrence and Webster, 1999]. A weakened monsoon circulation caused by an El Niño would lead to a deficient southward Ekman transport of heat and result in a less intense Australian monsoon during boreal winter. A weaker Australian monsoon has the equivalent effect of a weaker Asian

monsoon on Ekman dynamics. One year after the initial disturbance related to ENSO, there is a prevalence of above average sea surface temperature (SST) anomalies over the Indian Ocean. When boreal summer heats the Tibetan Plateau to set up a new Asian monsoon season, surface winds over positive SST anomalies collect more latent heat that will subsequently boost precipitation and atmospheric circulation over the continent. Stronger atmospheric circulation reinforces Ekman dynamics and north-south heat transport, bolstering an Australian monsoon during the next northern winter season. The initial disturbance, often associated with ENSO can also compel the biennial variations of the monsoon.

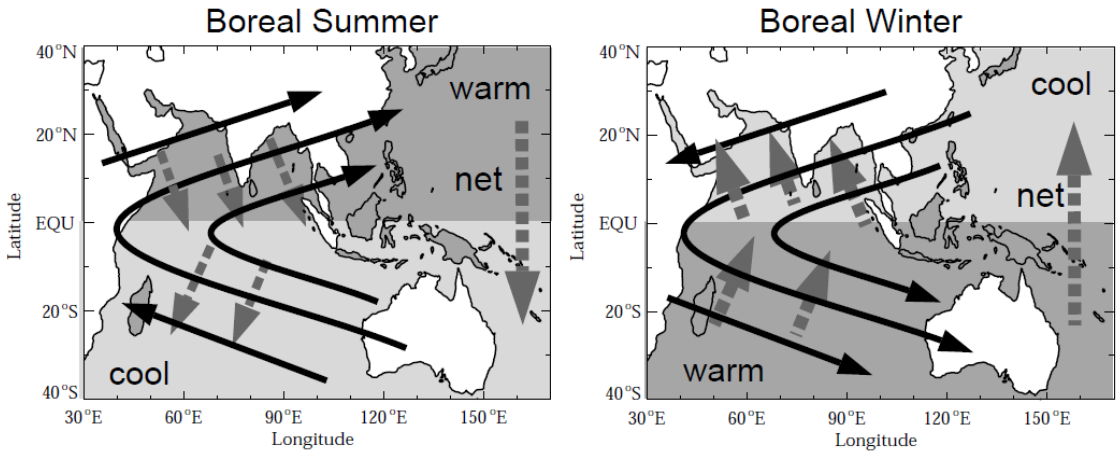

Figure 2.1: Schematic of the annual cycle of the Indian Ocean monsoon system for boreal summer (June-September) and winter (December-February). Black arrows denote surface winds, gray dashed arrows denote Ekman transport, and the vertical gray arrows indicate the direction of the net ocean heat transport (from Webster et al. [2002]).

The monsoons over South Asia and Australia usually display short periods of active convection and rainfall set apart by dry intervals. The periodicity of these active and break phases fall within the intraseasonal frequency band (20-90 days) and the associated variance is greater than the interannual variability [Webster and Hoyos, 2004].

Tropical Intraseasonal Variability

The ability to extend and improve the range of tropical weather forecasts into periods longer than a week and shorter than a season may allow the mitigation of human

and economic losses for some of the most populated regions of the world. The MJO is an intraseasonal 30-60-day eastward propagating oscillation stronger in boreal winter and spring (December to May) over the tropical Indian and West Pacific Oceans [Zhang, 2005]. The signal presents maximum power and coherence in sea level pressure (SLP) and zonal winds [Madden and Julian, 1972 and 1994; Hendon and Salby, 1994]. Although the physical mechanisms behind MJO organization and evolution are still unclear, the framework commonly used to describe the oscillation is based on the theoretical atmospheric response to a large-scale tropical diabatic heating anomaly [Matsuno, 1966; Webster, 1972; Gill, 1980]. The anomalous heating with prescribed frequency generates a Kelvin-Rossby couplet, with the Kelvin wave propagating to the east and the Rossby wave to the west. Observed differences between winter and summer intraseasonal variations are not restrict to the signal strength or its ability to propagate to the east. There is also a clear northward propagation of convective anomalies from the North Indian Ocean into the Asian continent during the boreal summer season that is not observed during winter [Wang and Rui, 1990; Lawrence and Webster, 2001]. This contrast leads to a dispute on whether the Asian monsoon intraseasonal variations represent a Northern Hemisphere summer counterpart of the MJO, especially because some of the Asian monsoon active/break cycles display weaker eastward penetration into the tropical West Pacific.

After Madden and Julian [1971, 1972] described an eastward propagation of a 40-50 day oscillation around the global tropics, the equatorial Kelvin wave became a major candidate to explain a phenomenon not predicted by theory. These early observations of tropical intraseasonal oscillations noted a strong variation in zonal winds and SLP. Both variables were nearly in phase near the surface with an apparent first baroclinic mode structure in the vertical. Madden and Julian [1971] speculated that the oscillation was a manifestation of a large-scale zonal circulation cell encompassing the entire troposphere. Madden and Julian [1972] noted that the oscillation was very similar to interannual east-

west displacements of the Walker circulation cells over the Pacific Ocean but with a much shorter time scale.

Perhaps the first attempt to fit the MJO to a Kelvin wave portrayed an eastward propagating zonal wavenumber 1 oscillation all around the equator using 100 hPa zonal winds and temperature, with variations sufficiently similar to a Kelvin wave with a period slightly longer than a month [Parker, 1973]. However, the theoretical phase speed of a free, dry, first baroclinic Kelvin wave mode is much faster than that commonly observed for the MJO (~40 m s^{-1} for the free Kelvin wave and ~10 m s^{-1} for the MJO) and some kind of damping was necessary to match theory and observations [Chang, 1977]. A few years later, a pulsating 40-day heat forcing was used in models to obtain a Kelvin-Rossby wave pair with a slower propagating speed [Yamagata and Hayashi, 1984]. The main problem with this result was the comparable magnitude of eastward and westward propagating components of the solution, whereas the MJO has a clear and dominant high-amplitude eastward propagation. Observational studies seemed to confirm that the forced atmospheric response assumes the form of a Kelvin-Rossby wave pair over the warm pools of the Eastern Hemisphere, with the eastward propagating signal resembling a radiating Kelvin wave over the colder eastern Pacific [e.g. Hendon and Salby, 1994].

The sense of a circumnavigating oscillation that emerged from the observations of Madden and Julian [1971, 1972] and Parker [1973] induced the hypothesis that one MJO cycle could help to trigger the next [Knutson and Weickmann, 1987]. The MJO time scale would be determined by the time an upper-level disturbance would take to travel around the globe. A major drawback of the circumnavigating hypothesis is that further analysis demonstrated that the decorrelation time of the MJO is shorter than the time the signal would take to circumnavigate the tropics, suggesting that one cycle does not depend on the previous one [Hendon and Salby, 1994]. This independence is additionally supported by the fact that the propagation of intraseasonal oscillations presents a high

degree of seasonality (Asian monsoon intraseasonal variations versus the austral summer MJO).

Two mechanisms together could explain the eastward propagation of the MJO during boreal winter and assimilate both its forced and radiating Kelvin wave responses [Matthews et al., 1999; Matthews, 2000] (Figure 2.2). First, a local mechanism involving the Kelvin-Rossby wave pair explains the eastward movement of convection over the warm pools of the Eastern Hemisphere. When convection is active over the Indian Ocean, the Rossby wave response to the west encompasses a region of surface divergence, disfavoring convective activity. To the east of convection, the Kelvin wave response includes an area of surface convergence, pulling the packet of active convection further to the east. In a congruent way, the MJO ocean-atmosphere coupling can be viewed as a self-regulated system [Stephens et al., 2004]. The period of the oscillation would be determined by the time required to destabilize the troposphere through sea surface temperature warming, heat fluxes from the ocean into the atmosphere, and radiative cooling at higher levels. Active and break cycles of the south Asian monsoon during boreal summer are also characterized by a feedback argument: convection over the eastern Indian/West Pacific Ocean produces strong subsidence over the western Indian Ocean, reducing cloudiness, allowing destabilization under clearer sky conditions, and consequent initiation of a new cycle [Wang et al., 2005]. This destabilization seems to be instrumental for the following convective phase of the intraseasonal oscillation, as well as for setting its correct time scale [Agudelo et al., 2006].

The second mechanism of eastward propagation seems to be related to previous research on the comparative roles of fast and slow Kelvin waves, reviving the circumnavigation arguments to accommodate the radiating (fast) Kelvin wave response. These disturbances are better detected in SLP anomalies and possess phase speeds exceeding 30 m s^{-1} over the equatorial eastern Pacific [Milliff and Madden, 1996]. Positive and negative SLP anomalies cross the tropical Pacific as fast Kelvin waves and

are subsequently blocked by the Andes [Matthews, 2000]. After reaching the mountain range, the anomalies propagate north and south as a coastal wave, trapped by the topographic barrier. Negative pressure anomalies finally overcome the Andes through the Panama gap and then propagate again as a Kelvin wave over the Atlantic before being blocked one more time by the East African Highlands. Upper-level anomalies are apparently disrupted by wave trains crossing the equator over the eastern Pacific, suggesting that disturbances aloft play a minor role on the circumnavigation of the MJO signal [Matthews, 2000]. The wave would finally reach the Indian Ocean by the start of the following MJO cycle. The Kelvin-Rossby forced mode over the warm pools is slower (~6 m s^{-1}) compared to the radiating response over the western hemisphere (which averages around 20 m s^{-1}), with a faster propagating mode (30-40 m s^{-1}) being blocked by orography [Kikuchi and Takayabu, 2003].

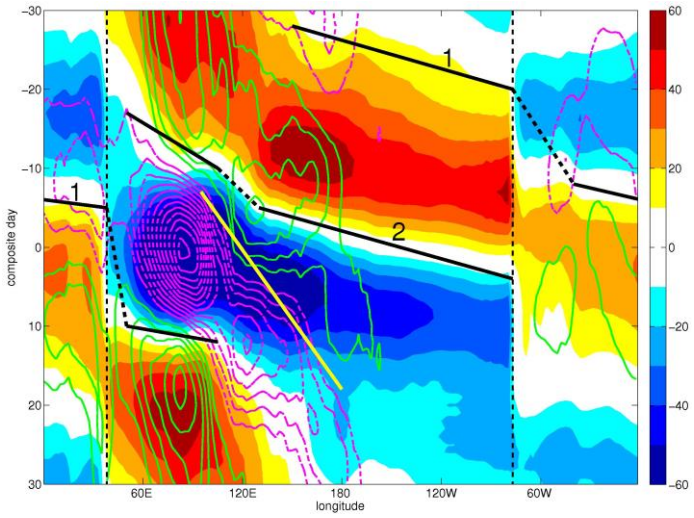

Figure 2.2: Composite time-longitude diagram of band-passed (20-90 days) SLP (shadings in Pa) and OLR anomalies (contours, green and magenta indicate positive and negative anomalies, respectively) relative to maximum intraseasonal convection over the Indian Ocean (composite day 0). Black lines (1 and 2) represent approximate eastward propagation of two radiating, fast Kelvin waves in SLP. Yellow line represent the eastward propagation of the convective center (forced Kelvin wave). When maximum convection approaches 120ºE, strong positive OLR anomalies develop to the west. To the east, surface easterlies associated with the radiating Kelvin wave promote convergence, pulling the convective packet to the east.

Circumnavigating Kelvin waves are usually blocked by the Andes and the East African Highlands [Hsu and Lee, 2005]. These topographic features, aligned in the north-

south direction throughout the tropical belt not only block Kelvin waves but act to lift easterly winds associated with equatorial waves. This lifting would lower SLP and contribute to initiate convection to the east of the mountains. Hsu and Lee [2005] suggest that when an eastward propagating wave is blocked by the western slopes of mountain ranges, circulation anomalies tend to develop convection to the east, resulting in another Kelvin wave. Therefore, the circumnavigating signal would be composed by more than one Kelvin wave.

A distinct role of orography emphasizes both eastward and westward propagating components of the MJO and the fact that westward propagating Rossby waves can be reflected to assume the form of eastward moving Kelvin waves [Roundy and Frank, 2004]. A strong eastward propagating component of the MJO over the Indian Ocean would tend to form as a resonance between the reflected and the arriving wave in the surroundings of mountain ranges. Even though Roundy and Frank [2004] do not mention the origin of the Kelvin waves reaching the western slopes of the East African Highlands, it is reasonable to assume that these waves may be either a reminiscence of MJO-radiated Kelvin waves or new waves formed over the Atlantic sector.

While the association between new intraseasonal cycles and Kelvin wave-like disturbances propagating over the warm pools of the Eastern Hemisphere is somewhat straightforward (Figure 2.2), the relationship of the MJO with Kelvin waves flared-up to the east of the Andes is still unclear. The amplitude of convective anomalies over South America and Africa, coherent with MJO activity, is small and the dynamical response to this convection is apparently weak [Matthews, 2000]. This fact supports the idea that the Kelvin wave coming from the Pacific basin is only delayed by the mountains, in contrast with Hsu and Lee's point of view, in which a new wave is formed to the east after the previous one stalls to the west.

There are two maxima in Kelvin wave filtered variance along the equator during southern summer with small differences in amplitude [Wheeler and Kiladis, 1999]. One,

over the warm pools, coincides with the region of maximum variance in the MJO band (maximum around 10°S between 100°E and 160°E). The second maximum lays over the equatorial Atlantic, linking South America to Africa. Boreal winter Kelvin wave activity over the Atlantic follows three distinct precursors [Liebmann et al., 2009]. The first one is a preexisting Kelvin wave propagating into the continent from the eastern Pacific. Nonetheless, there is low correlation between the occurrences of Pacific "convectively coupled" waves and an active MJO. The second precursor of a "convectively coupled" Kelvin wave is a synoptic disturbance associated with extratropical wave trains propagating equatorward. The third case involves a local wave neither related to preexisting Kelvin waves or to synoptic disturbances.

The association between Pacific and South American Kelvin waves and the correlations with MJO activity regards only cases of waves coupled with convection. However, there are evidences of different Kelvin waves, uncoupled with convection, preceding the development of convectively coupled ones. Uncoupled Kelvin wave circulations may act as initial forcing for coupled waves partly based on Wheeler et al. [2000] observations of fast (~44 m s^{-1}) eastward propagating SLP anomalies just before the development of coupled Kelvin waves over the Indian Ocean. Similar waves were also observed in the boreal summer Straub and Kiladis, [2003]. Matthews et al. [1999] also observed dry Kelvin waves propagating in the latter half of their MJO cycle extracted from model integrations, giving the impression that active and break phases of the boreal winter MJO are related to the Kelvin wave circulation cited by Straub and Kiladis [2003].

Another fraction of intraseasonal variability of the Asian monsoon, also associated with active and break periods of rainfall, is a shorter 10-20 days signal. Similarly to the 30-60 days signal, this shorter periodicity is usually described by equatorial wave dynamics, either being a mixed Rossby-gravity [Mao and Chan, 2005] or a pure Rossby mode modified by the background flow [Kikuchi and Wang, 2009]. The

spatial structure corresponds to the gravest meridional mode of an equatorial Rossby wave displaced about 5 degrees to the north of the geographical equator by the background summer conditions. Moreover, the horizontal scale of this shorter mode (half wavelength of 3,000 km) is smaller than that of the 30-60 days mode (half wavelength of 10,000 km) [Chatterjee and Goswami, 2006].

Extratropical Activity Associated with the MJO

As the MJO propagates eastward past the West Pacific warm pool, convection weakens close to the equator and strengthens along the South Pacific Convergence Zone (SPCZ) [Salby and Hendon, 1994]. The enhancement of convective activity into the subtropics is thought to be a response to convection over the Maritime Continent through the Rossby wave component of the MJO [Matthews et al., 1996].

Convection in subtropical latitudes acts as Rossby wave sources that propagate energy along ray paths of constant group speeds [Hoskins and Karoly, 1981]. More specifically, energy propagation along these rays occur at a speed that is two times that of the zonal component of the background wind and waves excited in subtropical latitudes initially propagate energy poleward and, at some latitude, the propagation turns equatorward. Ray paths are defined by the ratio between the meridional and the zonal wavenumbers of the disturbances. Kinematic wave theory implies that zonal wavenumber and frequency of waves are constant along rays. Therefore, the variation of the meridional wavenumber provides the latitude where the ray paths bend equatorward. Assuming that the stationary wavenumber is a decreasing function of latitude (because atmospheric zonal winds usually increase with latitude in subtropical and midlatitudes), a stationary wave of zero frequency (the meridional gradient of absolute vorticity is defined by the basic zonal wind field and the horizontal scale of the Rossby wave) propagating energy poleward would experience a decrease in meridional wavenumber and the ray path would become more zonally oriented. At latitudes where the meridional

wavenumber tends to zero, the stationary wavenumber tends to be equal to the zonal wavenumber, and the Rossby wave ray path curves equatorward.

Teleconnections are defined as contemporaneous correlations between geopotential heights on a given pressure surface at two distant locations of the planet [Wallace and Gutzler, 1981]. Some of the correlation patterns described by Wallace and Gutzler [1981] are, in fact, Rossby waves predicted by the theoretical work of Hoskins and Karoly [1981]. Among these teleconnection patterns, a zonally symmetric alternation of wintertime SLP between polar and middle latitudes extending from the Pacific sector to North America was identified and it is now known as the Pacific/North American (PNA) pattern. The growth of the PNA pattern on intraseasonal timescales is sometimes linked to a Rossby wave train excited by the MJO [Mori and Watanabe, 2008].

The Southern Hemisphere presents two wavenumber 3 patterns in midlatitudes with large amplitudes between the Pacific and South America. These patterns are leading modes of empirical orthogonal function (EOF) analysis of 500 hPa height and 200 hPa streamfunction anomalies from intraseasonal to decadal time scales and, due to their similarity to PNA patterns, they are called Pacific/South American (PSA) modes [Ghil and Mo, 1991; Mo and Higgins, 1998]. The PSA1 pattern is related to SST anomalies in the central and eastern Pacific on decadal time scales and to ENSO on interannual scales while PSA2 is also associated with ENSO, but on higher frequency bands (22 to 28 months) [Mo and Nogués-Paegle, 2001]. Both PSA1 and PSA2 are also linked to tropical intraseasonal convection over the Eastern Hemisphere warm pool. Mo and Nogués-Paegle [2001] showed that the positive PSA1 pattern is associated with enhanced MJO convection over the Pacific east of 150^{o}E and convection associated with the PSA2 pattern is in quadrature with that related to PSA1. These modes encompass high intraseasonal variance on the MJO frequency band (correspondent to periods around 40 days) and to shorter 22-day signals over South America expressed as a see-saw pattern of concurrent wet and dry anomalies over the South Atlantic Convergence Zone (SACZ)

and the subtropics to the south [Nogués-Paegle and Mo, 1997; Nogués-Paegle et al. 2000].

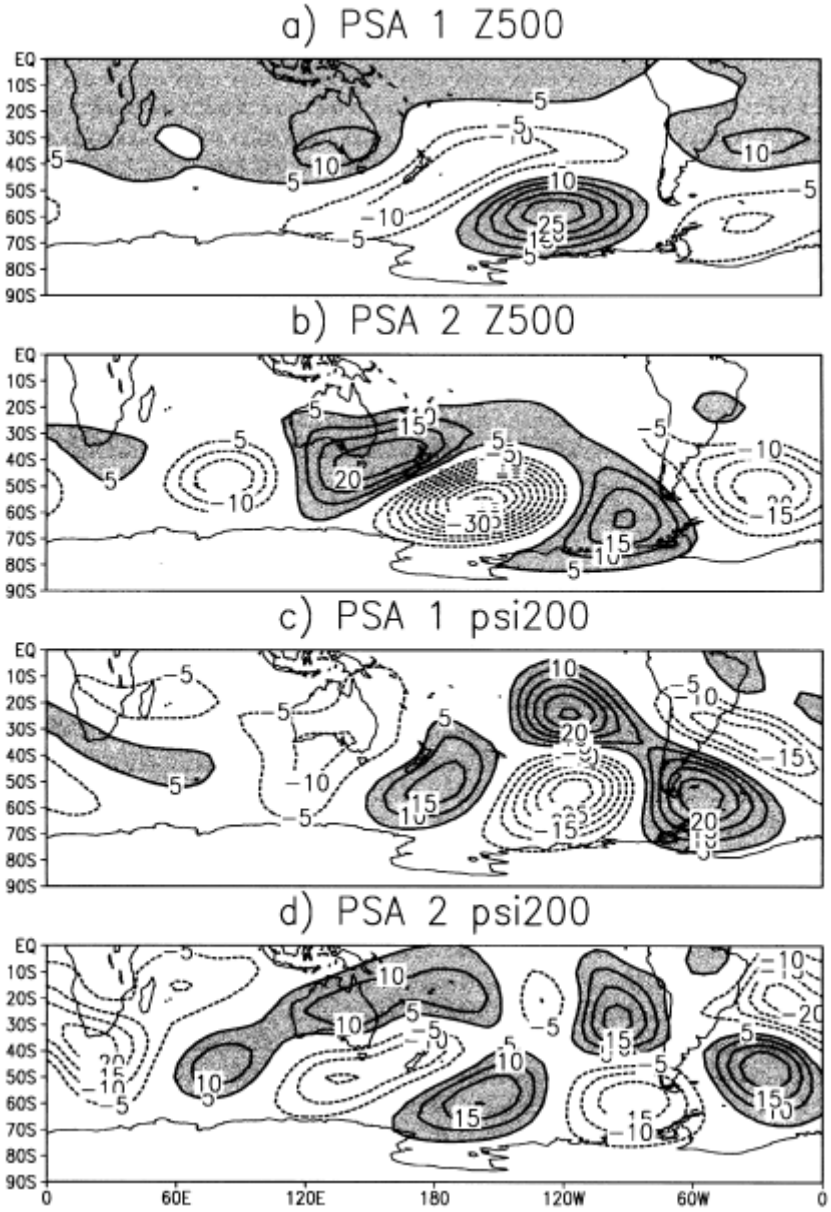

Figure 2.3: (a) PSA1 (EOF2) and (b) PSA2 (EOF3) of 500 hPa mean height anomalies. Positive values are shaded. PSA1 explains 13 % and PSA2, 11% of the total variance. (c) PSA1 (EOF3) and (d) PSA2 (EOF4) of 200 hPa streamfunction anomalies (mean zonal winds removed). PSA1 explains 8.2% and PSA2, 7.6% of the total variance (from Mo and Nogués-Paegle [2001]).

The South American Monsoon and its Variability

Compared to the widely investigated Asian monsoon, the South American summer monsoon (SASM) was characterized only relatively recently. According to early strict definitions of monsoons, the South American climate is not classified as monsoonal even though a large area of the continent experiences a dry winter and a wet summer. The discrepancy arises from the fact that traditional criteria for the definition of a monsoon require clear wind shifts associated with the seasonal variation of the atmospheric temperature gradient [Ramage, 1971].

Initial heat budget estimates, however, indicated that the summer diabatic heating over the central Andes Mountains in January 1979 was similar to that observed over the Tibetan Plateau in July 1979 [Rao and Erdogan, 1989]. Later on, a series of studies revealed that the Amazon rainforest was also important as a heat source and could support the characteristic summertime upper-level circulation over the continent [Silva Dias et al., 1983 and 1987; Figueroa et al., 1995]. Numerical modeling results suggest that the summer circulation over South America is not completely dependent on orography, but the presence of the Andes seems to be important for the observed intensity and, to a lesser extent, for the location of major SASM features described in the literature [Lenters and Cook, 1995 and 1997]. Variations of the South American summer circulation are tied to equatorial Atlantic wind perturbations and, although the Atlantic trade winds are prevalent during the entire year, a seasonal reversal of wind direction is observed in anomalies relative to the annual mean [Zhou and Lau, 1998].

Rainfall amounts over central Brazil quickly increase during September and November, and decrease sharply in April, with 90% of the total annual precipitation falling between October and April [Gan et al., 2004]. Over the southern Amazon and central eastern Brazil, around 87% and 79% of the total annual rainfall is observed between October and April, respectively, with peaks in January (Figure 2.4). Northern

Amazon receives around 60% of total annual precipitation during the same period, but the annual cycle peaks between April and May.

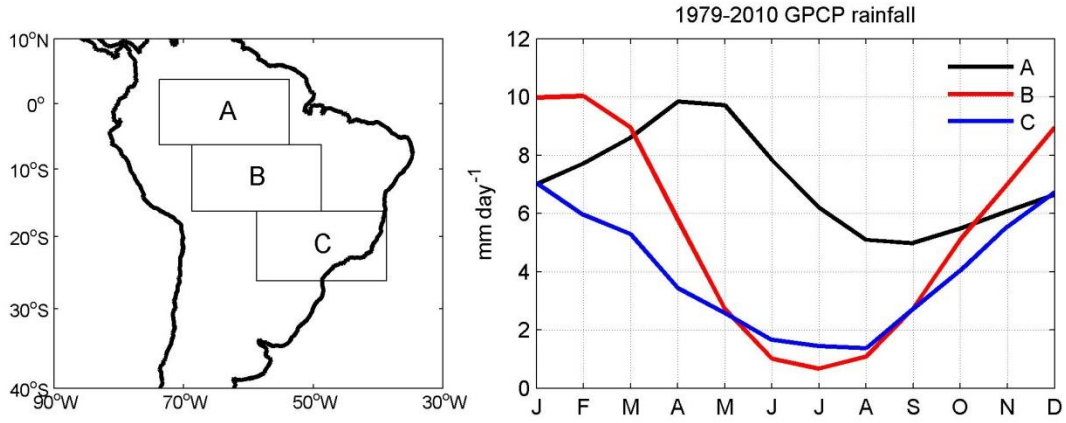

Figure 2.4: Global Precipitation Climatology Project (GPCP) 1979-2010 monthly rainfall average over A) northern Amazon; B) southern Amazon; C) central eastern Brazil.

From the austral spring to summer, the lower atmosphere over Amazonia experiences a buildup of moisture and rainfall that migrates from northwest to southeast following the southward march of the sun [Marengo et al., 2001]. Increasingly warm and humid conditions eventually reach the proximities of the central Andes. Moisture is entrained into the boundary layer as a result of diurnal expansion and contraction [Fu et al. 1999]. By the end of the calendar year, a very moisten environment developed over southern Amazon climbs the eastern flanks of the Andes towards the Bolivian Altiplano. A strong latent heat flux is driven by the peak seasonal solar radiation south of the equator. The gradual establishment and intensification of an upper-level high pressure center (known as the Bolivian High) determine the mature phase of the SASM [Zhou and Lau, 1998] (Figure 2.5).

Like the Asian monsoon, the SASM system presents strong intraseasonal variance particularly concentrated over eastern Brazil (Figure 2.6). Wavelet analysis of area-averaged OLR anomalies from the region of maximum intraseasonal variance over eastern Brazil depicts a wide signal on intraseasonal time scales, a semi-annual cycle (correspondent to a period around 182 days), and three peaks on interannual timescales

(2-4 years). Intraseasonal variations are divided in two distinct dominant signals of 22-28 days (submonthly) and 36-40 days [Nogués-Paegle et al., 2000]. Over northern and northwestern Amazon only submonthly variability is observed, while both signals influence summer variability to the south and to the east [Liebmann et al., 1999; Jones and Carvalho, 2002].

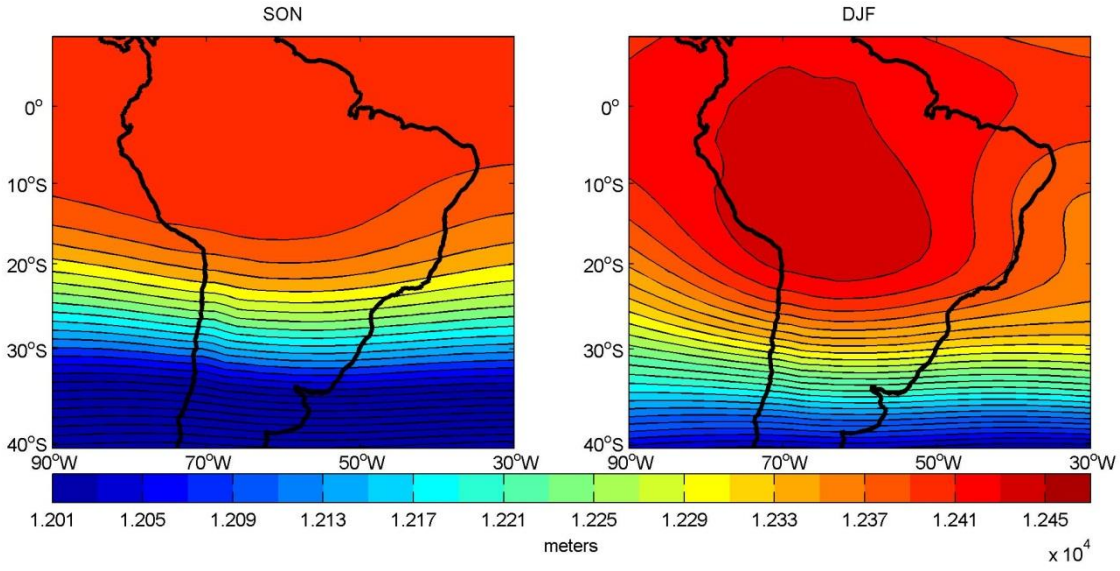

Figure 2.5: ERA-Interim SON (left) and DJF (right) 200 hPa average geopotential height illustrating the seasonal formation of the upper-level Bolivian High.

Over southeastern Brazil, submonthly variations of convection are commonly associated with extratropical Rossby wave activity while the 36-40-day signal has been statistically related to the tropical MJO [Liebmann et al. 1999; Carvalho et al., 2004]. Active (break) cycles of the SASM within the intraseasonal frequency band show a particular signature in low-level westerly (easterly) winds and positive (negative) rainfall anomalies over central Brazil [Jones and Carvalho, 2002]. Even though convective anomalies within the active MJO phase tend to weaken as they propagate over relatively colder SST in the eastern Pacific, the upper-level divergent signal often reaches South America, modulating local convection [Souza and Ambrizzi, 2006]. When upper-level divergence anomalies coming from the west are established over tropical South America,

rainfall is enhanced over southeastern Amazon and northeastern Brazil and oftentimes over the SACZ [Carvalho et al. 2004; Souza and Ambrizzi, 2006].

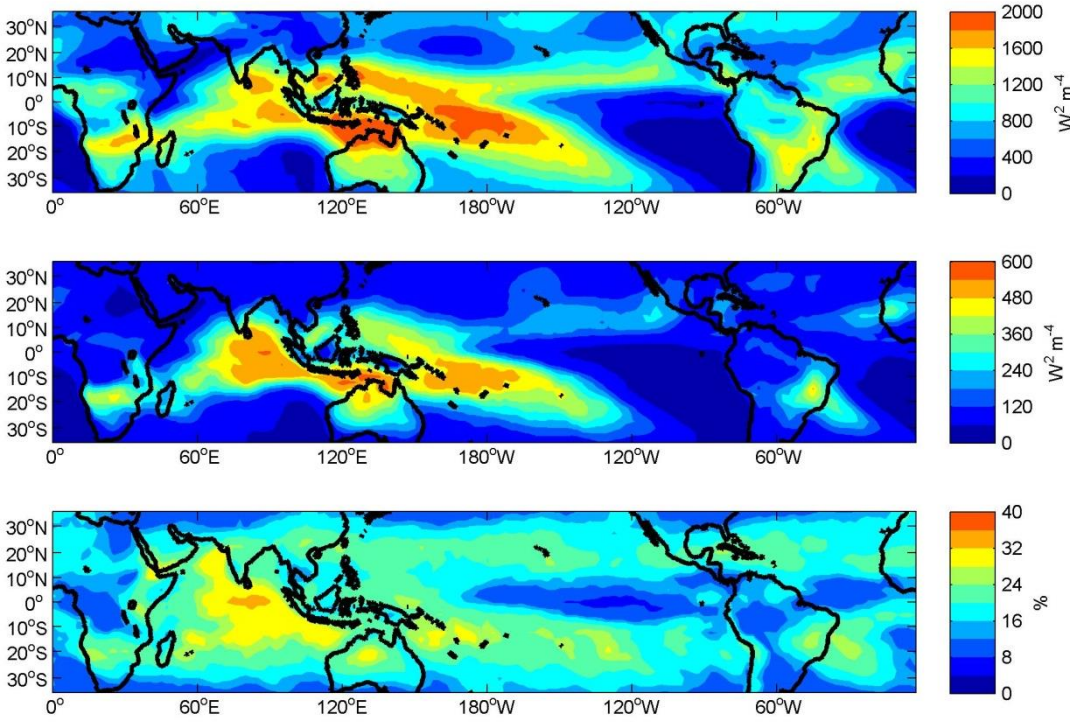

Figure 2.6: October-March OLR unfiltered variance (upper panel); band-passed intraseasonal (20-90 days) variance (middle panel); Percentage of intraseasonal relative to unfiltered variance (lower panel).

On longer time scales, SAMS interannual variability (Figure 2.7) is strongly associated with ENSO. The impact of ENSO on South American precipitation is regionally heterogeneous. El Niños tend to suppress convection over northern Amazon through changes in the zonal Walker circulation [Liebmann and Marengo, 2004]. Over southern Brazil, rainfall is enhanced during spring (November) of a warm ENSO event, with a weakening or even a reversal of these anomalies in January [Grimm et al., 1998]. Anomalous wet spring conditions are related to a strengthening of the South American upper-level subtropical jet and anticyclonic anomalies equatorward of the jet axis, due to the development of the Bolivian High, that favor baroclinic developments below. Spring anomalies are driven by a modulation of an extratropical Rossby wave train

teleconnection pattern excited by the anomalous heat source in the south Pacific associated with El Niños [Grimm and Silva Dias, 1995]. The reversal of anomalies in January seems to occur due to stronger local forcing during peak summer and is dependent on rainfall anomalies in late spring, when teleconnections are favored by the basic state [Grimm et al., 2007]. Long term variations in ENSO-related SST anomalies in the tropical Pacific apparently affect the location of the atmospheric anomalous heating and consequently influence precipitation variability over South America, with diluted anomalies associated with central Pacific El Niños [Hill et al., 2011].

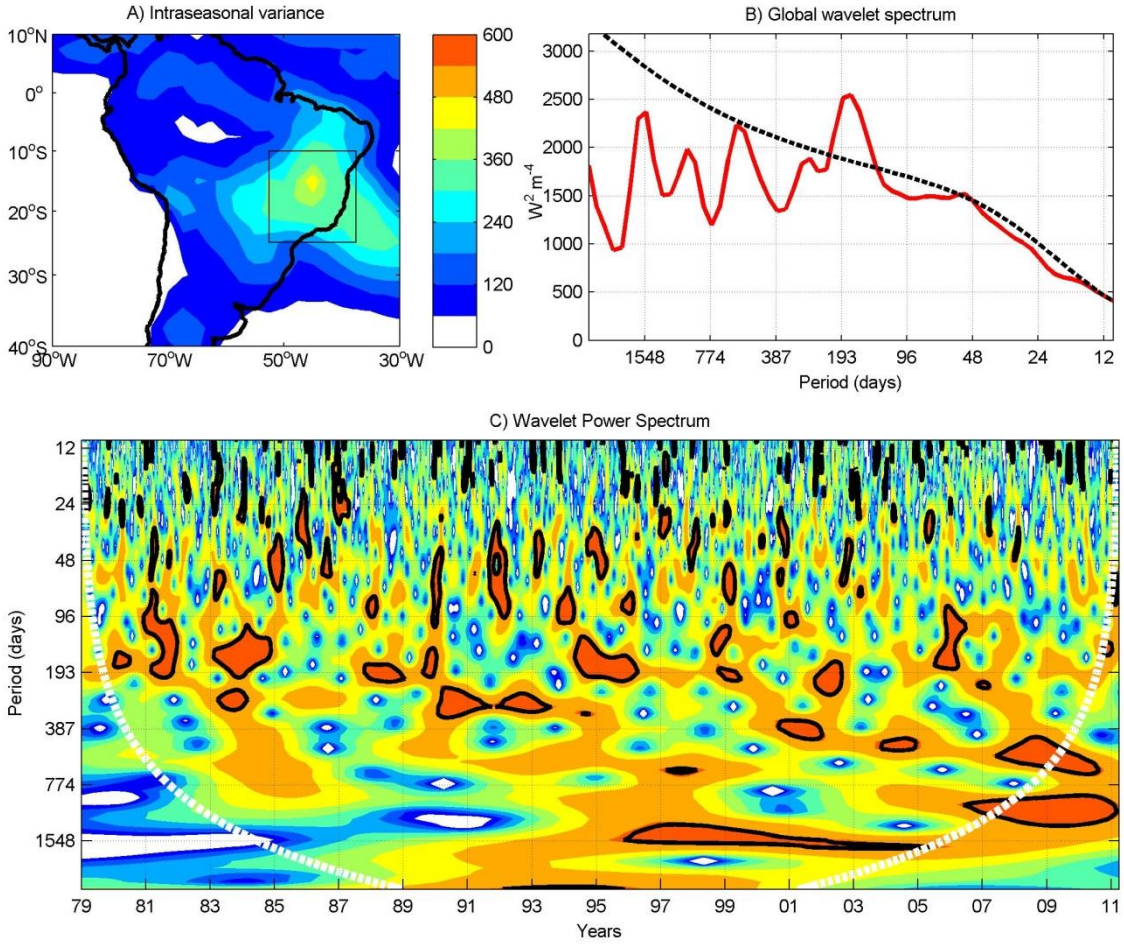

Figure 2.7: A) Oct-Mar intraseasonal (20-90 days) OLR variance; B) Global wavelet spectrum of area-averaged OLR anomalies taken from the box displayed on A; C) Wavelet power spectrum for the same OLR time series. The annual cycle was removed prior to the analysis. Red noise spectrum in B (dashed black line) was calculated using the time series lag-1 autocorrelation value of 0.7.

Decadal cycles and trends of precipitation and river flows have been identified in most of the South American continent [Genta et al., 1998; Robertson and Mechoso, 1998; Marengo et al., 1998; Rusticucci and Penalba, 2000; Marengo, 2004]. Station data from various sources revealed a significant trend toward wetter summers (January to March) south of the SACZ from 1976 to 1999, expressed by an increase in the percent of rainy days and the intensity of precipitation events [Liebmann et al., 2004]. The observed trends are related to a weakening and southward shift of the SACZ associated with a receding of the South Atlantic subtropical high pressure center. El Niño influences on observed trends were discarded by the lack of a significant correlation between JFM rainfall over southern Brazil and Niño 3.4 index and by the non-significant trends in SST anomalies in the Niño 3.4 region. The observations, however, did correlate JFM rainfall and both eastern tropical Pacific and South Atlantic SST, with stronger positive correlation observed when Atlantic SST lags precipitation by one month.

Upward trends of rainfall and rainfall extremes were also identified from 1960 to 2000 using gauge station data over Ecuador, northern Peru, and southeastern South America (southern Brazil, Paraguay, Uruguay, and northern and central Argentina) [Haylock et al., 2006] (Figure 2.8). Canonical correlation patterns between annually averaged Pacific Ocean SST and several annual rainfall indices led the hypothesis that a shift to more El Niño-like conditions may have caused these changes. This hypothesis is in line with long-term observations of Pacific Ocean variability impact over South America. When warm ENSO events occur during Pacific Decadal Oscillation (PDO) positive phases, teleconnections from the Pacific basin to South America are intensified [Kayano and Andreoli, 2007].

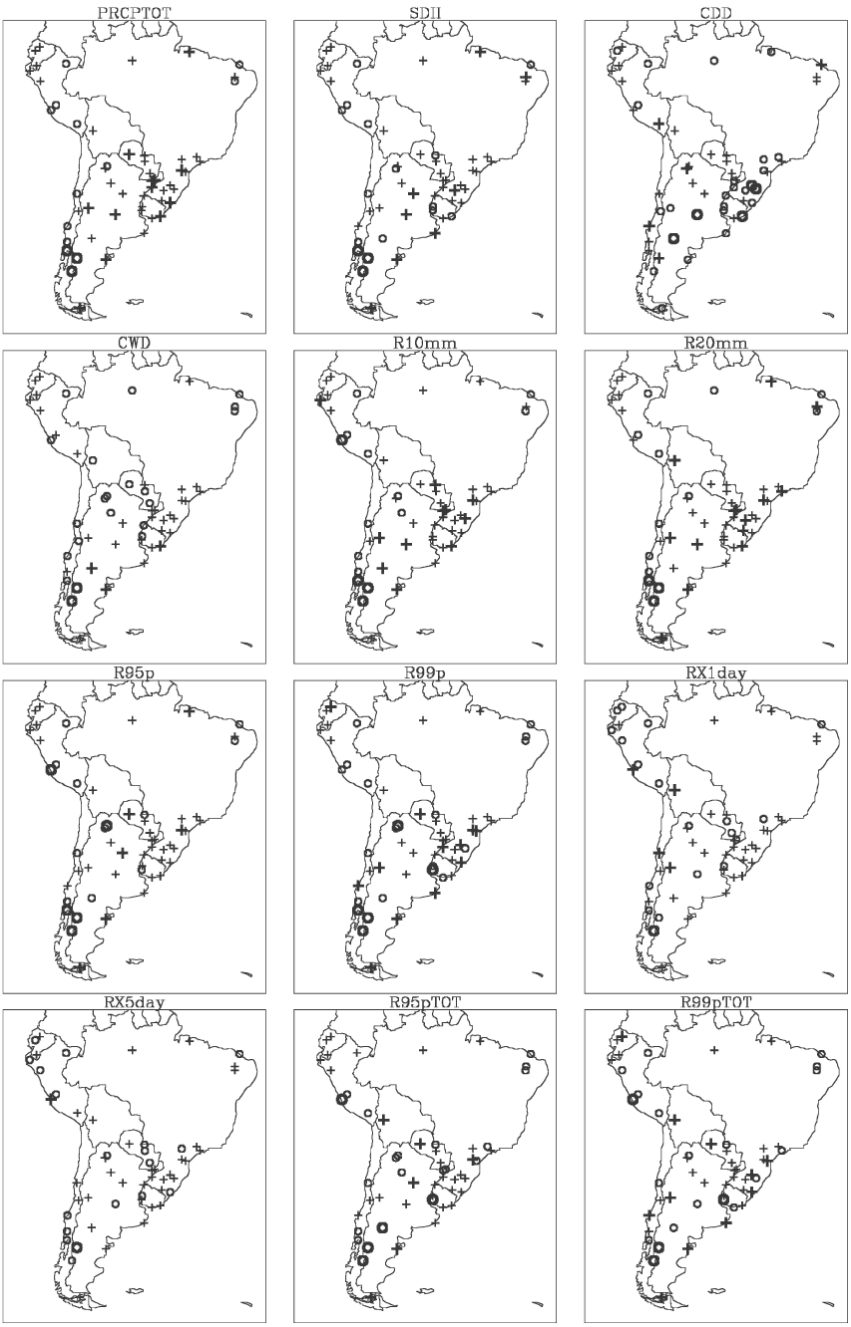

Figure 2.8: Sign of linear trends for 12 rainfall indices from Haylock et al. [2006]. An increase is shown by a plus sing, a deacrese is shown by a circle. Trends significant at 0.05 levels are indicate by bold signs. PRCPTOT is the annual total precipitation during wet days, SDII is the average precipitation during wet days, CDD is the maximum number of consecutive dry days, CWD is the maximum number of consecutive wet days, R10mm is the number of days with rainfall rate RR ≥ 10 mm, R20mm is the number of days with RR ≥ 20 mm, R95p is the total annual precipitation when RR > 95th percentile (1961-1990), R99p is the total annual precipitation when RR > 99th percentile (1961-1990), RX1day is the annual maximum 1-day precipitation amount, RX5day is the annual maximum 5-day precipitation amount, R95pTOT is the percentage of annual total precipitation from days with RR ≥ 95th percentile (1961-1990), and R99pTOT is the percentage of annual total precipitation from days with RR ≥ 99th percentile (1961-1990). A wet day means RR ≥ 1mm and a dry day means RR < 1 mm.

CHAPTER 3

AUSTRAL SUMMER TROPICAL INTRASEASONAL OSCILLATIONS

Large-scale tropical intraseasonal convection over the Eastern Hemisphere warm pool presents striking event-to-event variations. The most prominent austral summer mode of variability within the intraseasonal frequency band in the region is the Madden-Julian Oscillation (MJO). However, an important fraction of the total intraseasonal variance of tropical convection over the Indian and West Pacific Oceans does not necessarily exhibit the same features of the observed MJO archetypal that has been developed by the scientific community since it was first depicted by Madden and Julian [1971].

Traditionally, the MJO is defined as a planetary-scale eastward propagation of convection with a period between 30 and 90 days, stronger over the tropical Indian Ocean and West Pacific during austral summer [Zhang, 2005]. Although we do not challenge this notion, we hypothesize it hinders the understanding and limits the potential predictability of a significant fraction of tropical intraseasonal variability. Around 40% to 60% of the intraseasonal variance in tropical convection over the eastern Indian Ocean and West Pacific fit the traditional MJO definition, as measured by the simultaneous amplitude of the principal components (PCs) associated with the first two empirical orthogonal functions (EOFs) of one or more atmospheric variables [Wheeler and Hendon, 2004]. This strategy reveals fundamental real-time information about the location and amplitude of the MJO around the tropics. Nevertheless, there is still a comparable percentage of intraseasonal variance that falls somewhere in between the coherent MJO signal and other large-scale disturbances that permeate the tropics. Some episodes of

large-scale intraseasonal convection are similar to the MJO ideal during early stages of their life cycles but fail to propagate as far east as canonical events. Other events present much weaker or an absence of convective anomalies over most of the Indian Ocean, but grow enough over the Maritime Continent to be often called MJOs. Such distinct manifestations of tropical intraseasonal convection are commonly excluded from the dataset by studies focusing on the MJO, but some of them also produce strong convection and rainfall over the region indicating a path to improve the prospects for overall intraseasonal predictability. The main motivation for the present effort is to describe and explain significant differences within the broad spectrum of tropical intraseasonal variability that go beyond the classic MJO conception and seek a characterization of these differences.

The goal of this chapter is to show that there are enough statistical and dynamical reasons to recognize the existence of more than one distinct form of large-scale tropical intraseasonal convective events, each being significantly different from the conventional MJO. In particular, it is suggested that these differences should not be neglected nor treated simply as weak MJOs. To label them all as MJO events may diminish signal-to-noise ratio and lessen potential predictability. To neglect them completely may deprive us of a better understanding of intraseasonal convection growth and propagation and the different sectoral influences that these other categories possess, including unique teleconnection patterns. The premise of limited categories of intraseasonal events sheds light on outstanding issues about tropical dynamics on intraseasonal time scales and may represent an improvement of extended-range weather forecasts in regions where these signals are important (e.g. South America).

Definition of Intraseasonal Events

The statistical definition of tropical intraseasonal events closely follows the arguments of Kessler [2001], which consistently identifies large-scale slow eastward

propagating intraseasonal patterns over the warm pools. Band-passed (20-90 days) outgoing longwave radiation (OLR) data [Liebmann and Smith, 1996] averaged between 5ºN and 5ºS during the austral summer season (Oct-March, from 1979 to 2011) is decomposed to simple empirical orthogonal functions (EOF). The first two EOF modes (Figure 3.1a) are significantly correlated with each other with maximum lag-correlation of 0.65 when EOF1 principal component time series (PC1) leads EOF2 series (PC2) by approximately 11 days (Figure 3.2). Together, they explain most of the intraseasonal variance over the Indian Ocean, Maritime Continent, and western Pacific Ocean (Figure 3.1b). Thus, these two modes are used to describe intraseasonal variations of large-scale convection and its following propagation over the tropics of the Eastern Hemisphere.

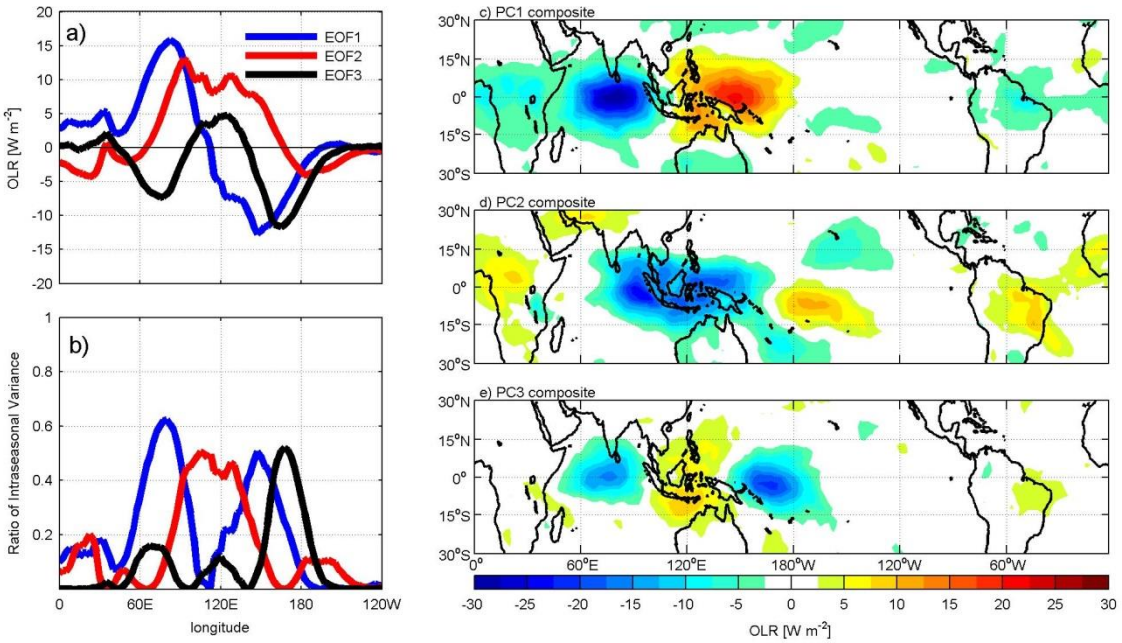

Figure 3.1: a) Austral summer EOF modes of averaged (5ºN to 5ºS) intraseasonal OLR. b) Ratio of intraseasonal variance as a function of longitude for each EOF mode. c) Composite day 0 for PC1 events with minimum below -1 standard deviation. d) Composite day 0 for PC2 events with minimum below -1 standard deviation. e) Composite day 0 for PC3 events above +1 standard deviation, representing strengthened convection over the Indian and West Pacific Oceans.

Three sets of distinct large-scale intraseasonal convective events are defined as combined evolution of EOF1 and EOF2 (Figures 3.1c,d). The first set encompasses the

MJO: the fraction of planetary-scale intraseasonal convection that begins over the tropical Indian Ocean initiation region (between 70°E and 90°E) and propagates eastward, reaching the western Pacific Ocean a few days later. These events are defined when PC1 presents a minimum below -1 standard deviation and PC2 also falls below -1 standard deviation within 25 days after the PC1 minimum. The 25-day time window is chosen in order to identify all PC1 minima followed by PC2 minima. This selection criterion resulted in an average lag of 10.8 days (Table 3.1), very close to the best correlation lag between the two time series (11 days). The day of minimum PC1 value is the referred to as MJO composite day 0.

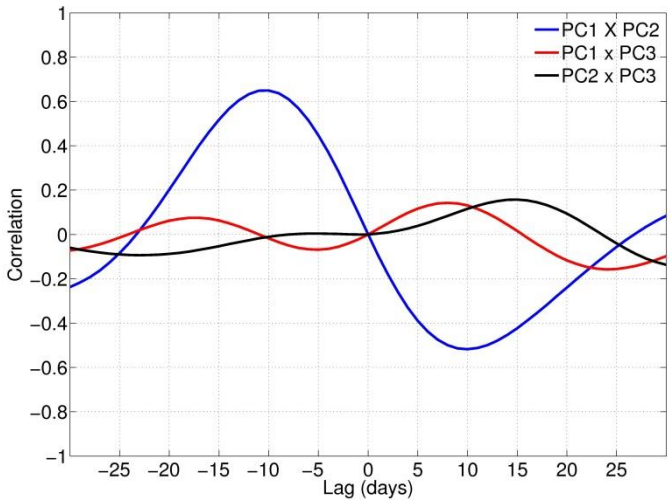

Figure 3.2: Lag-correlation among PC1, PC2, and PC3. Negative lags indicate that, for each pair of PCs identified by the legend, the first leads the second.

Table 3.1. Categories of EOF-based intraseasonal events

	Number of events	**Average lag (days)**
Canonical MJO	52	10.8
Eastward decayed	25	-
Eastward intensified	13	-
Others	5	-
TOTAL	95	-

A second set of intraseasonal events is defined whenever PC1 presents a minimum below -1 standard deviation (this minimum is referred to as composite day 0 for this cycle) but a subsequent minimum below -1 standard deviation is not observed on PC2 within a period of 25 days. Events matching this criterion are referred to as *eastward decaying events* (EDs) due to the observed weakening of convective activity over the Maritime Continent. The third category comprises intraseasonal events in which PC2 falls below -1 standard deviation (the composite day 0 for this cycle) but it is not preceded by a minimum PC1 below -1 standard deviation. This last category describes weak or absent convection over the tropical eastern Indian Ocean but later strengthens over the Maritime Continent. These are referred to as *eastward intensifying events* (EIs).

The threshold of one standard deviation is used to include relatively strong convective events and to state that ED and EI events are not merely weak MJO events. Five other events presented minima in PC1, PC2, or both, with varied lags much longer than 25 days and are neglected. An important result is that more than 40% of the total 93 intraseasonal events identified through this method do not fall into the canonical MJO category (Table 3.1).

Other variables used in this study were obtained from ERA-Interim Reanalysis dataset. We also use NOAA's daily Optimum Interpolation (OI) AVHRR-only [Reynolds et al., 2007] and TRMM Microwave Imager (TMI) 3-day average sea surface temperature (SST) data [Wentz, 1997]. All data were band-passed using the same procedure applied to OLR. Gaps in TMI data were linearly filled, including a 15-day hiatus from 16-31 July 2007. The boreal summer period was not used in our analysis but will be examined separately in another study.

Both infrared (such as the Advanced Very High Resolution Radiometer - AVHRR) and microwave sensors (such as the TMI) have limitations to retrieve SST data. Satellite infrared SST retrievals are limited to cloud-free conditions and microwave imagery measurements are limited to rain-free conditions [Wentz et al., 2000]. These

limitations are of great concern when one is trying to associate deep convection and intense rainfall with SST anomalies in the tropics. A comparison between daily OI AVHRR-only and TMI datasets was carried out to ensure that the choice of SST product does not affect our conclusions about the importance of SST anomalies for the initiation and eastward propagation of tropical intraseasonal convection.

The OI AVHRR-only dataset has three advantages over microwave products: it covers a much longer time span (1981 to present), it uses in-situ data from buoys and ships, and it retrieves SST near land [Reynolds et al., 2007]. Daily OI SST also offers a product that includes AMSR (Advanced Microwave Scanning Radiometer) data but it only starts in 2002. The following figures display a series of band-passed SST composites for each of the intraseasonal events described in the article (Figures 3.3, 3.4, and 3.5).

Composites were computed for events that occurred during austral summer seasons from December 1997 to March 2011 to coincide with the TMI coverage analyzed in this study. Although the magnitudes of the anomalies are slightly different, their horizontal structure and phase with respective to the event life cycle are approximately the same for all three categories. Figure 3.3, for instance, displays the eastward migration of positive SST intraseasonal anomalies from the equatorial Indian Ocean to the Maritime Continent from composite days -14 to 0. The signal is stronger in TMI composites but the AVHRR depicts the same features. The same characteristics are observed in the composites for ED and EI events, although the contrast between the two datasets is not as clear as in the case of the MJO cycle. The lack of significance and spatial coherency of SST anomalies during ED and EI cycles seem to be an important feature of the intraseasonal variability of the Indian Ocean and Maritime Continent.

Once both SST datasets give qualitatively similar results and we use OI data in our composites because of its longer temporal coverage (1981 to present) and smaller biases near land [Reynolds et al., 2007]. This latter point is vital to observations within

the MC during convective breaks. Statistical significance was assessed by a Monte Carlo method [Livezey and Chen, 1983].

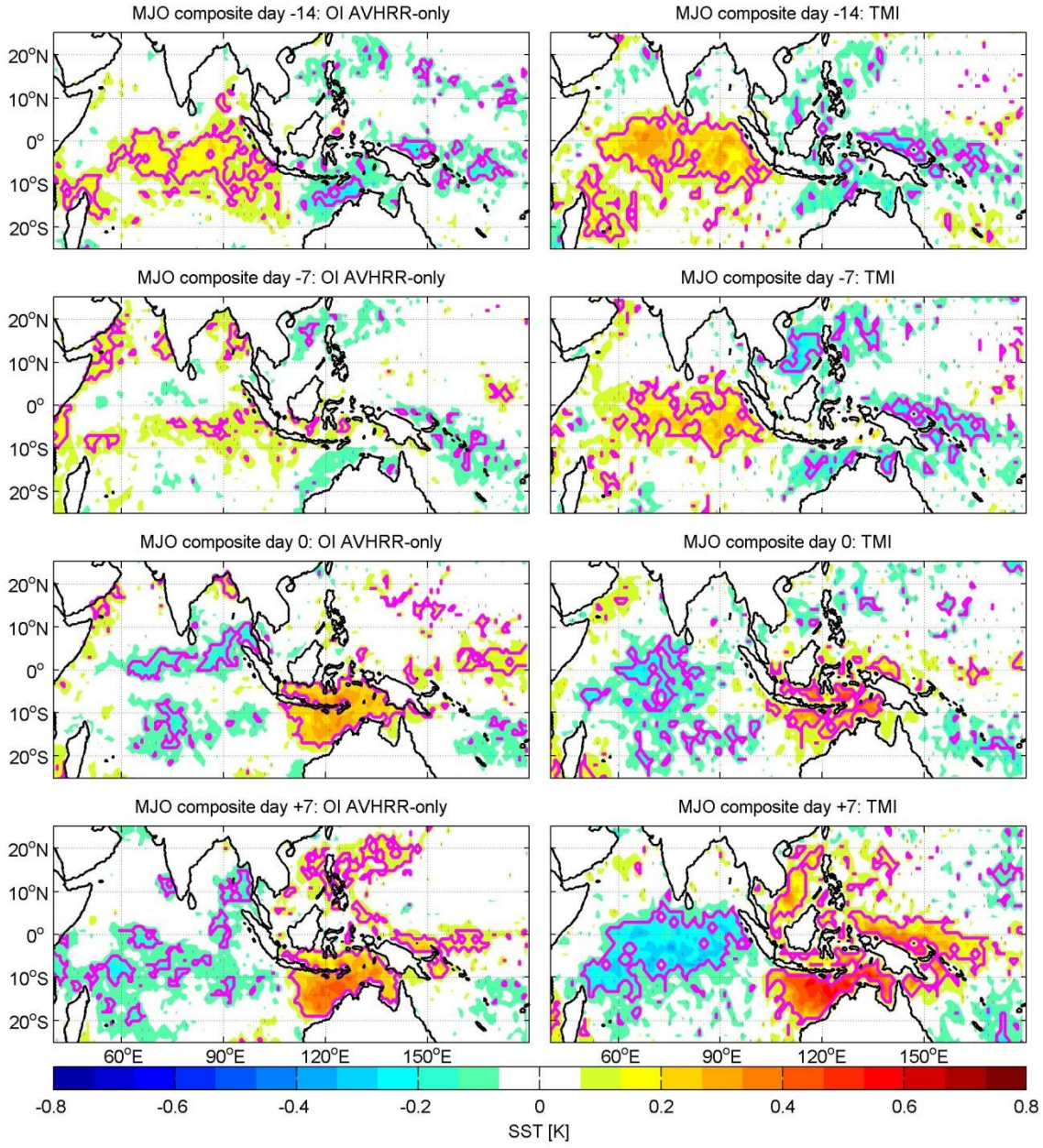

Figure 3.3: Band-passed SST composites for canonical MJO events (days -14, -7, 0, and +7). Right-hand side: OI AVHRR-only; left-hand side: TMI. Pink contours indicate significant SST anomalies at 95% confidence level.

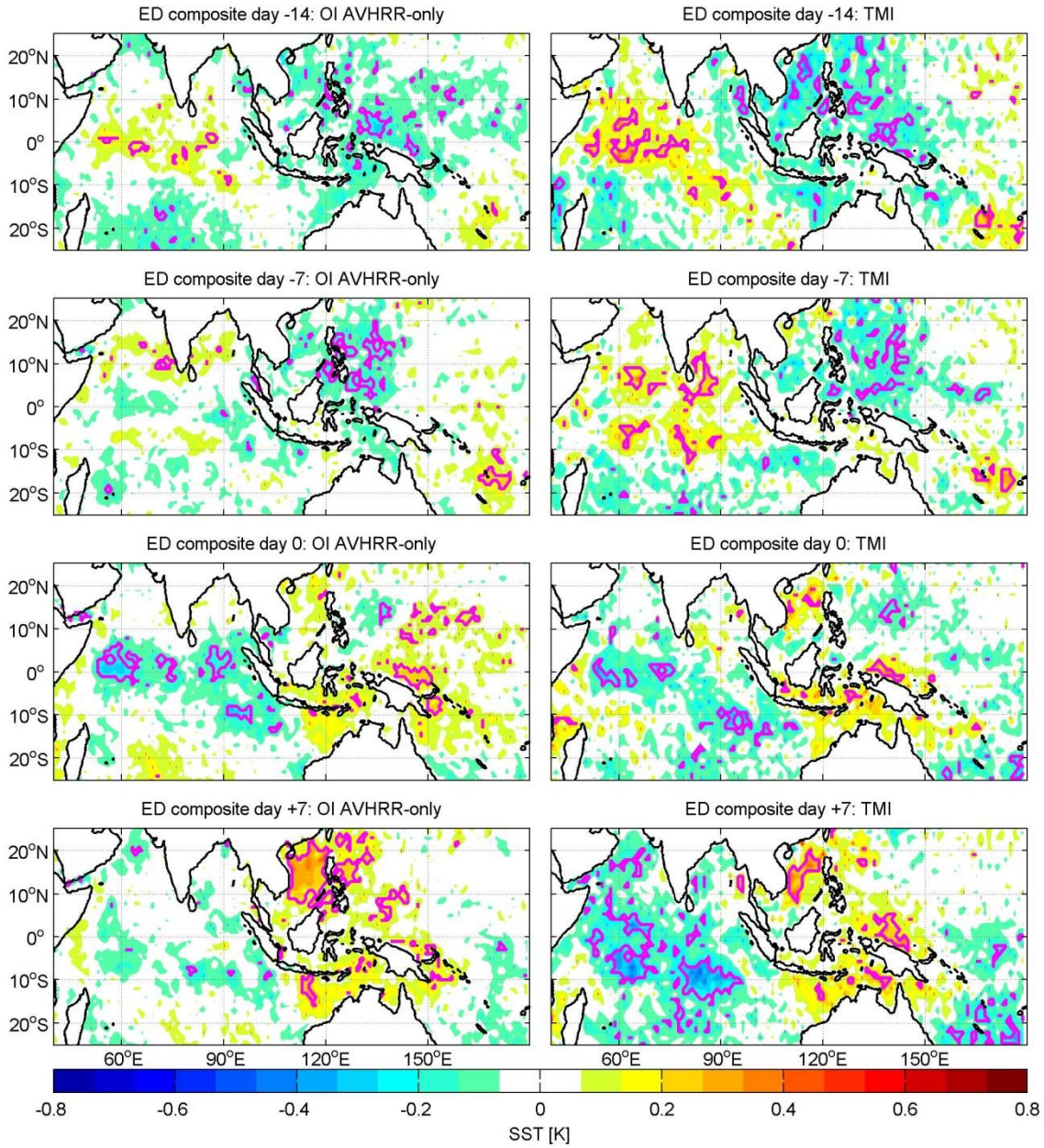

Figure 3.4: Band-passed SST composites for eastward decaying events (days -14, -7, 0, and +7). Right-hand side: OI AVHRR-only; left-hand side: TMI. Pink contours indicate significant SST anomalies at 95% level.

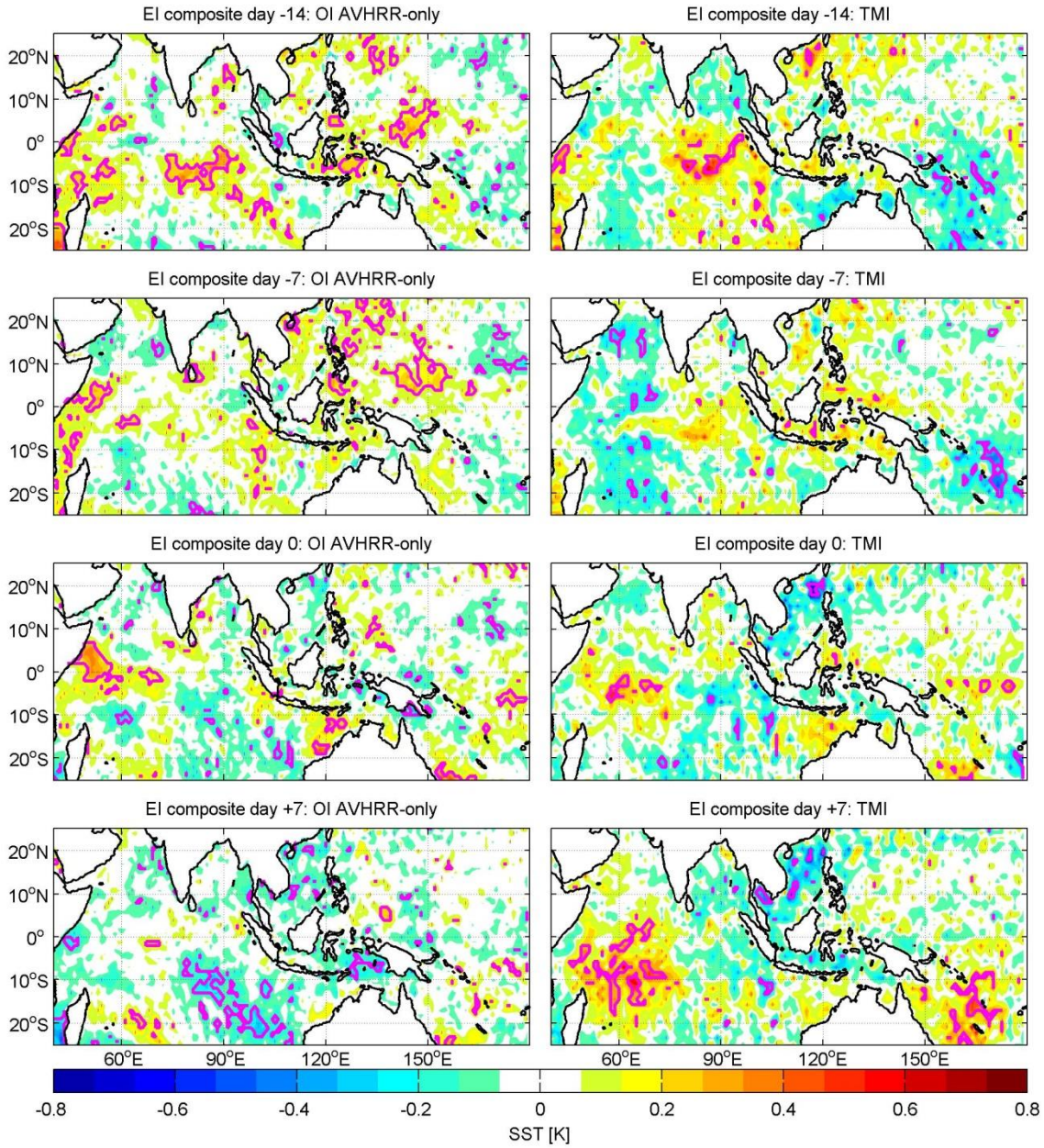

Figure 3.5: Band-passed SST composites for EI events (days -14, -7, 0, and +7). Right-hand side: OI AVHRR-only; left-hand side: TMI. Pink contours indicate significant SST anomalies at 95% level.

Intraseasonal Life Cycles of Convection

Previous studies proposed that intraseasonal convectively active phases over Eastern Hemisphere tropics are, at least in part, a consequence of atmospheric destabilization during the preceding quiescent conditions [Stephens et al., 2004; Agudelo et al., 2006]. The dynamical mechanism that allows this destabilization period would be

an atmospheric Rossby wave response to convective activity to the east, promoting subsidence to the west of convection, sea surface warming and atmospheric energy build-up [Wang et al., 2005]. Sea surface warming is observed during the earlier half of the MJO life cycle (Figure 3.6a). Overall, OLR lead SST anomalies by around one week.

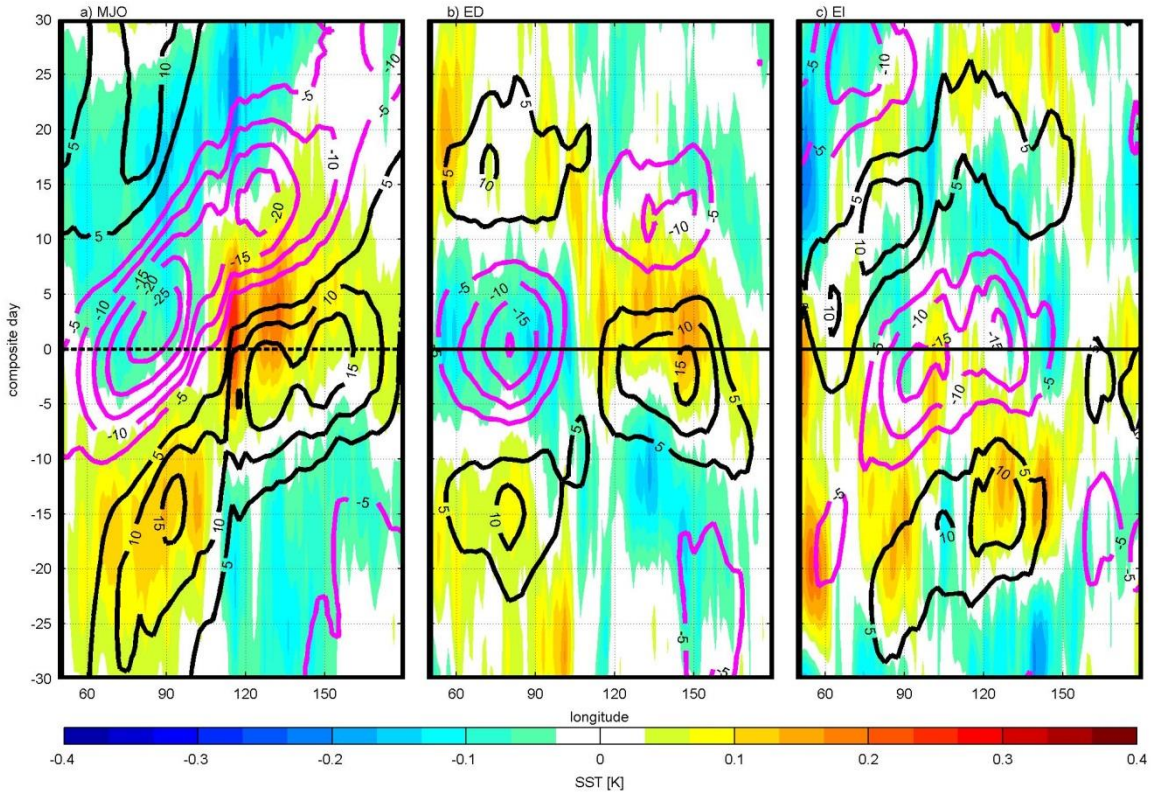

Figure 3.6: a) Longitude-time diagrams of composite life cycles for the canonical MJO, b) ED, and c) EI events. Shading (contours) represent band-passed SST (OLR) anomalies averaged between 5ºN and 10ºS to highlight stronger SST anomalies south of the equator in the surroundings of the MC (Figure 3.7).

Two weeks prior to maximum MJO convection over the eastern Indian Ocean, easterly anomalies become significant over an anomalously warm equatorial Indian Ocean, while significant cold anomalies prevail under westerlies in the tropical West Pacific (Figure 3.7a,b). The wind and surface pressure anomalies suggest low-level divergent conditions associated with Rossby wave subsidence. The eastward propagation of a Kelvin wave from this region of enhanced subsidence (Figure 3.7b) suppresses convection along the way and allows warm SST anomalies to grow within the Maritime

Continent. This Kelvin-Rossby wave pair is similar to the large-scale tropical atmospheric response to heating but with the opposite sign.

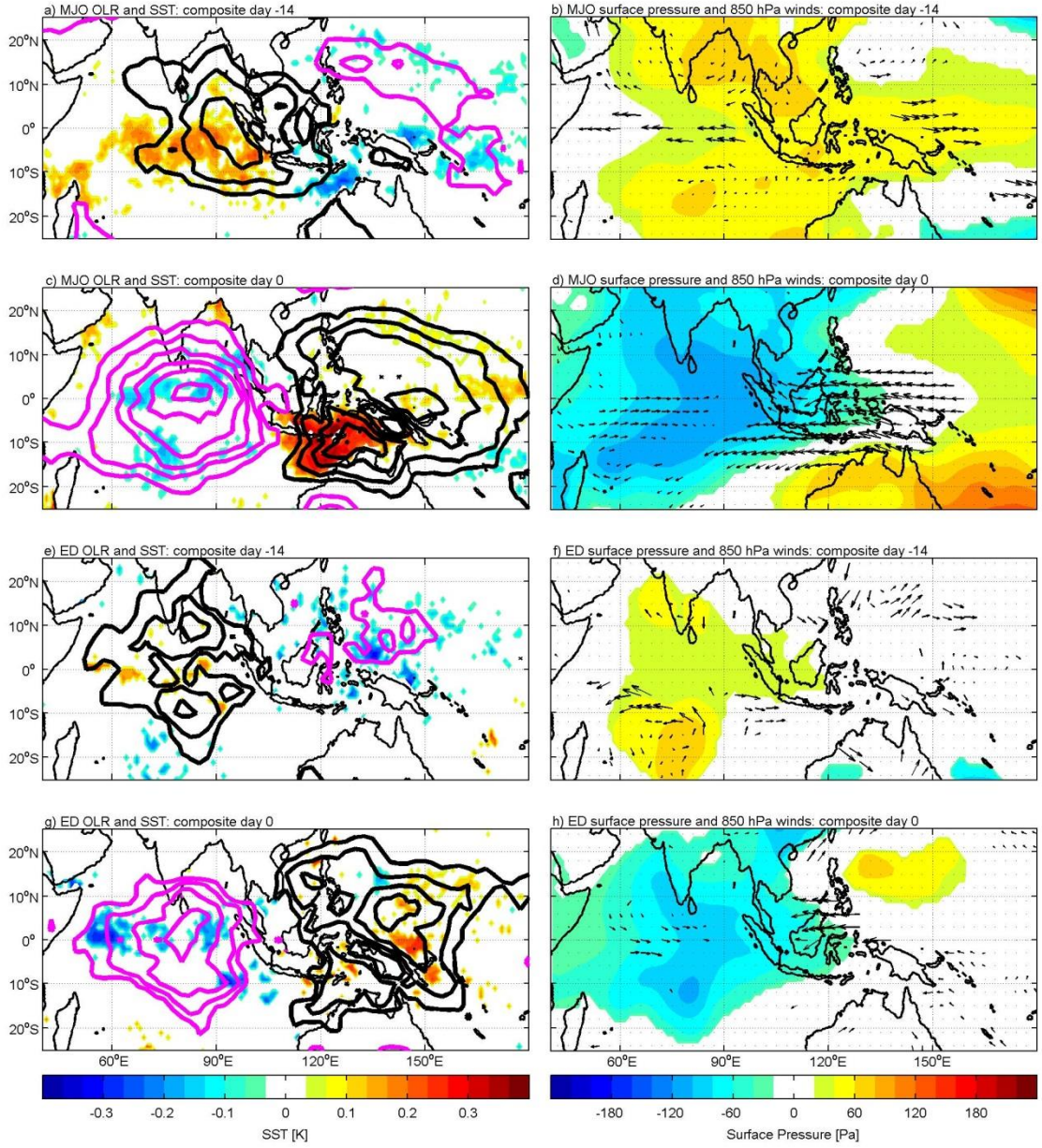

Figure 3.7: Composites for the canonical MJO (a-d) and ED events (e-h). Right-hand side: shading represents significant SST anomalies and black (magenta) contours represent significant positive (negative) OLR anomalies (5 W m^{-2} intervals). Left-hand side: shading represents significant surface pressure anomalies and vectors represent 850 hPa winds with significant speed (90% significance level; maximum wind anomalies of -4.5 m s^{-1} on panel d).

One week before MJO composite day 0 (Figure 3.6a), convective anomalies grow east of 60^{o}E while strong positive OLR anomalies sit over the Maritime Continent and the West Pacific Ocean. On composite day 0, warm SST anomalies are observed south of the equator from Sumatra to New Guinea, under significant low-level easterly anomalies flowing towards the low-level convergence maximum as part of the large-scale wave response to convective heating (Figure 3.7c,d). These easterly anomalies observed in a region of climatological westerly wind stress indicates decreased evaporative cooling, allowing shortwave flux to raise SST anomalies to the east of active convection [Woolnough et al., 2000; Vialard et al., 2012]. Convection weakens over the Maritime Continent, but anomalies near -15 W m^{-2} continue to travel eastward favored by the positive SST anomalies east of 100^{o}E: these SST anomalies having developed during the convective break and wave-related subsidence. The amplitude of easterly anomalies diminishes after the convective peak on composite day 0, suggesting an increase in latent heat flux over the region of anomalously warm SST. The combination of positive intraseasonal SST anomalies and a tendency to more westerly wind stress incrementally increases surface heat fluxes to the atmosphere, fuelling further eastward motion. As in the depiction of the boreal summer intraseasonal events of Wang et al. [2006], sea surface warming is followed by surface convergence and, subsequently, convection. Propagation is less pronounced for ED and EI events (Figure 3.6b,c). Neither of these two intraseasonal categories exhibit comparable sea surface warming leading convection within the Maritime Continent.

The convective phases of ED events begin around one week prior to maximum convection, as in the traditional MJO cycle (Figure 3.6b). Weak and incoherent SST anomalies over the initiation region are observed after an earlier break in convective activity. The convective break moves to the east following a tendency of suppressed convection promoted by the eastward propagation of a dry Kelvin wave. The dynamical signature of the large-scale waves can be identified, but the anomalies are smaller in

amplitude and less significant compared to the MJO cycle (Figure 3.7e-h). Hence, warm SST anomalies within the Maritime Continent are also weaker and less significant. It appears that ED events are somehow triggered before the atmosphere-ocean system is able to generate sufficiently strong positive SST anomalies around the Maritime Continent that sustain further eastward propagation. The weaker influence of large-scale wave dynamics renders the cycle less effective to promote optimal conditions for the growth of SST anomalies to the east and damps the propagation of the convective envelope. Two scenarios could explain the debilitation of further eastward propagation: (1) the Rossby wave does not last long enough and the combination of radiative warming and suppressed evaporative cooling is not able to raise SSTs within the Maritime Continent (Figure 3.6a,b) or (2) easterly anomalies associated with the Rossby wave during the convective break are not sufficiently intense to suppress evaporative cooling (Figure 3.7f,h).

In the case of EI events, the Rossby and Kelvin waves are completely absent from the composite life cycle (Figure 3.8). There are only small amplitude convective anomalies over the tropical Indian Ocean from day -21 to -14 (Figure 3.8a,c,e). During the intraseasonal break, the region of stronger positive OLR anomalies are centered at 120^{o}E (day -14, Figure 3.8e), with weak negative anomalies near 60^{o}E and east of 150^{o}E. There is a tendency for SST warming, but positive pressure anomalies observed during the break of convection rapidly decline and negative anomalies predominate mostly off the equator (Figure 3.8d,f). Significant intraseasonal perturbations of the zonal circulation over the western Indian Ocean suppress convection to the east two weeks before the EI convective maximum, leading to sea surface warming and consequent atmospheric destabilization (Figure 3.9a). As convection crumbles in the west, negative OLR anomalies grow over the warmest sea surface anomalies, east of the MJO initiation region (Figure 3.7c). One week prior to the convective maximum, negative OLR anomalies begin to deepen over these warm SSTs. A Kelvin-Rossby wave pair only arises after

convection develops over the Maritime Continent. Further eastward, propagation seems to be solely due to Kelvin waves propagating out of the region. One week after the convective peak over the Maritime Continent, cold SST anomalies are widespread. A new convective break seems to develop over the initiation region while the active intraseasonal phase fades away with almost no significant surface circulation anomalies (Figure 3.8i,j).

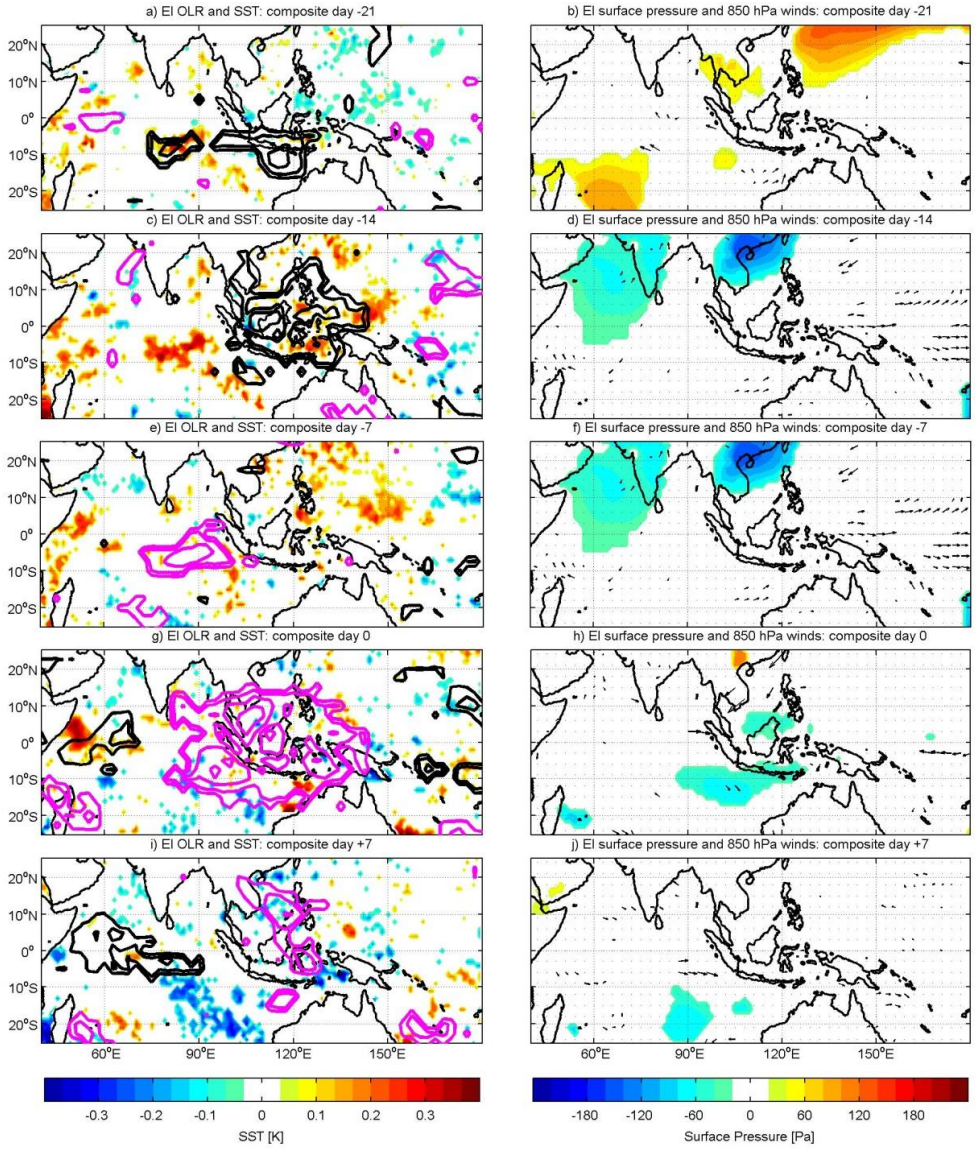

Figure 3.8: Composites for EI events. Right-hand side: shading represents significant SST anomalies and black (pink) contours represent significant positive (negative) OLR anomalies (5 W m^{-2} intervals). Left-hand side: shading represents significant surface pressure anomalies and vectors represent 850 hPa winds with significant wind speed (90% significance level; maximum wind anomalies of 5.1 m s^{-1} on panel g).

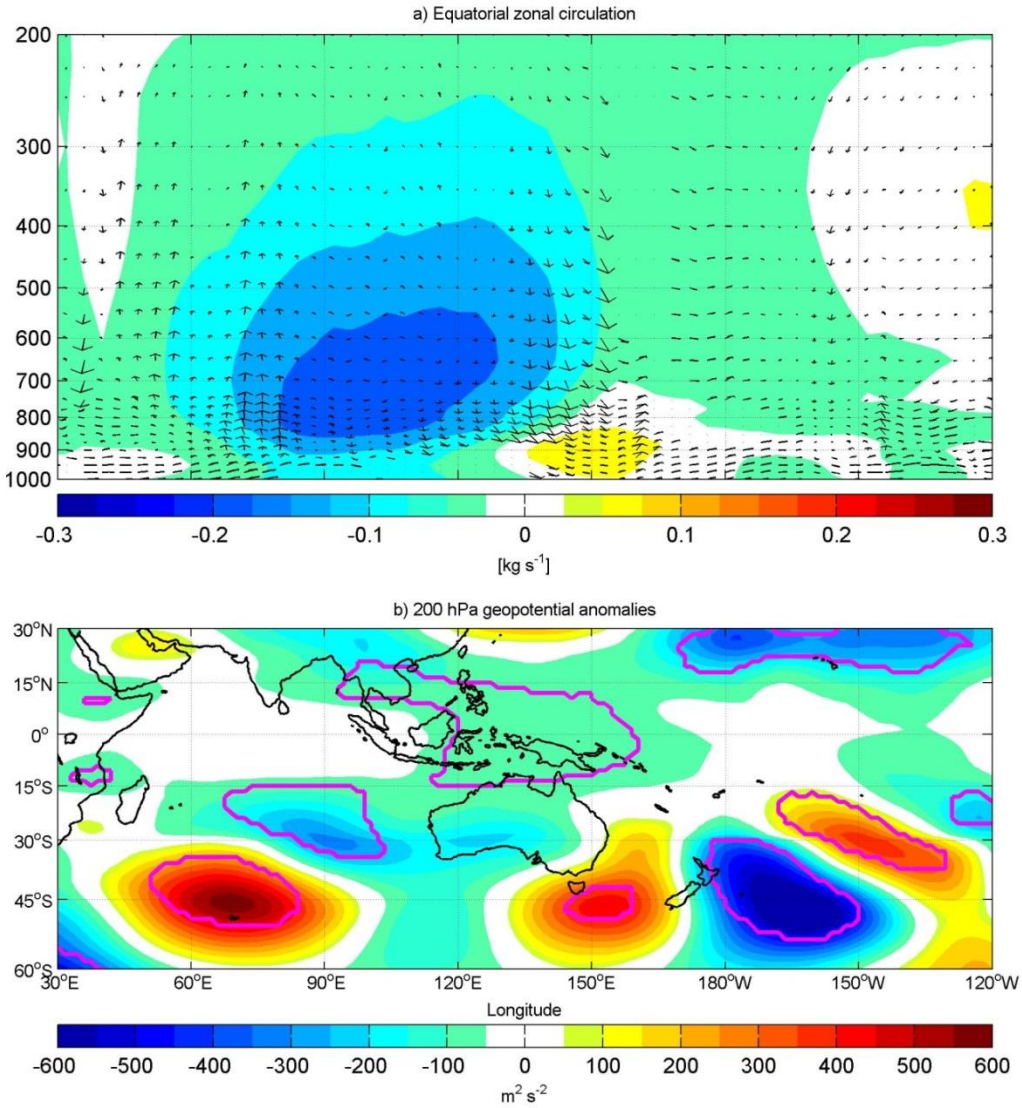

Figure 3.9: EI composite day -14: a) Vectors represent the zonal component of the wind field (m s^{-1}) and omega (Pa s^{-1}) along the equator. Only vectors with significant magnitude at 90% level are plotted. Shading denotes streamfunction anomalies. b) Band-passed 200 hPa geopotential anomalies from ERA-Interim Reanalysis. Pink contours indicate significant anomalies at 90% level.

EOF3 and ENSO Dependence

Following the guidelines for the separation of EOF modes by North et al. [1982], a third mode (EOF3) is found to be statistically significant and represents a large fraction of intraseasonal variance near the dateline (Figure 3.1a,b,e). This mode represents low-frequency eastward extensions of convection associated with the ENSO [Kessler, 2001]. We found some degree of correlation among EOF1, EOF3, and ENSO, but there is no

significant difference in occurrence of any intraseasonal modes during a particular ENSO phase, in agreement with the lack of association between ENSO and the MJO on interannual time scales [Hendon et al. 1999; Slingo et al. 1999].

During El Niño events, EOF3 would act to weaken convection over the Eastern Indian Ocean and strengthen it over the West Pacific. This occurs because the modes have opposite signs near the initiation region (EOF1 is positive, EOF3 is negative) and have the same sign east of 120^{o}E (both negative). Although there is an apparent lack of lag correlation between PC1 and PC3 (Figure 3.2), Kessler [2001] showed that zero lag correlations of 400-day windows between PC1 and PC3 series revealed a coherent behavior correlated with the Southern Oscillation Index (SOI). We calculated zero lag correlation between PC1 and PC3 seasonal averages and there is a weak but highly variable tendency of stronger positive correlations during El Niño austral summers and negative correlations during La Niña austral summers, even though the average seasonal correlation during the entire period is nearly zero (Figure 3.10). The correlation with seasonal averages of the standardized SOI is significant (-0.5 with a p-value of 0.0033 at 95% confidence level), confirming some degree of association among EOF1, EOF3, and ENSO. Nevertheless, a t-test fails to reject the null hypothesis that there is a difference in event occurrence of any intraseasonal category during a particular ENSO phase. Therefore, anomalies observed during the intraseasonal cycle are unlikely associated with ENSO anomalies on interannual time scales.

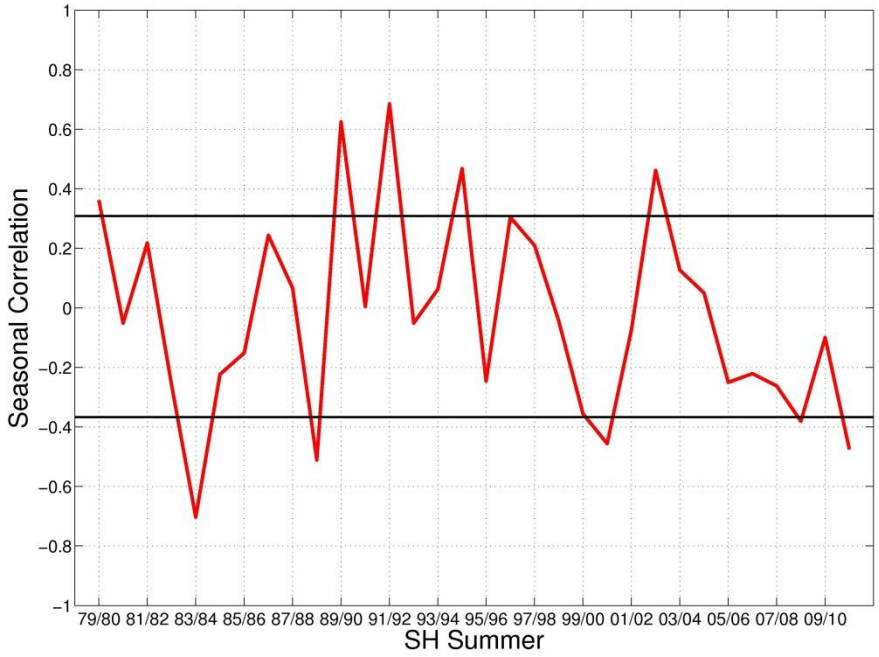

Figure 3.10 Zero-lag correlations between Southern Hemisphere summer seasonal averages of PC1 and PC3. Horizontal black lines indicate ±1 standard deviation.

Conclusion

The evolution of large-scale tropical intraseasonal convection into an MJO event depends on the strength of interaction between large-scale wave dynamics and radiative processes that begins during a convective break, in agreement with the processes leading to a primary MJO [Straub, 2013]. The cycles of an MJO and an ED event begin over the Indian Ocean initiation region, where subsidence generates positive OLR anomalies and surface anticyclones straddling the equator as Rossby waves (Figure 3.11a). A dry Kelvin wave propagates eastward away from this region, damping convection to the east. These conditions allow sea surface warming by a combination of lower evaporative cooling (the easterlies counteract the climatological westerlies to give weaker winds) and radiative heating due to minimum cloud cover. With warm SST anomalies, convection is initiated, generating a Kelvin-Rossby wave response to heating to the west of the convective break (Figure 3.11b). After the convective phase is active, the entire system propagates to the east. In the MJO cycle, the subsiding Rossby wave that precedes the convective phase is

stronger and lasts longer, resulting in warmer SST anomalies within the Maritime Continent. These warmer SST anomalies combine with the Kelvin wave propagation to favor the eastward propagation of the entire system across the Indonesia. This subsiding wave is weaker in ED events, resulting in lower or absent positive SST anomalies within the Maritime Continent and lack of eastward propagation.

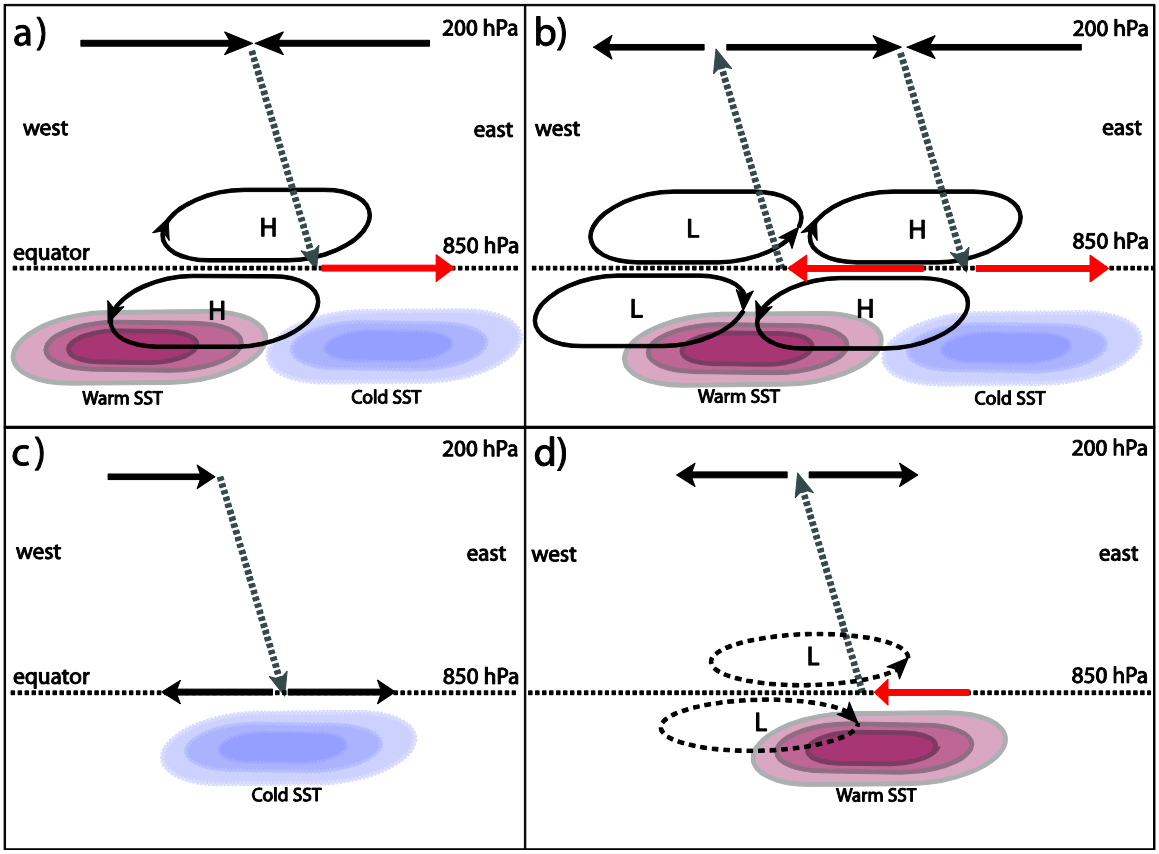

Figure 3.11: Schematic diagram for: a) Convective breaks before canonical MJO. b) Convective phase for canonical MJO. c) Break phase before EI events. d) Convective phase during EI events. Horizontal dashed lines represent the equator at 850 hPa (above SST anomalies). Dashed arrows represent upward/downward motions between 850 and 200 hPa. Black arrows represent the direction of wind anomalies. Red arrows along the equator indicate 850 hPa winds associated with Kelvin waves (easterlies for a wave associated with convection). L (H) indicates low-level negative (positive) pressure anomalies within cyclonic (anticyclonic) anomalies. Both (a) and (b) also depict ED life cycle, but the amplitude of the anomalies is smaller and less significant when compared to canonical MJO events.

Previous studies proposed self-regulation [Stephens et al., 2004] or self-induction [Wang et al., 2005] mechanisms for the maintenance of these convective cycles in which

opposite phases would act in a cooperative manner to sustain the oscillation. Our results show that convective breaks are essential for the development of active phases. However, it is not clear that the break phase bears any relationship with a previous intraseasonal event as it is suggested by the term *primary MJO* [Matthews, 2008]. The amplitude of peak convective anomalies are slightly different for each category and located over different regions but the amplitude of positive OLR anomalies generated to the west as convection moves to the east is nearly the same (Figure 3.6). Moreover, intraseasonal convection generally decorrelates after around one cycle as indicated by Hendon and Salby [1994]. Therefore, the intensity of intraseasonal convection is not a good predictor of the subsequent break phase but the break phase seems to be a good indicator of the following active phase, independent of any autocorrelation or circumnavigation signals.

One may speculate that the life cycle of an intraseasonal event is tied to initiation mechanisms in the sense that different triggers could induce distinct convective patterns. Our categorization identifies the event analyzed by Hsu et al. [1990] in early January 1986, influenced by extratropical disturbances as an MJO. Extratropical systems play important roles in triggering or organizing intraseasonal activity through the tropics (see Ray and Zhang [2010] and references therein). Nonetheless, the evolution of convection into an MJO event seems to rely more on the mutual interactions of the tropical atmosphere-ocean system immediately before large-scale convective development than on the convective trigger. ED events are somehow triggered before the large-scale wave is able to produce sufficiently large SST anomalies within the Maritime Continent and debilitates eastward propagation. The triggering mechanism may assume a variety of forms but the event development and propagation depends on the ability of an intraseasonal break to generate SST anomalies to the east of convection. Energy is stored in the ocean during the preceding convective break to be consumed by the subsequent convective disturbance as it progresses to the east. It would be worthwhile to use an

independent satellite-determined surface flux data set (e.g. SEAFLUX [Curry et al., 2004]) to confirm the sequence of ocean-atmosphere interactions proposed here.

The initiation of EI events occurs independently of equatorial Rossby wave subsidence over the tropical Indian Ocean (Figure 3.11c). Without the Rossby wave influence, no SST anomalies are generated over the usual initiation region and the convective phase is restricted to a narrower longitude range, exactly where intraseasonal convection experiences a minimum in the MJO cycle (Figure 3.6a,c). There is some sea surface warming within the Maritime Continent that eventually favors convection that approaches from the west. These convective anomalies tend to form closer to Indonesia, to the east of the traditional MJO initiation region. The life cycle indicates that small amplitude convective anomalies east of the dateline are possibly triggered by extratropical disturbances propagating into lower latitudes due to the existence of a westerly duct over the East Pacific [Webster and Holton, 1982; Webster and Chang, 1997]. However, equatorial zonal circulation suggests that the subsidence forcing is located to the west and a westerly duct does not exist over the Indian Ocean in austral summer and extratropical disturbances would not able to trigger convection over the tropical western Indian Ocean. The mechanisms behind EI event initiation are not clear as yet and deserve further investigation.

CHAPTER 4

INTRASEASONAL DEPENDENCE, WAVE ACCUMULATION AND INTENSE SACZ EVENTS

Variations in convective activity and rainfall over South America are a result of complex interactions among different phenomena, on distinct time scales. Over land, the tropical diurnal cycle during summer (December-February) is characterized by a fast afternoon build up and slow decay, with cloudiness aligned to the coastline or topographic barriers [Garreaud and Wallace, 1997]. The seasonal cycle is marked by the SASM [Zhou and Lau, 1998]. These conditions are modulated by submonthly, intraseasonal, and interannual phenomena that consequently determine extreme events of rainfall over the continent. The SASM variability on this diverse range of time scales have been associated with extratropical Rossby wave activity, the MJO, and ENSO [Liebmann et al., 1999; Grimm, 2003; Carvalho et al., 2004].

The most prominent feature of the SASM variability is the SACZ. It is usually defined as a band of deep convection oriented from northwest to southeast, extending from the Amazon basin to the South Atlantic Ocean with a varying spectral structure along its axis (Figure 4.1a,d-f). Close to the equator, intraseasonal and synoptic variations are less energetic. To the southeast, intraseasonal variability peaks near the Brazilian coast, south of 12^{o}S. Synoptic disturbances are relatively more important in the subtropics over the ocean. The spectral structure and orientation of the SACZ strongly resembles features found in the SPCZ [Widlansky et al., 2010].

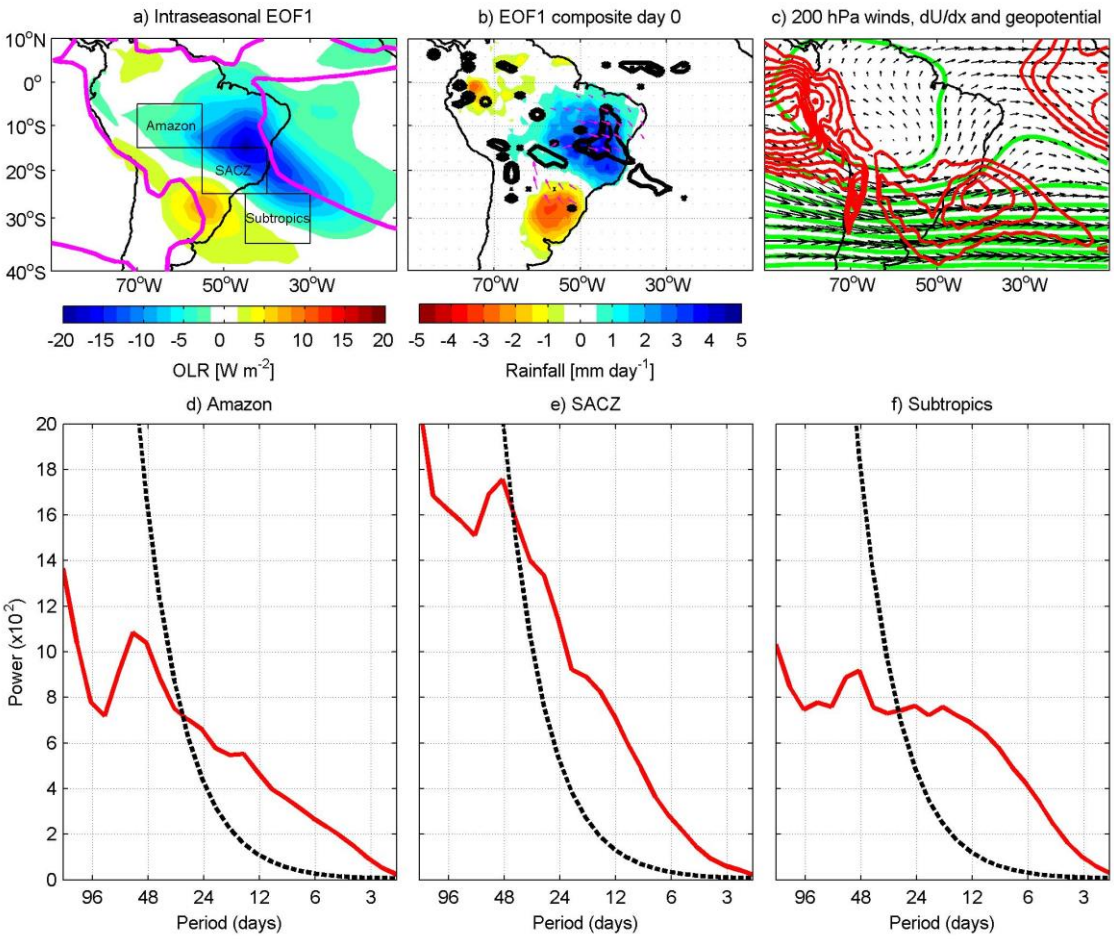

Figure 4.1: (a) First intraseasonal EOF calculated from daily filtered OLR data. Magenta contour outlines the 245 W m^{-2} October-March mean OLR. Boxes indicate the areas used to calculate the spectra in d-f. (b) SACZ composite day 0 for CPC rainfall (shading) and ERA-Interim 850 hPa winds (vectors) and negative 500 hPa omega(black contours at -5 and -2.5 x 10^{-2} Pa s^{-1}. (c) Mean October-March Era-Interim 200 hPa winds, geopotential (green), and negative zonal stretching deformation (red). (d-f) Global wavelet spectra [Torrence and Compo, 1998] of unfiltered area-averaged OLR taken from the boxes in (a). Dashed lines indicate significance level based on 95% autocorrelation.

The association of a subtropical convergence zone with a monsoonal circulation is commonly observed worldwide. Moisture convergence and abundant rainfall near the boundary between an upper-level high pressure system generated by the monsoon and subtropical jet streams occur in the SPCZ, the SACZ, and in the Baiu frontal zone [Kodama, 1992]. In South America, the establishment of the upper-level high has been suggested to be fundamental for the first SACZ of the season [Nieto-Ferreira et al., 2011]. The upper-level high pressure system over South America (known as Bolivian

High) alters the wind field, forcing a change in behavior of propagating synoptic disturbances. The seasonal formation of the Bolivian High, driven mostly by Amazon convection [Lenters and Cook, 1997], enhances anticyclonic wind shear in the northern flank of the subtropical jet, leading to thinning and westward tilting of transients and promoting the diagonal orientation of the quasi-stationary SACZ [Nieto-Ferreira et al., 2011].

The influence of the Bolivian High on upper-level winds also deepens the negative zonal stretching deformation (200 hPa $\partial \bar{U}/\partial x < 0$) over south and eastern Brazil (Figure 4.1c) in a region that coincides with the SACZ climatological position (Figure 4.1a). The location and orientation of the SPCZ is determined by the location of a region of negative zonal stretching deformation set up by the zonal SST gradient across the South Pacific [Widlansky et al.,2010]. Webster and Chang [1988] derived two expressions relating the zonal stretching deformation to longitudinal wavenumber (k) and wave energy density (ξ) under the conditions that the background wind field varies gradually in space and the frequency of synoptic-scale Rossby waves is conserved:

$$\frac{dk}{dt} = -k\frac{\partial \bar{U}}{\partial x}$$

$$\frac{d\xi}{dt} = -\xi\frac{\partial \bar{U}}{\partial x}$$

Negative zonal stretching deformation increases the longitudinal wavenumber of synoptic Rossby waves propagating eastward (which leads to a reduction of the longitudinal group speed) and increases wave energy density. The local increase of wave energy density (*wave accumulation*) results in intense convective activity that forms the diagonal band of low OLR, characteristic of the SPCZ [Widlansky et al., 2010]. Similarities between the background summertime conditions in the SPCZ and the SACZ lead to the hypothesis that wave energy accumulation also plays a role in the SACZ dynamics.

The SACZ presents important submonthly (2-30 days) and intraseasonal (30-90 days) variations. Extensive research has focused on the influence of the MJO on SACZ variability. The basic idea about the MJO influence over South American convection is that there is a zonal tropical connection and a tropical-extratropical connection. The zonal connection is directly tied to the MJO and is characterized by a more northward-displaced SACZ while the tropical-extratropical connection represents the influence of extratropical wave on both synoptic and intraseasonal frequencies [Cunningham and Cavalcanti, 2006]. The SACZ would develop whenever the synoptic and the intraseasonal frequencies (MJO or a PSA-like pattern) become in phase. Liebmann et al. [1999] argued that extratropical systems act to tap moisture flowing southward from the Amazon and are, therefore, a vital mechanism for SACZ variability.

Extratropical wave activity has been suggested to link variations of the SPCZ and the SACZ on both submonthly [Liebmann et al., 1999], intraseasonal and interannual time scales [Grimm and Silva Dias, 1995]. Grimm and Silva Dias [1995] showed that a divergent forcing (heating) southeastward of the SPCZ climatological position, consistent with that imposed by the MJO or ENSO, is able to trigger a barotropic wave train that enhances the SACZ approximately 5 days later. With an enhanced SACZ, the subtropical plains experience relatively dry conditions [Nogués-Paegle and Mo, 1997]. When the SACZ is weak or absent, a low-level jet east of the Andes transports moisture poleward and the subtropics experience wetter periods. Statistically, when convection is suppressed over the Maritime Continent, SACZ events tend to be stronger and persist for a longer time [Carvalho et al., 2004]. These intense and long-lived SACZ events are closely related to excessive precipitation over southeastern Brazil [Carvalho et al., 2002].

The main goal of this chapter is to demonstrate that a region of upper-level negative zonal stretching deformation over the eastern Brazilian coast acts to accumulate high frequency wave energy, resulting in the occurrence of SACZ events. Accumulation of high frequency energy provided by synoptic disturbances seems to be particularly

important for SACZs associated with intraseasonal convection over the Eastern Hemisphere tropics. The most intense SACZ events are associated with the MJO and represent nearly 27% of all identified SACZs from 1979-2011. Intense SACZ events tend to precede the initiation of MJO events over the Indian Ocean but their intraseasonal precursors are intimately related to large-scale wave acting during the MJO convective break. On the other hand, most of the identified SACZ events (55%) showed weaker convective anomalies associated with the global intraseasonal cycle. Apparently, these SACZ events are not associated with strong MJOs, but atmospheric circulation anomalies triggered by weaker intraseasonal convection over the Indian Ocean and Maritime Continent are sufficient to interact with extratropical waves, resulting in synoptic wave accumulation in the SACZ.

Definition of the SACZ

There is a maximum of South American intraseasonal variance from the Amazon basin into the South Atlantic as indicated by an OLR minimum (Figures 4.1). Here, the SACZ is defined as the first EOF of filtered (20-90 days) OLR over South America (hereafter referred to simply as SACZ, Figure 4.1a). This first mode explains 41% of the intraseasonal variance and is not significantly affected by variations in domain size. Unlike intraseasonal EOF modes of the Eastern Hemisphere tropics, the first two South American patterns depicted by simple EOF decomposition are not significantly correlated, indicating that the first mode can be considered independent of the second.

The SACZ mode depicts a dipole-like structure along the eastern Brazilian coast and within the region of summertime OLR minimum (Figure 4.1a). To confirm the close dynamical similarity of this statistical mode with the structure of the SACZ commonly described in the literature, a composite based on the SACZ principal component time series maxima exceeding +1 standard deviation during austral summer (Oct-Mar, 1979-2011) is shown in Figure 4.1b using CPC unified gauge-station daily rainfall [Chen et al.,

2008] and ERA-Interim reanalysis variables. These maxima are referred to as SACZ events and serve as the reference for the composites (composite day 0). Significant positive rainfall and negative omega anomalies coincide with a region of negative OLR anomalies depicted by the SACZ mode. The predominance of low level westerlies north of 15ºS associated with a low level cyclonic flow to the south resembles an active phase of the SASM [Jones and Carvalho, 2002] and a combination of the intraseasonal modes of variability described by Grimm and Ambrizzi [2009]. Negative rainfall anomalies are observed over southern Brazil and Uruguay and this dipole matches the see-saw pattern of relativelydry subtropical plains concurrent with an active SACZ [Nogués-Paegle and Mo, 1997; Carvalho et al., 2004]. The dipole is also consistent with SACZ intraseasonal, interannual, and interdecadal variations [Nogués-Paegle et al., 2000; Robertson and Mechoso, 2000]. Although this statistical definition differs from those used by Liebmann et al. [1999] and Zhou and Lau [1998], the dynamical structure showing a region of high convective variability over eastern Brazil during summer is preserved. Carvalho et al. [2004] used a more complex definition of the SACZ to incorporate some of the spatial, temporal, and intensity differences in deep convection over Brazil. However, in their analysis, intense and weak SACZ events are defined regardless of their spatial structure and more oceanic or continental SACZ events are defined regardless of their intensity. Therefore, the principal components of this first EOF mode of intraseasonal OLR variability over South America are be used to represent South American intraseasonal variations of convection and will be referred to as the SACZ mode.

SACZ Correlation with Tropical Intraseasonal Events

The three distinct categories of tropical intraseasonal oscillation defined based on the combined evolution of the first and second EOF modes of intraseasonal OLR over the Eastern Hemisphere tropics defined in the previous chapter are used here to investigate connections with the SACZ. Lag correlations between SACZ and the principal

component time series of the Eastern Hemisphere EOF1 (PC1) and EOF2 (PC2) indicate that the best significant relationship is between the PC2 and the SACZ (-0.37 with the SACZ leading PC2 by 1 day, Figure 4.2). This association is readily observed in EOF2 spatial pattern (Figure 3.1d). Furthermore, PC1 and the SACZ exhibit significant negative correlation at lag +8 (PC1 leads SACZ). These correlations indicate the traditional association between tropical intraseasonal oscillations and the SACZ: active (inactive) convection over the Maritime Continent is concurrent with a break (active) phase in SACZ convective activity [Carvalho et al., 2004]. It is also worth noting the positive correlation at lag -12 with the SACZ leading PC1. This correlation suggests that SACZ activity can feedback into the intraseasonal convection cycle over the Eastern Hemisphere.

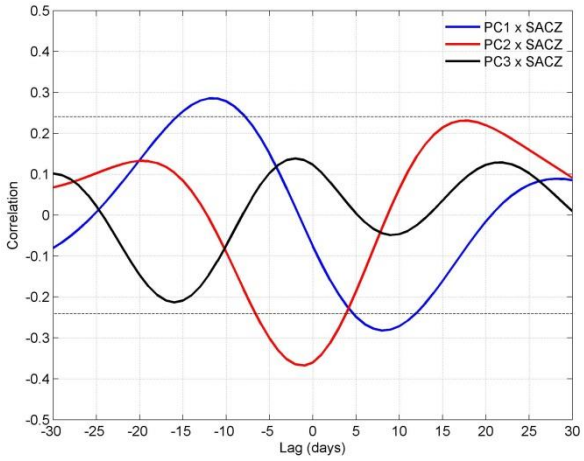

Figure 4.2: Lagged cross-correlations between each PC of the tropical modes of intraseasonal oscillations (Figure 3.1) and the PC associated with the SACZ mode (Figure 4.1a) for Oct-Mar, 1979 to 2012. Horizontal lines indicate the 0.05 significance level assessed by a two-sided t-test assuming 4 degrees of freedom per season.

Tropical intraseasonal oscillation events can be used to determine whether a SACZ event occurred within their life cycles or not, indicating possible connections between each of these distinct intraseasonal categories and the SACZ. Table 4.1 summarizes the findings of this procedure. The number of SACZ events is much higher than the combined number of intraseasonal events identified in the previous chapter,

suggesting that SACZ occurrences are not influenced only by intraseasonal convection over the Eastern Hemisphere warm pool. Overall, the SACZ seems to be more important for warm pool intraseasonal activity than the other way around: the number of SACZ preceding MJO events (26) is larger than the number of MJO events preceding the SACZ formation (11). In addition, most of the time a SACZ is observed independent of any type of intraseasonal event in the Indian or West Pacific (63 events).

Table 4.1. Lead-lag relationship between SACZ events and intraseasonal events identified in chapter 2.

	Number of events	**Average lag (days)**
MJO leading SACZ	9	4.5
ED leading SACZ	2	4
EI leading SACZ	2	5
SACZ leading MJO	24	9.1
SACZ leading ED	7	9
SACZ leading EI	4	9
Independent	63	-
Number of SACZ events	113	-

In the next section, composites are constructed to investigate the life cycle of three cases highlighted on Table 4.1: (1) SACZ independent of the MJO, (2) SACZ preceding the MJO, and (3) MJO preceding the SACZ.

Independent SACZ

As expected, the composite cycle for independent SACZ events shows little connection to strong intraseasonal convection in the Eastern Hemisphere tropics and it is very similar to the average SACZ life cycle (which considers all identified SACZ events). Nevertheless, the dynamics structure associated with tropical intraseasonal oscillations is clear and significant in surface pressure anomalies (Figure 4.3). Positive pressure

anomalies propagate eastward across the tropical Pacific Ocean as the Kelvin-Rossby wave couplet described in the previous chapter, but there is no evidence that the negative anomalies growing over the tropical Atlantic are directly linked to a Kelvin wave associated with previous intraseasonal oscillations. The pressure and OLR anomalies support the lag-correlation results with a convective break over the Maritime Continent concurrent with the development of an active SACZ.

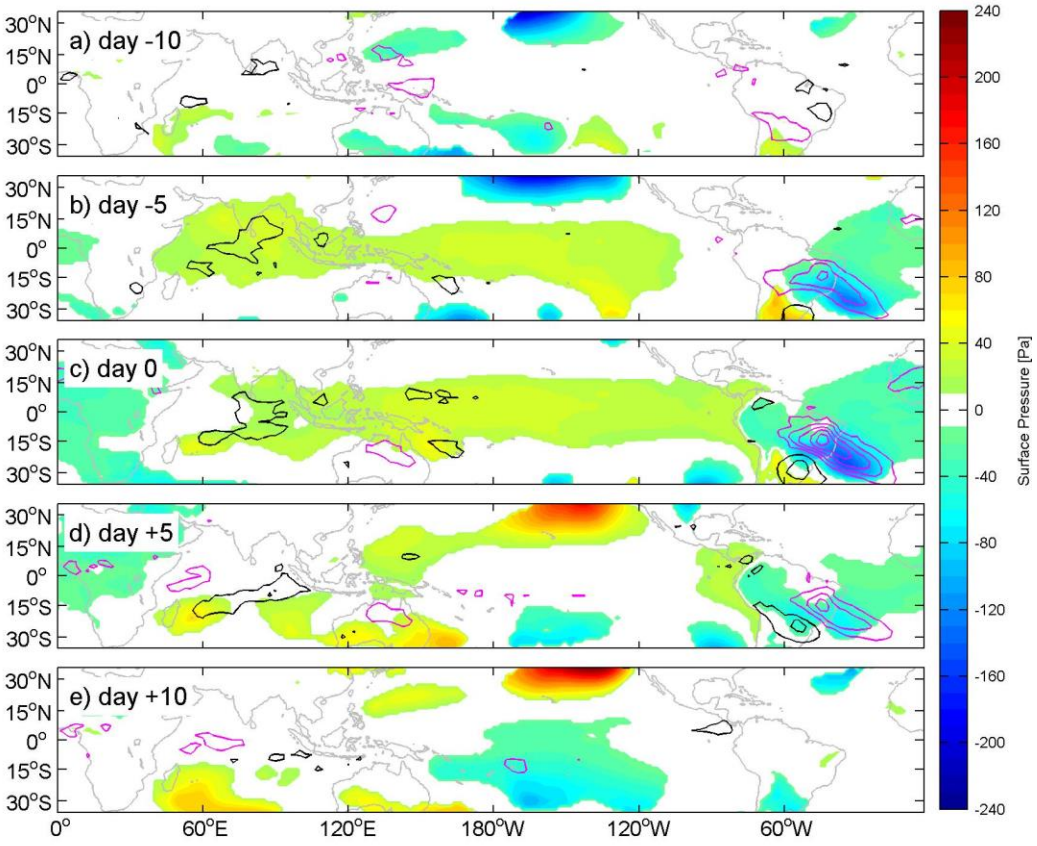

Figure 4.3: OLR (contours) and surface pressure (shadings) composite cycle for independent SACZ events. Black (magenta) contours represent positive (negative) OLR anomalies from at 5 W m^{-2} intervals. Zero contour is omitted. Only values significant at 95% confidence levels are displayed.

It is possible to observe that off equatorial pressure anomalies are stronger over the North Pacific, once the seasonal cycle favors teleconnections through the winter hemisphere westerly winds. However, significant anomalies are also present south of 20°S. Upper-level geopotential anomalies (Figure 4.4) suggest that, as the positive pressure anomalies propagate eastward across the tropical Pacific, extratropical

anomalies are organized and connect the central Pacific to South America. Upper-level anomalies on composite day -10 (Figure 4.4f) assume a zonal wavenumber 3 pattern along 60^{o}S. The extratropical anomalies east of the dateline are apparently influenced by the eastward propagation of the Kelvin-Rossby wave pair to the north. On day -5 (Figure 4.4g), the wave train over the Western Hemisphere bridges the central Pacific to southern South America. The orientation of the wave train enhances a dipole of positive geopotential anomalies over southern South America and negative anomalies to the north, while SACZ convection initiates (Figures 4.3b and 4.4b). This upper-level dipole, characteristic of the intraseasonal see-saw associated with the SACZ, is present on composite day 0 in all SACZ cycles displayed on Figure 4.4.

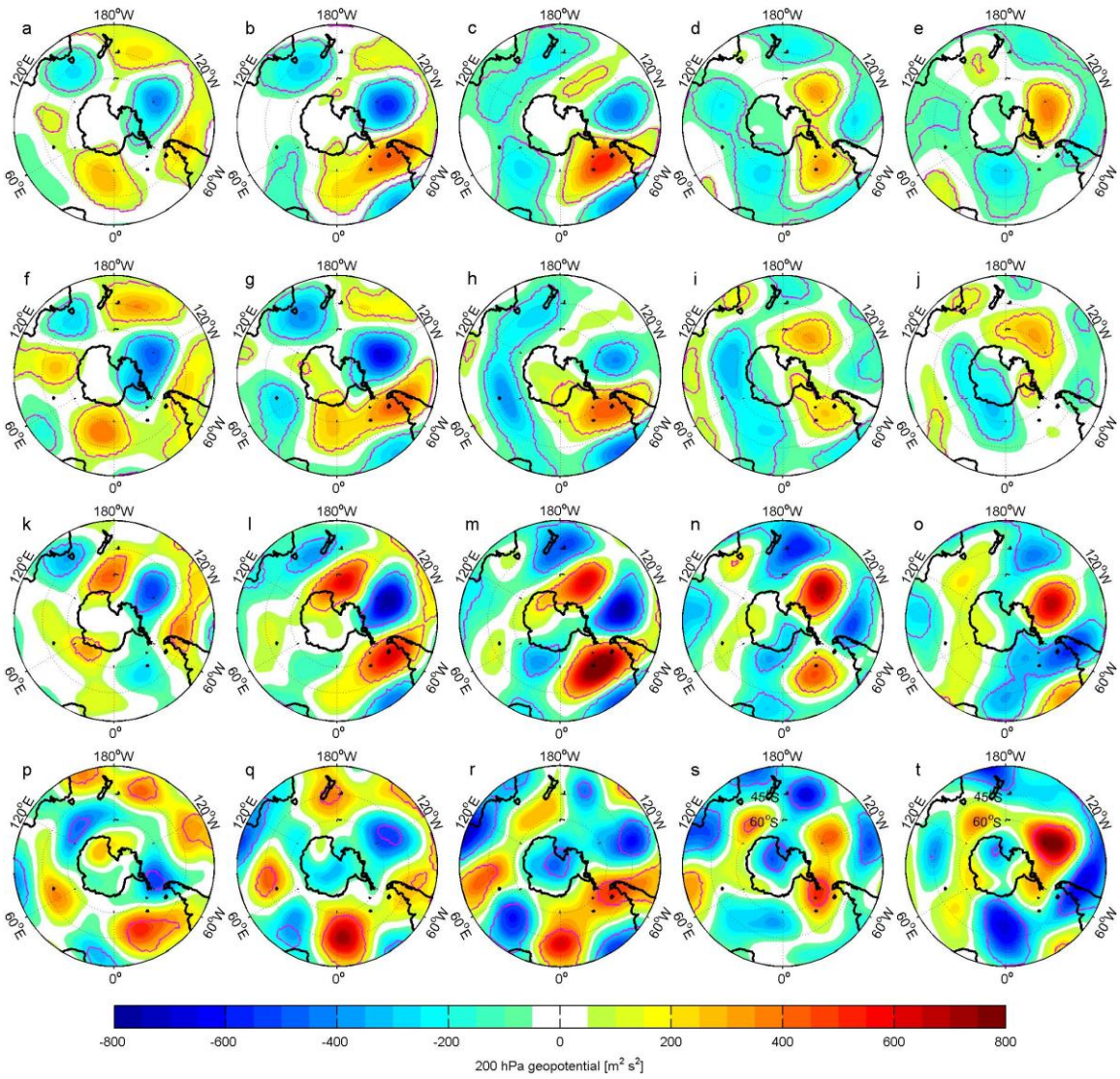

Figure 4.4: 200hPa geopotential composites. (a-e) -10, -5, 0, +5, and +10 composite days for the average SACZ cycle. Contour indicates 95% significance. (f-j) Same, but for independent SACZ. (k-o) Same, but for SACZ preceding MJO events. (p-t) Same, but for MJO preceding SACZ events.

SACZ preceding the MJO

Composites for SACZ events preceding the MJO possess stronger intraseasonal anomalies (Figure 4.5). On day -10, the large-scale Kelvin-Rossby wave pair is more defined and the negative pressure anomalies are present over the North and South Pacific. There are some significant convective anomalies at the equator, near the dateline and to the east of the leading edge of the Kelvin wave. Negative pressure anomalies are already

observed over the tropical Atlantic, with convective anomalies over continental South America. In the upper-levels, a well-defined wave train connects southeastern Australia to the East Pacific.

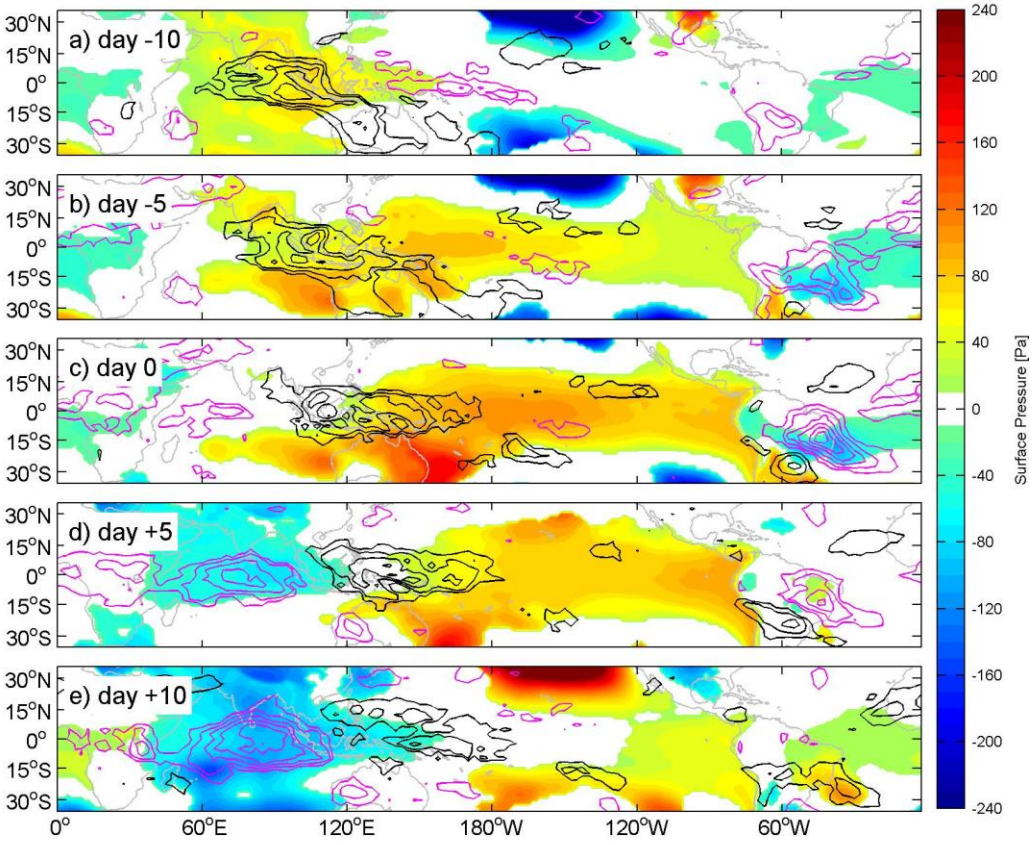

Figure 4.5 Same as Figure 3.3 but for SACZ events preceding the MJO.

On day -5, the leading edge of the Kelvin wave already reached South America. To the east of the Andes, convective anomalies are observed over the Intertropical Convergence Zone (ITCZ) and the SACZ. With the eastward propagation of the Kelvin-Rossby wave pair, the extratropical wave bends towards the Atlantic to the east of 120°E and the upper-level dipole along 30°W, associated with the SACZ, is established.

The evolution of OLR anomalies before composite day 0 shows convective anomalies around the SPCZ region, with some activity east of the dateline. At lower levels, negative surface pressure anomalies south of convective anomalies over the

tropical West Pacific assume a northwest-southeast orientation near the dateline at composite day -10 (Figure 4.5a). This set up resembles a weakening SPCZ. The negative pressure anomalies off the equator from days -10 to -5 resemble Rossby waves (Figure 4.5a,b). In this sense, the composite cycle based on SACZ events preceding MJO convection is very similar to the traditional MJO life cycle around the tropics [e.g. Matthews, 2000].

Peak convection over South America and the adjacent South Atlantic Ocean occurs at composite day 0 (Figure 4.5c), with OLR anomalies comparable in magnitude to the ones observed over the Indian Ocean a few days later (Figure 4.5e). This is the strongest SACZ among all categories inspected here. Maximum convective anomalies over the Indian Ocean are strong after an intense SACZ, indicating again that the relationship between the MJO and the SACZ still holds: convective breaks over the Maritime Continent are observed while convection grows over South America and around 10 days later, the MJO experiences an active phase. This description provides evidence of the dependency of intense SACZ events on the MJO life cycle.

The 200 hPa geopotential composites before these intense SACZ events (Figure 4.4k-m) are very similar to streamfunction anomalies for pentad lag zero of an intraseasonal event over the warm pool identified on 3 January 1986 [Hsu et al. 1990; Berbery and Nogués-Paegle, 1993]. Hsu et al. [1990] reported that the wave pattern established over the entire Northern Hemisphere could be traced back to the tropical West Pacific on 19 December 1985 associated with convective activity. Berbery and Nógues-Paegle [1993] showed that another wave pattern was excited in the Southern Hemisphere driven by the same intraseasonal forcing over the Maritime Continent.

Here, one of the SACZ events preceding an MJO was identified on 27 December 1985, precisely before the MJO on 3 January 1986. Thus, the extratropical wave pattern along the Southern Hemisphere observed on composite day -10 matches the upper-level geopotential pattern on 19 December, although there are no evidences that the trigger was

an MJO or any other category of intraseasonal oscillation. Nevertheless, 11-day mean vertically integrated diabatic heating calculated by Hsu et al. [1990] for 24 December (their Figure 3) showed values greater than 50 W m^{-2} over South America and the tropical North Atlantic. Their 11-day mean 250 hPa streamfunction anomalies also displayed a wave train from the Indian to the Atlantic, along the Northern Hemisphere, at the same day (Figure 4.6). The wave pattern in the Southern Hemisphere is not clear, but 5 days later, 29 December, a wave train seems more organized from Indonesia to the East Pacific. The same wave train can be observed in Berbery and Nógues-Paegle [1993] between the last pentad of December 1985 and the second pentad of January 1986 (Figure 4.7). The upper-level wave train displayed on Figure 3.4k,l apparently represents the link between the SPCZ and the SACZ, characterizing a response to intraseasonal variations in agreement with the modeling results by Grimm and Silva Dias [1995].

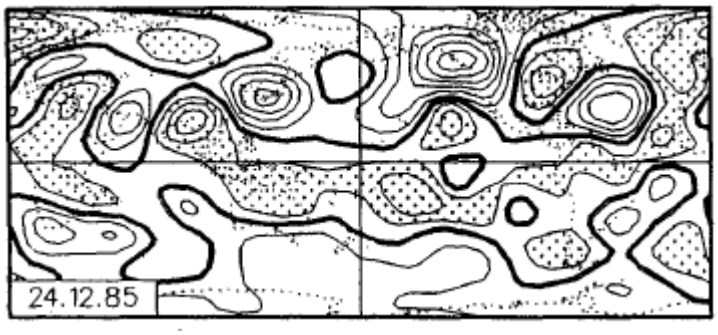

Figure 4.6: Hsu et al. [1990] 11-day means of 250 hPa streamfunction anomaly centered at 24 December 1985. The contour interval is 5 x 10^{-6} m^2 s^{-1}. The thick contour is indicates zero values and shading indicates values smaller than -5 x 10^{-6} m^2 s^{-1}.

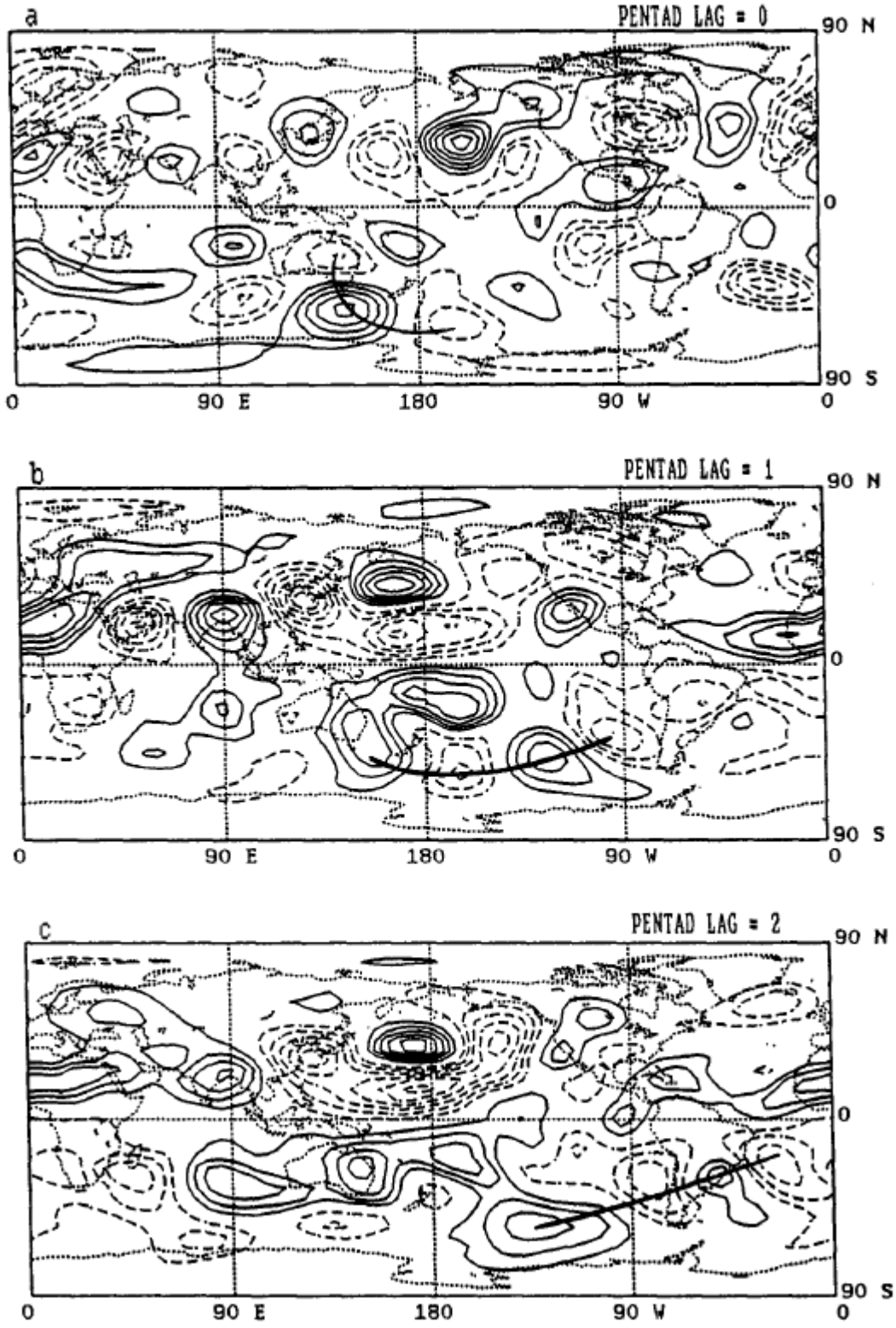

Figure 4.7: Berbery and Nógues-Paegle [1993] streamfunction anomalies at (a) pentad 73 of 1985, (b) pentad 1 of 1986, and (c) pentad 2 of 1986. Contour interval is 5 x 10^{-6} m^2 s^{-1}. Negative values are dashed and zero line is omitted.

MJO preceding the SACZ

Although the number of MJO events preceding the SACZ is small, the composite cycle exhibits significant features very different from the ones described so far. Moreover, it is important to note that although the MJO does precede the SACZ, the MJO lead is only of a few days (5 out of 9 events occur with the MJO leading by 3 days or less), meaning that convection development is almost concurrent.

On day -10, the large-scale wave signature is present over the warm pool, with a convective break over the Maritime Continent (Figure 4.6a). Convective anomalies are observed to the east, around the SPCZ, and to the west. Negative pressure anomalies in the North and South Pacific are not as strong as observed in the other SACZ cycles. The upper-level anomalies are less organized (Figure 4.4p) and there is no evidence of a wave train linking MJO activity to South America.

On day -5, the leading edge of the Kelvin wave reached South America and SACZ convection is initiated, but there are no significant negative pressure anomalies over the Atlantic basin. In addition, SACZ convective anomalies, although exhibiting approximately the same magnitude compared to other SACZ categories, occupy a smaller area. Contrary to the other SACZ cycles, the upper level dipole in geopotential is not formed yet.

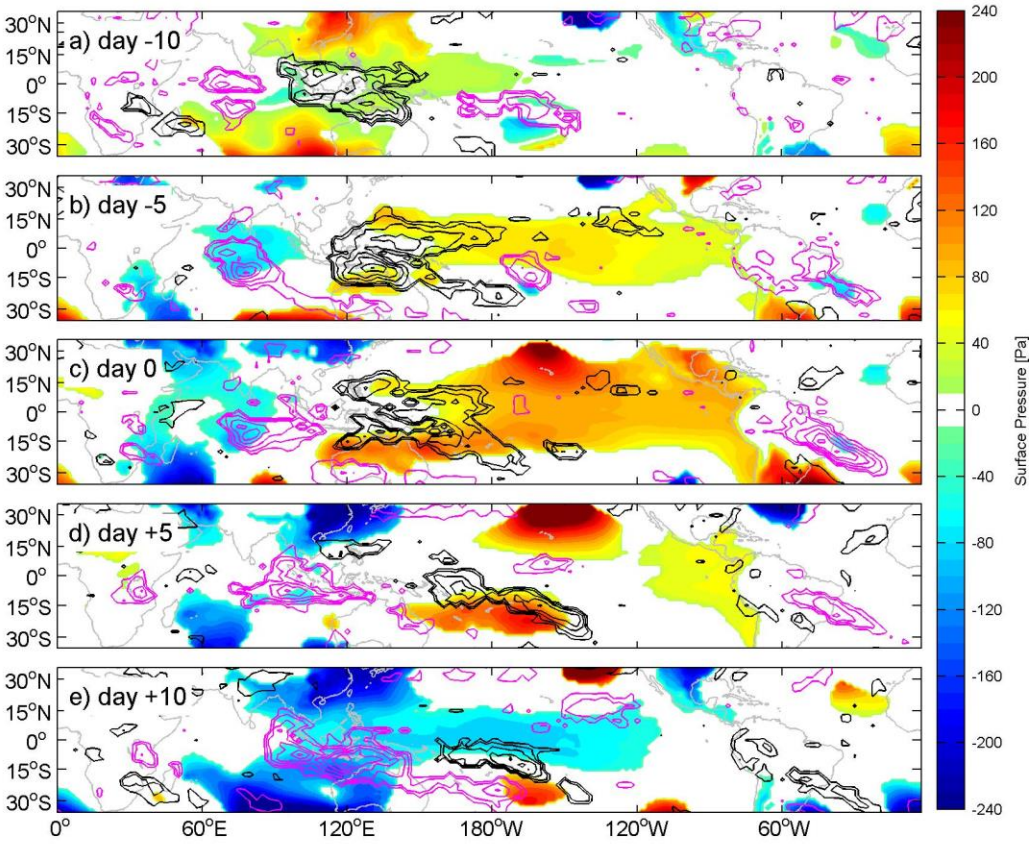

Figure 4.8: Same as Figure 4.3 but for MJO events preceding the SACZ.

Convection in the SACZ peaks at day 0 while strong surface pressure anomalies are present over the Pacific. Intense positive pressure anomalies appear over South America south of 15ºS. This feature is observed in all cycles and indicates the equatorward propagation of a surface anticyclone following the passage of a cyclonic disturbance.

The influence of high-frequency synoptic disturbances on SACZ convection was discussed before by several studies [Cavalcanti and Kayano, 1999; Siqueira and Machado, 2004; Cunningham and Cavalcanti, 2006; Raia and Cavalcanti, 2008]. Cunningham and Cavalcanti [2006] suggested that the SACZ would develop whenever the intraseasonal signal and the high-frequency extratropical wave train become in phase. The evolution of the extratropical intraseasonal anomalies associated with the MJO

preceding the SACZ (Figure 4.4p-t) suggests that this phase locking occurs very late in the life cycle (Figure 4.4r), probably due to the small lead-lag relationship between the MJO and the SACZ. In the next section a dynamical explanation for the association of extratropical disturbances and the SACZ will be proposed.

Negative Zonal Stretching Deformation and Synoptic Disturbances

During summer, over South America and the adjacent Atlantic Ocean south of 20ºS there is a region of upper-level negative zonal stretching deformation that coincides with the climatological position of the SACZ subtropical extension (Figures 4.1a,c). The same feature is observed in the SPCZ, where this region of negative zonal stretching deformation acts to increase wave energy density and boost convection [Widlansky et al., 2010]. Figure 4.9 display intraseasonal OLR composites on day 0 for all identified SACZ and for the other three SACZ categories described in the previous section with color shadings representing unfiltered 200 hPa zonal stretching deformation anomalies. In all cases, significant negative stretching deformation anomalies are observed off eastern Brazil, coinciding with the extension of deep convection over the Atlantic Ocean. The anomalies are stronger for the few cases when the MJO precedes the SACZ and in all cases the zonal stretching deformation minimum is located to the east of the convective maximum. The northwest-southeast orientation of the stretching deformation minima suggests a local increase of energy density, promoting the convective extension of the SACZ over the adjacent South Atlantic Ocean.

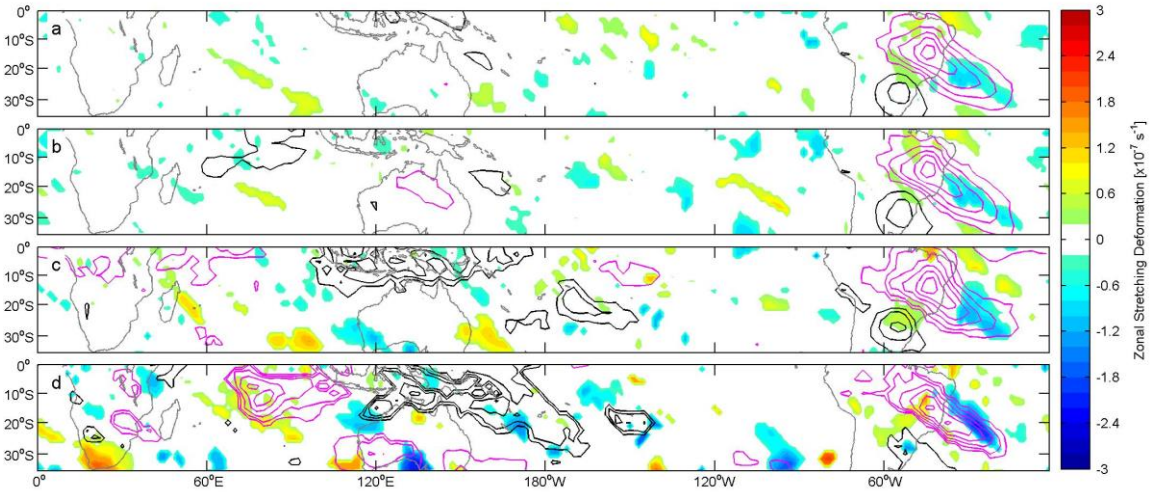

Figure 4.9: Intraseasonal OLR anomalies (contours) and zonal stretching deformation (shading) for composite day 0 of (a) all identified SACZ events; (b) MJO-independent SACZ; (c) SACZ events preceding the MJO; and (d) MJO preceding the SACZ. OLR contours are plotted at 5 W m^{-2} intervals (zero contour omitted). Only values significant at 95% are shown.

The behavior of high-frequency synoptic disturbances in the SACZ is displayed on Figure 4.10 using OLR 3-6-day filtered OLR and zonal stretching deformation anomalies relative to minima below -1 standard deviation at 24^{o}S, 45^{o}W. From 1979 to 2011, this method identified 462 high-frequency minima below -1 standard deviation, each representing the presence of a synoptic disturbance nearby the SACZ. This estimate results in an average of approximately 14 disturbances per season with a recurrence period of around 12 days. Previous studies have estimated higher numbers of surface cyclones propagating along the coast. Less conservative estimates found as much as 47 systems per summer [Gan and Rao, 1991]. Their criteria for cyclone identification are: (1) at least one closed isobar (at 2 hPa intervals) around a surface low pressure and (2) the low pressure must persist for at least 4 days. On the other hand, Garreaud and Wallace [1998] used OLR anomalies along 60^{o}W to estimate the frequency of convective anomalies associated with summertime midlatitude air incursions over South America and found recurrence periods between 7 and 12 days. Thus, the identification of synoptic systems presented here agrees well this more conservative estimate, at least with respect

to the frequency of occurrence of the disturbances. In any case, it is clear that not all synoptic disturbances trigger an SACZ during summer.

Negative stretching deformation anomalies are present over the SACZ climatological position ahead of weak negative OLR anomalies two days before the convective maximum (Figure 4.10). As the high-frequency system propagates along the coast, both stretching deformation and OLR anomalies intensify, always with negative stretching deformation leading negative OLR anomalies. Moreover, the zonal extension of the anomalies to the northeast of the SACZ climatological position is smaller than the zonal extension observed to the southwest, indicating a decrease in longitudinal scale as the disturbances propagate across the SACZ and veer northeastward.

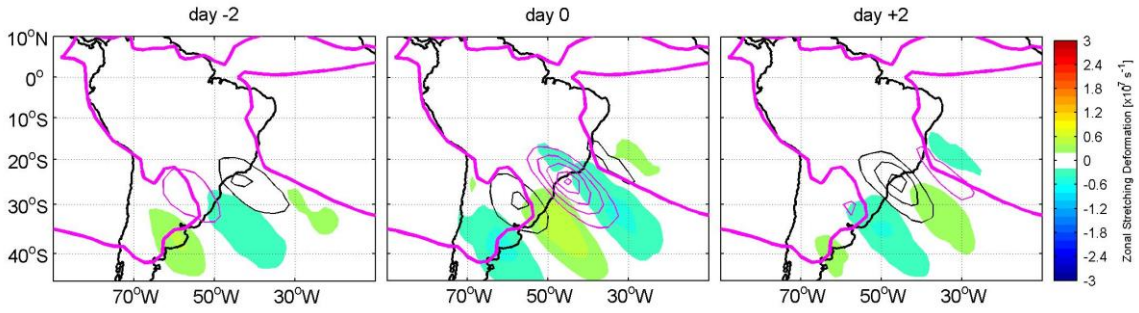

Figure 4.10: High-frequency 3-6-day composite cycle relative to minima OLR below -1 standard deviation at 25ºS, 45ºW. Thin black (magenta) lines represent positive (negative) OLR anomalies at 5 W m^{-2} intervals. Thick magenta lines indicate October-March mean -245 W m^{-2} and it is used as a reference for the climatological SACZ position. No significance test applied.

From all 113 identified SACZ events, 70% (80) occurred with a synoptic system within the climatological bounds of the SACZ, leading the convergence zone convective maximum by an average of 3 days (Table 4.2). Slightly higher percentages of SACZ events associated with synoptic disturbances are found for cycles somehow associated with the MJO (MJO preceding SACZ and SACZ preceding the MJO, with 77% and 75% respectively).

The high percentage of SACZ events observed during the passage of a strong high-frequency disturbance suggests that summertime cold fronts are not only a fundamental dynamic component of the SACZ development, but that these synoptic systems are usually more intense (OLR minima exceeding -1 standard deviation) when the SACZ is triggered. This fact does not necessarily mean that SACZ formation requires the passage of an intense synoptic disturbance through the region. Note that 30% of all SACZ events still form without the presence of a strong frontal system. However, on the high-frequency composite cycle (Figure 4.10), the negative OLR anomalies are not particularly strong on day -2 but they reach -25 W m^{-2} on composite day 0.

Table 4.2. Number of high-frequency (3-6-day) disturbances identified by OLR minima below -1 standard deviation at 25ºS, 45ºW. The lag refers to the number of days the high-frequency synoptic disturbance was observed before the SACZ (SACZ lags the high-frequency).

	Number of events	**Concurrent with synoptic systems**	**Average lag (days)**
MJO leading SACZ	9	6	3
ED leading SACZ	2	1	4
EI leading SACZ	2	1	3
SACZ leading MJO	24	18	3
SACZ leading ED	7	5	1
SACZ leading EI	4	2	3
Independent	63	47	3
Total	113	80	-

The composites on Figure 4.10 are calculated based on all identified high-frequency events. In order to further confirm the behavior of these synoptic systems during observed SACZ events, two distinct composite cycles are calculated based on the two most frequent categories of SACZ events (Table 4.2): (1) independent SACZ, and (2) SACZ leading the MJO. Composite day 0 is defined by the high-frequency OLR

minimum observed at 25ºS, 45ºW correspondent with the concurrent synoptic system indicated on Table 4.2. Therefore, in both cases, high-frequency composite day 0 occurs 3 days before maximum intraseasonal SACZ convection.

Both MJO-independent SACZ events (Figure 4.11) and SACZ events leading the MJO (Figure 4.12) display a synoptic disturbance at day 0 with significant negative zonal stretching deformation anomalies ahead, in a very similar pattern to the one displayed on Figure 4.10. Two days later (one day prior to maximum SACZ convection), high-frequency negative OLR anomalies have propagated eastward, weakened, and their longitudinal extent have clearly decreased. Positive OLR anomalies are centered over the climatological SACZ, indicating clearer skies associated with colder air and higher pressures trailing the passage of the initial frontal system. Meanwhile, a subsequent disturbance is ready to enter the SACZ domain. A secondary system, weaker compared to the first, moves into the SACZ region between days +2 and +4, when intraseasonal convection is maximum.

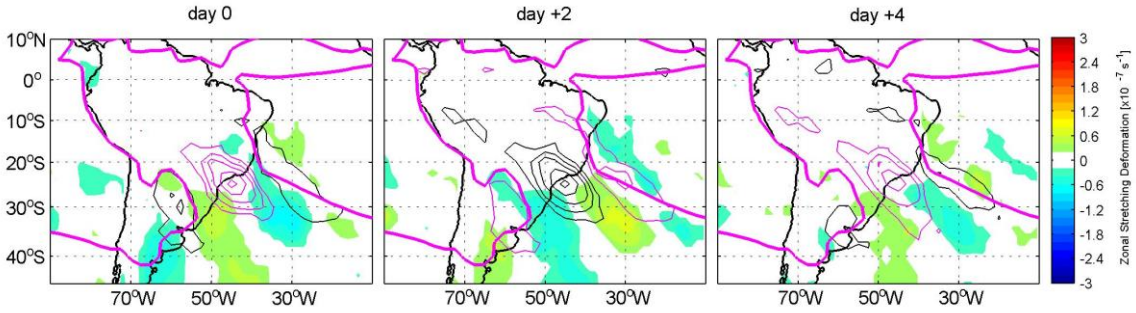

Figure 4.11 Same as Figure 3.8 but for composite days 0, +2, and +4 of high-frequency disturbances concurrent with MJO-independent SACZ events (Table 4.2). Here, only significant anomalies at 90% are shown.

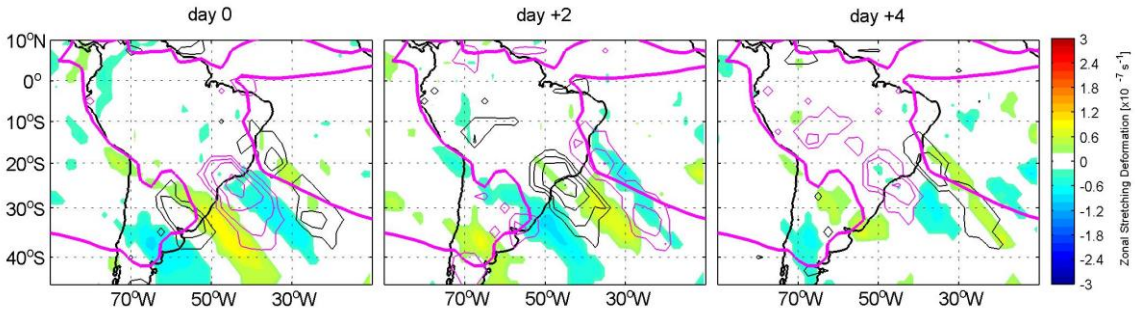

Figure 4.12 Same as Figure 4.10 but for SACZ events preceding the MJO (Table 4.2).

Time-longitude diagrams for these two high-frequency composite cycles (Figures 4.13 and 4.14) are used to estimate period, phase speeds, and longitudinal wavelengths of synoptic disturbances associated with the SACZ. Garreaud and Wallace [1998] identified bands of enhanced convection moving from midlatitudes (40°S to 35°S) into the tropics (as far as 5°S) in around 5 days, at average speeds of approximately 10 m s^{-1}, and longitudinal scales of about 3,000 km.

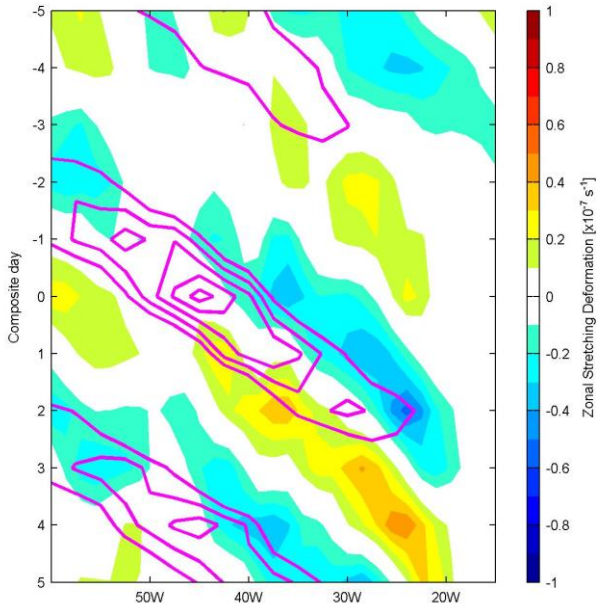

Figure 4.13: Time-longitude composite cycle at 25°S for synoptic disturbances associated with MJO-independent SACZ events. Magenta contours indicate negative OLR anomalies at 5 W m^{-2} intervals.

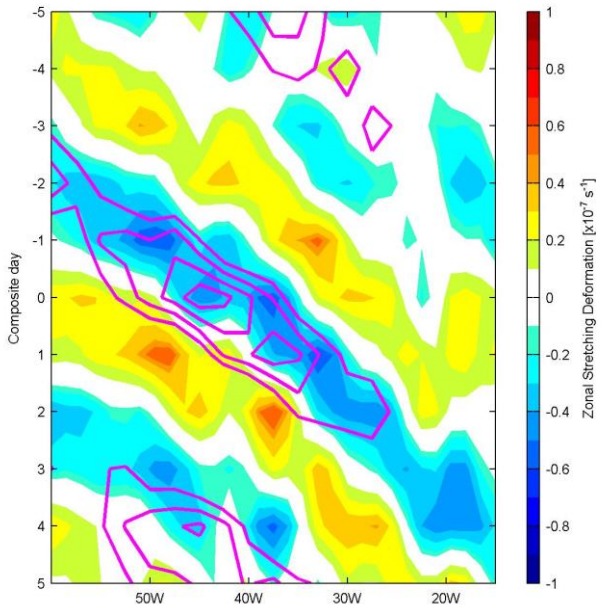

Figure 4.14: Same as Figure 4.13 but for synoptic disturbances associated with SACZ events preceding the MJO.

Based on Figure 4.13, the propagation speed of negative OLR anomalies during MJO-independent SACZ events seems to be nearly constant from around day -2 to day +2, immediately before the intraseasonal maximum in convection. Zonal stretching deformation, on the other hand, indicates the existence of two regimes. The first, west of 45^{o}W, with zonal phase speeds of approximately 12 m s^{-1} from day -2 to 0. East of 45^{o}W, the phase speed slows down to 7 m s^{-1} after day 0. The longitudinal wavelength on day 0, based on zonal stretching deformation, is near 4,400 km, decreasing to approximately 2,800 km on day +2. Synoptic disturbances propagating through the SPCZ exhibit similar behavior, with phase speeds and wavelength decreasing from 15.2 m s^{-1} to 7 m s^{-1} and 5,800 km to 2,700, respectively, between days -2 and 0 [Widlansky et al., 2010].

The high-frequency cycle associated with SACZ events preceding the MJO is clearer, with shorter, slower, and convectively weaker disturbances. Zonal stretching deformation anomalies indicate that, west of 45^{o}W, the mean phase speed is around 8 m s^{-1} with the wavelength decreasing from 3,200 km to 1,600 km from day-2 to day 0. East

of 45^{o}W, the mean phase speed drops to 4.6 m s^{-1} and the wavelength further decreases to 1,200 km from day 0 to day +2.

Conclusions

Even though all categories of intense SACZ are related to large-scale wave signatures of intraseasonal variability over the tropical Indian and West Pacific Oceans, the strongest SACZ convection is associated with the MJO. More specifically, these SACZ events occur during convective breaks preceding an MJO convective phase. Around 46% of all MJO identified on chapter 2 occur a few days after an intense SACZ. Thus, the identification of a robust break in intraseasonal convection over the tropical Indian and Pacific Oceans together with the occurrence of an intense SACZ may be useful to predict the formation of an MJO.

This chain of events is not merely statistical. First, previous studies have argued that negative SLP anomalies propagating eastward as equatorial Kelvin waves are delayed by mountain ranges but are able to circumnavigate the globe to trigger the following MJO convective cycle [Matthews, 2000]. Others have proposed that the Kelvin waves do not overcome mountain barriers, but easterly anomalies linked to Kelvin waves blocked to the west contribute to the development of deep heating anomalies on the windward side of the Andes and the East African Highlands [Hsu and Lee, 2005]. Under this point of view, the Kelvin wave would not able to circumnavigate the global tropics, but the signal is transmitted as a series of Kelvin waves. Although the results on this chapter are not able to confirm neither of these two hypotheses, negative pressure and OLR anomalies over the Atlantic basin during the active SACZ phase do precede the growth of same sign significant anomalies over the eastern Indian Ocean, east of the African Highlands (Figure 4.5). Thus, independent of the mechanisms of propagation, significant anomalies are propagating eastward around the tropics and the same negative

anomalies linked to intense SACZ convection may help to initiate the subsequent MJO convection over the Indian Ocean.

Second, previous studies suggest the existence of wave-like connection between the SPCZ, the SACZ, and the western Pacific on intraseasonal time scales, with the SACZ convection triggering a wave train through the Northern Hemisphere [e.g. Grimm and Silva Dias, 1995]. The composite sequence of intraseasonal upper-level geopotential anomalies presented on Figure 4.4k-o and associated with SACZ events preceding the MJO shows a relatively weaker wave train, apparently excited by the strong dipole over the South Atlantic generated by SACZ convection, propagating towards the eastern Indian Ocean (Figure 4.4n). Therefore, it is possible that extratropical anomalies triggered by SACZ convection affect the tropical intraseasonal cycle over the Eastern Hemisphere.

The method used to separate SACZ categories relative to their lead-lag relationship with strong intraseasonal modes of the tropical Indian and West Pacific Oceans identify a few cases in which the MJO precedes SACZ convection by a few days. The most striking feature of this composite cycle is the absence of significant negative pressure anomalies over the Atlantic basin before SACZ formation (Figure 4.8a,b). It is important to note that the cycle indicates the eastward propagation of Kelvin waves across the Pacific in a similar way as all other cycles. Another distinguished feature is that the SACZ convective band is more sharply defined in these cases (the gradient of negative OLR anomalies is stronger when compared to the other SACZ convective bands – Figure 4.9). This particular characteristic suggests that synoptic transients are able to trigger SACZ convection even when tropical intraseasonal connections are not significant east of the Andes.

The importance of extratropical disturbances for the formation of the SACZ has been recognized by previous studies. For instance, Nieto-Ferreira et al. [2011] suggested that the increase in anticyclonic shear in the northward side of the subtropical jet over

South America induces a change in extratropical system's behavior, causing them to thin and tilt westward and triggering the formation of the first SACZ of the season. Others have speculated that two distinct wave trains, one on synoptic and another on intraseasonal time scales, become in phase over South America, allowing the formation of the SACZ [Cunningham and Cavalcanti, 2006]. The motivation for this chapter is to demonstrate that a region of climatological negative zonal stretching deformation coincides with the mean SACZ position and is important to accumulate high-frequency wave energy and deepen convective activity over the South Atlantic Ocean during intense SACZ events. The impact of wave accumulation is also observed in the SPCZ [Widlansky et al., 2010] and it is significant for all strong SACZ cases investigated here. Even when the SACZ is not linked to the MJO or any other mode of strong intraseasonal convection over the warm pools of the Eastern Hemisphere, negative zonal stretching deformation anomalies are observed ahead of synoptic disturbances propagating equatorward along the eastern South American coast.

Although the results presented here do not reject other mechanisms for the SACZ formation, evidence is presented to support the idea that the accumulation of wave energy are important, at least, for the intensification of convective activity over the adjacent Atlantic Ocean, contributing to the subtropical extension of the SACZ. Both anticyclonic shear and negative zonal stretching deformation depend upon the establishment of the upper-level Bolivian High. The growth of this anticyclone alters the wind patterns and the subtropical jet over South America increasing both anticyclonic shear on the equatorward side of the jet and negative zonal stretching deformation as it enhances convergence in the jet exit region. Hence, both mechanisms can act in concert to promote favorable conditions for the triggering of the SACZ by synoptic systems. With stronger negative zonal stretching deformation over the Atlantic Ocean, high-frequency disturbances become more efficient in tapping southward moisture influx from the Amazon, strengthening convection over the region.

Composite cycles for MJO-dependent and MJO-independent SACZ events indicate that an upper-level wave train on intraseasonal time scales appears to become more organized and similar to PSA waves as intraseasonal Kelvin waves propagate cross the tropical Pacific. On the other hand, high-frequency disturbances propagating equatorward along the eastern South American coast seem to be very common, even during summer. Thus, the suggested phase locking between the two wave trains apparently occurs whenever tropical waves are able to interact with the extratropics. The formation of the upper-level intraseasonal dipole as a consequence of SACZ convection, with negative anomalies centered at 30^{o}S and positive anomalies to the south, indicate more favorable conditions for baroclinic developments over the region once it is indicative of decreased zonal winds. This configuration may contribute to amplify synoptic disturbances further during the SACZ convective phase and the presence of an intense high-frequency system in the region 3 days prior to maximum SACZ convection does not appear to occur by chance.

Last, high-frequency disturbances present during MJO-dependent and MJO-independent cycles possess distinct propagation characteristics. Systems associated with SACZ events preceding the MJO seem to be more intense, with stronger negative zonal stretching deformation anomalies suggesting a more important role for wave accumulation mechanisms. Furthermore, these high-frequency transients are apparently shorter and slower than their MJO-independent counterparts. A comparison of Figures 4.4g (for MJO-independent) and 4.4l (for MJO-dependent) indicate that the geopotential anomalies are stronger for SACZ events preceding the MJO, especially the ones forming the upper-level dipole along the eastern South American coast. These intraseasonal meridionally-oriented dipoles on intraseasonal time scales are usually present in jet exit regions indicating strong variations of zonal winds [e.g. Blackmon et al., 1984]. The higher-amplitude anomalies associated with MJO-dependent life cycles indicate sharper

deceleration of the subtropical jet, explaining the slower, shorter, and more intense anomalies observed in this case.

CHAPTER 5

SUMMERTIME LONG-TERM RAINFALL VARIATIONS AND THE SACZ

The SACZ interannual variability is characterized by variations in position and intensity [Barros et al., 2000; Doyle and Barros, 2002]. The stationary Rossby wave structure of intense SACZ events also modulates precipitation anomalies to the south, over the subtropical plains of southern Brazil, Uruguay, and northern Argentina [Robertson and Mechoso, 2000] and this variability has been associated with variations in extratropical wave activity [Liebmann et al., 1999]. Although some studies describe an important impact of ENSO phase on the SACZ [e.g. Carvalho et al., 2002], there are also some indication of independence between SACZ interannual variations and ENSO, with interdecadal variations apparently more consistent with SST variability in the South Atlantic [Robertson and Mechoso, 2000].

Trends and interdecadal cycles of precipitation and streamflow are ubiquitous over South America [Genta et al., 1998; Robertson and Mechoso, 1998; Marengo et al., 1998; Rusticucci and Penalba, 2000; Marengo, 2004]. The focus here, though, is on long-term variations of rainfall in the vicinity of the SACZ, where the intraseasonal signal is stronger. More intense and frequent rainfall events south of the climatological SACZ have been associated with variations of the South Atlantic high pressure center [Liebmann et al., 2004] and to more frequent El Niño conditions [Haylock et al. 2006]. Liebmann et al. [2004] suggested that a southward shift of the SACZ from 1976 to 1999 could be caused by a weakening of the South Atlantic subtropical high pressure system

and discarded ENSO influences on observed trends due to a lack of significant correlation between January-March rainfall trend over southern Brazil and Niño 3.4 SST anomalies. However, Liebmann et al. [2004] did identify correlations between January-March precipitation and South Atlantic SST anomalies, with SST lagging precipitation by one month. On the other hand, Haylock et al. [2006] found canonical correlation patterns between annually averaged Pacific Ocean SST and several rainfall indices over South America from 1960 to 2000 and hypothesized that a shift to more El Niño-like conditions may have caused these changes. They also reported a secondary mode of long-term dry tendencies in southern Chile that would be connected to a weakening of the South American continental trough that forced a southward shift of the storm tracks.

The dispute of whether long-term variations of rainfall in the vicinity of the SACZ are related to the South Atlantic or the Pacific variability also extends to the debate about the drivers of interdecadal cycles over the region. Atmospheric response to interdecadal basin-wide variations in Pacific SST may interact with ENSO-related anomalies to alter teleconnections towards South America. When an El Niño occurs during a positive phase of the PDO, teleconnections between the Pacific basin and South America seems to be intensified [Kayano and Andreoli, 2007]. Strong El Niños suppress convection over northern Amazon [Liebmann and Marengo, 2004] and displaces the subtropical jet to the east, forcing the SACZ to form over the Atlantic Ocean [Carvalho et al., 2002]. However, recent observations of a tendency of more frequent central Pacific warming events are associated with weaker rainfall anomalies over Brazil [Hill et al., 2011]. Regarding the role of Atlantic SST anomalies over long-term variations of the SACZ, Chaves and Nobre [2004] and Almeida et al. [2007] argue that warm South

Atlantic SST anomalies actually intensify the SACZ and that cold SST anomalies concurrent with strong SACZ events are generated after an initial atmospheric response to positive SSTs. Moreover, on interannual time scales, an intense northward-shifted SACZ accompanied by reduced precipitation over southern Brazil and Uruguay are related to cold Atlantic SST anomalies south of 20^{o}S and west of 30^{o}W [Barros et al., 2000; Doyle and Barros, 2002]. These observations between Atlantic SST anomalies and South American rainfall are similar to the correlations found by Liebmann et al. [2004], with SST lagging rainfall by one month.

So far, the mechanisms driving long-term variations of the SACZ remain unclear. In particular, the relative roles of Pacific and Atlantic SST anomalies in determining the SACZ position and intensity are not settled yet. The main goal of this section is to describe and explain how low-frequency variability of precipitation in the SACZ region was forced during the last three decades, focusing on the respective roles of SST and SLP anomalies over the Atlantic and the Pacific basins. In the previous chapter, the formation and structure of intense SACZ events was linked to extratropical activity propagating eastward from the Pacific basin. This is the basis of the present hypothesis: long-term trends in SACZ convection are more strongly influenced by Pacific SST trends through extratropical teleconnections that modulate the see-saw pattern of variability between the SACZ and the subtropics to the south.

Precipitation Trends from 1979 to 1999 over South America

January to March trends from 1979 to 1999 are evaluated using monthly data from the Global Precipitation Climatology Project (GPCP) [Adler et al., 2003], Extended Reconstructed SST (ERSST) version 3b, NOAA OLR [Liebmann and Smith, 1996], and ERA-Interim reanalysis data [Dee et al., 2011]. The period is chosen to facilitate a comparison with Liebmann et al. [2004] and Haylock et al. [2006] but a more thorough

examination is performed later on. Although the increase frequency of extreme events is an important component of the trends presented in previous studies, the main goal is to identify the origins of the long-term variations. Thus, only linear trends estimated by a least-square method are inspected here. Trend significance at 0.05 significance level is assessed by a Mann-Kendall test.

Significant summer precipitation trends are observed over South America (Figure 5.1a) and display a spatial pattern similar to that shown by Liebmann et al. [2004]. The apparent southward shift of the SACZ is characterized by negative rainfall trends to the north and positive trends to the south of the SACZ climatological position. Furthermore, there are significant positive trends in mean SLP over southern South America east and west of the Andes (Figure 5.1b) and in 200 hPa geopotential off eastern Brazil (Figure 5.1c). The large-scale patterns associated with this anticyclonic tendency are very similar to that presented by Grimm et al. [1998] for the spring of three El Niño events (1979, 1982, and 1986).

Summer South Atlantic SST has increased during this period off eastern Brazil, in a region commonly covered by SACZ convective clouds (Figure 5.1d). Liebmann et al. [2004] attributed this positive SST trend to short wave radiational forcing caused by the SACZ southward migration. Doyle and Barros [2002] hypothesized a positive feedback in which positive SST anomalies generated under weak or absent SACZ episodes are advected to the south by the Brazil current. Warmer SST to the south would favor rainfall over southern Brazil and Uruguay, perpetuating the cycle. On the other hand, Chaves and Nobre [2004] and Almeida et al. [2007] argue that warm south Atlantic SST anomalies actually intensify the SACZ. Under this point of view, cold SST anomalies that seem to favor strong SACZ events are a response to strong convection and not the cause. Long-term weakening of the SACZ and local SST warming suggests that the observed South Atlantic SST trends do not favor stronger SACZ events. The warm SST anomalies seem to be a product of the weaker and southward-shifted SACZ.

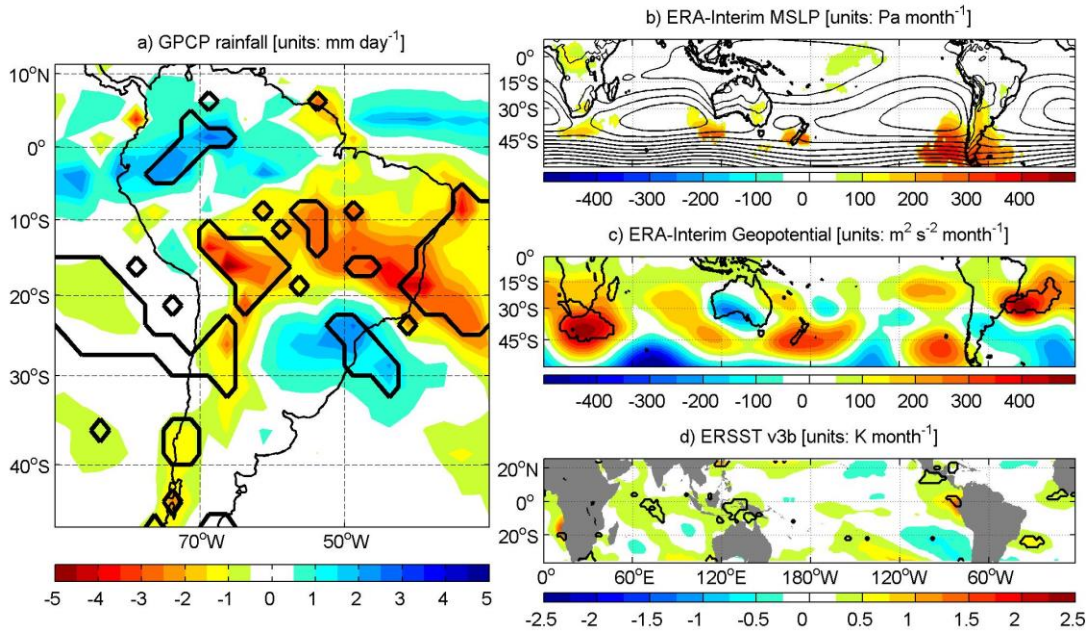

Figure 5.1: Linear trends from 1979 to 1999. (a) GPCP monthly precipitation. (b) ERA-Interim mean sea level pressure. (c) ERA-Interim 200 hPa geopotential. (d) NOAA ERSST. Think black contours in (a), (c), and (d) indicate values significant at 0.05. Contours in (b) represent climatological values of JFM mean sea level pressure. Only values significant at 95% are display in (b).

Liebmann et al. [2004] reported a lack of correlation between precipitation trends over South America and Niño 3.4 index, probably caused by the location of tropical Pacific SST trends. Small but significant SST warming is also observed in the equatorial eastern Pacific off South America and concentrated in Niño 1+2 region and the hypothesis of Pacific forcing of South American rainfall trends should not be dismissed. In addition, significant upward trends in 200 hPa geopotential off eastern Brazil (Figure 5.1c), indicating a significant anticyclonic trend in upper-level winds, further supports the idea of more El Niño-like influence on South American climate. This type of response is usually present over the region during the spring prior to El Niño events because background spring conditions are more favorable for teleconnection, while the summer season is more influenced by local land-atmosphere feedbacks. However, in the long-term, the significance of the upper-level anomaly may indicate that the eastern Pacific warming is important in driving the observed rainfall changes during the period.

Accordingly, mean SLP trends do not support a weakening of the South Atlantic subtropical high during the period (Figure 5.1b). In fact, SLP trends support the idea that the observed rainfall trends are a result of remote forcing. There is a tendency of higher SLP along the eastern slopes of the Andes Mountains that can be interpreted as a tendency of intensified northward cold air incursions associated with synoptic systems. Although stronger cold air incursions do not seem correlated with ENSO on interannual time scales [Seluchi and Marengo, 2000], upward trends in mean SLP over Argentina may reflect an increase in baroclinic developments and northward transport of colder air favored by ENSO teleconnections on the long run. West of the Andes, SLP anomalies present sharper positive trends off southern Chile. The combination of these SLP trends off Chile and significant dry tendencies over the Chilean coast from approximately 32^{o}S to 40^{o}S, resemble a pattern usually observed during El Niño events [Montecinos and Aceituno, 2003] and noted by Haylock et al. [2006] as a secondary pattern in canonical correlations with Pacific SSTs.

Pezza et al. [2007] detected significant increase in synoptic system strength along the southern Brazilian coast from the late 1970s to the late 1990s, with a decrease between 1997 and 2001. They related these changes to PDO variability. According to Kayano and Andreoli [2007], El Niño teleconnections are stronger during warm PDO regimes. A warm, or positive, PDO phase was active from 1976 until the mid to late 1990s, when a possible shift took place (Figure 5.2) [Bond et al., 2003; Peterson and Schwing, 2003]. Hence, the combination of all these observations, from independent datasets and using different variables, indicates that trends in South American rainfall during the 1979 to 1999 period are more strongly related to a tendency toward more El Niño-like conditions in the eastern tropical Pacific Ocean combined with a robust positive PDO phase initiated in the mid-1970s. ERA-Interim data does not support a strengthening of the South Atlantic high pressure and this is in agreement with Venegas

et al. [1996] description of a 15-year oscillation in South Atlantic SLP and SST that does not exhibit a noticeable trend during the same period analyzed here.

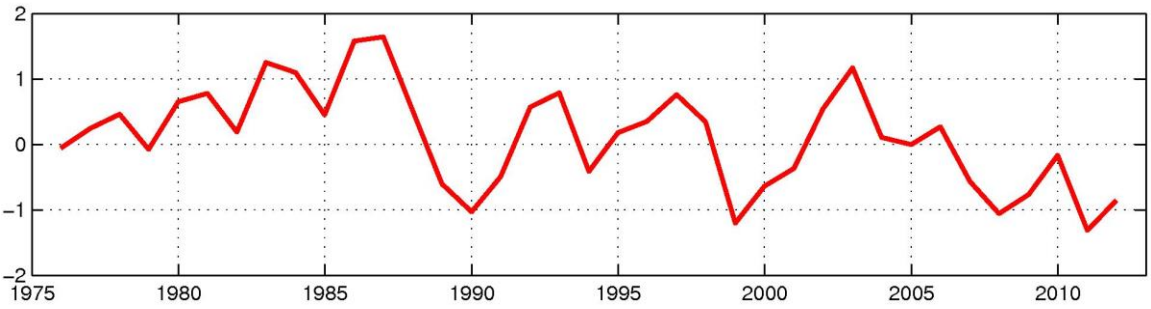

Figure 5.2: Average January to March PDO index obtained from the Joint institute for the Study of the Atmosphere and Ocean, University of Washington, calculated as standardized values of the leading PC of monthly SST anomalies in the Pacific Ocean north of 20°S [Mantua et al., 1997].

Precipitation Trends after 1999 over South America

From 1999 to 2011 there is a general absence of significant summer rainfall trends over the South American continent (Figure 5.3a). Tropical Pacific SST trends after 1999 are positive (but not significant) over the central part of the basin and there is no significant SST trend in the Niño 1+2 region (Figure 5.3d). The lack of Pacific SST trends indicates that the tendency of more eastern Pacific El Niño-like conditions have weakened during the last decade leading to a leveling off of rainfall anomalies over South America.

The PDO index also oscillates after 1990 (Figure 5.2) and there is a debate of whether or not a regime shift in the Pacific basin took place during the late 1990s [Bond et al. 2003; Peterson and Schwing 2003]. Nonetheless, a band of negative SST trends extending southeastward from the Maritime Continent to 120°W agrees with the hypothesis of a shift in the PDO regime from a warm to a cold phase. The leveling off of tropical Pacific SST trends after 1999 coincide with substantial changes in upper-level circulation with a widespread downward tendency of 200 hPa geopotential south of 15°S, even though this decrease is significant only southeast of Africa and in the Southeast

Pacific. The period is also marked by a hiatus in the increasing trend of global surface temperatures that has been recently linked to interdecadal ENSO-like variations in Pacific SST [Collins et al., 2013]. There are no significant trends in upper-level geopotential near the SACZ region. The wave train structure linking the Pacific to South America is not apparent anymore, possibly due to a lack of significant SST anomalies in the tropical Pacific Ocean. Positive SLP trends are not observed in the Atlantic sector or over South America. The configuration of trends after 1999 reinforces the hypothesis that long-term variability of rainfall in the SACZ region is associated with SST variations in the tropical Pacific basin. Stronger teleconnection patterns related to El Niños and positive PDO phases tend to increase rainfall south of the SACZ, decreasing precipitation to the north.

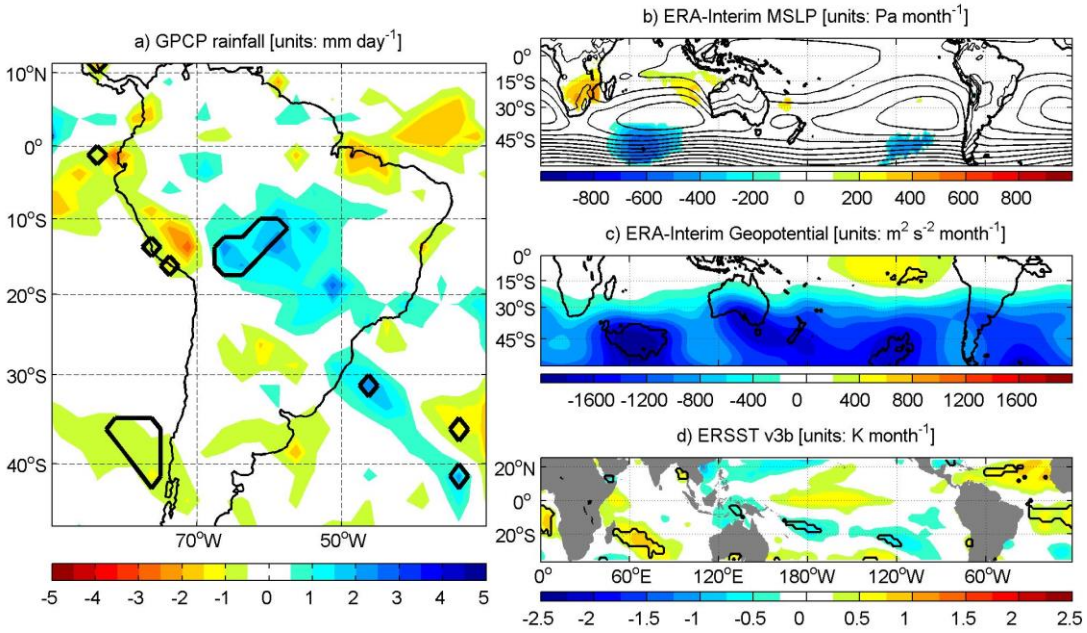

Figure 5.3: Linear trends from 1999 to 2011. (a) GPCP monthly precipitation. (b) ERA-Interim mean sea level pressure. (c) ERA-Interim 200 hPa geopotential. (d) NOAA ERSST. Think black contours in (a), (c), and (d) indicate values significant at 0.05. Contours in (b) represent climatological values of JFM mean sea level pressure. Only values significant at 95% are displayed in (b).

Submonthly variability

The pattern in upper-level geopotential trends (Figure 5.1c) resembles that of submonthly (10-30-day) perturbations leading SACZ episodes [Liebmann et al. 1999] but

with opposite sign. More specifically, positive geopotential and upper-level anticyclonic trends suggest a decrease in SACZ intensity [Robertson and Mechoso 2000]. Liebmann et al. [1999] showed that SACZ convection tends to be enhanced along the edge of upper-level troughs reaching the region from the extratropics. If the upper-level trends in Figure 5.1c are related to extratropical waves propagating from the Pacific and bending towards the equator along eastern South America, it seems reasonable to expect that upper-level trends are possibly indicating changes in submonthly variability of the SACZ.

The extratropical wave train pattern observed in Figure 5.1c is not significant over the South Pacific. However, concurrent SST warming in the eastern tropical Pacific and the weakening and southward shift of rainfall anomalies over eastern Brazil indicates that similarities with the see-saw pattern of wet and dry conditions over eastern South America, as described by Nogués-Paegle and Mo [1997], are not coincidental. The significance of upper-level trends in the vicinity of the SACZ may be explained by the fact that summertime regional circulation over South America is dominated by a stationary Rossby wave structure modulated by high-frequency transients [Robertson and Mechoso, 2000]. Therefore, small perturbations in high-frequency activity may be translated in significant changes in the dominant stationary wave pattern in the long term.

The first EOF of summer daily OLR (Figure 4.1a) used to identify strong SACZ events (Chapter 3) is now used to investigate the hypothesis that long-term changes in the SACZ are related to extratropical wave activity. Figure 5.4 shows the average summer spectra of the SACZ time series for three different periods (1979-1990, 1990-2000, and 2000-2011). All spectra exhibit power on submonthly time scales (correspondent to periods shorter than 30 days). However, spectra for the two later periods indicate that submonthly and higher frequency phenomena become more important after 1990. At first glance, the increase in submonthly activity, especially during the 1990s, seems to oppose the idea of less active or weaker SACZ from 1979 to 1999. However, our hypothesis is that teleconnections associated with more eastern Pacific El Niño-like conditions from

1979 to 1999 generated upper-level positive geopotential and anticyclonic trends near the SACZ region, favoring baroclinic developments south of the SACZ, once subsidence over the subtropics weakens as SACZ convection decreases. The increasing importance of submonthly variability related to the SACZ appears to be a manifestation of this chain of events: eastern Pacific warming during a positive PDO phase, enhanced teleconnections, upper-level anticyclonic trends off eastern Brazil, and increased baroclinic activity over southern Brazil.

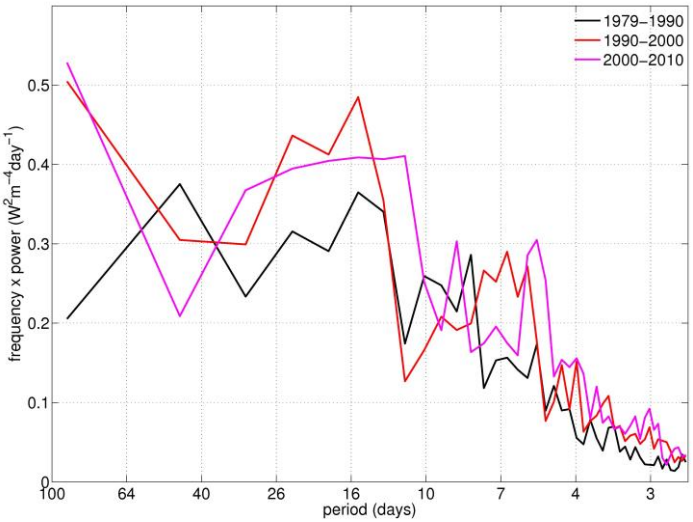

Figure 5.4: Average summer (October-March) SACZ principal component time series variance-preserving spectra for three distinct periods. Note that a 90-day cycle is sampled twice a year.

The ratio of submonthly to 30-90 day variance is smaller in the SACZ region and increases to the south [Liebmann et al., 1999]. Therefore, higher submonthly activity associated with the first EOF pattern after 1990 is possibly highlighting a suppressed or diffuse SACZ accompanied by enhanced convection over the subtropics driven by synoptic disturbances and associated cold fronts. This tendency is further supported by SLP trends observed in Figure 5.1b, as the intrusion of positive SLP anomalies east of the Andes are indicative of more intense or more frequent cold air incursions trailing frontal systems propagating northward over South America. The lack of SLP increases in the Atlantic suggests that there is no significant increase of low-level winds over the basin,

meaning that there is no significant trend in southward moisture transport (assuming that humidity levels have kept the same). Nonetheless, even if humidity availability increases, the results are in agreement with Liebmann et al. [1999] in the sense that submonthly variability of the SACZ is largely independent of southward flow from the Amazon and more strongly linked to the ability of extratropical disturbances to tap the incoming moisture and produce rainfall anomalies.

On the previous chapters, it is hypothesized that negative zonal stretching deformation acts to accumulate energy density that favors the formation of strong SACZ events. The fact that rainfall trends are apparently linked to a tendency of more El Niño-like conditions over the Pacific basin from 1979 to 1999 is further supported by interannual variations of zonal stretching deformation associated with ENSO events (Figure 4.5).

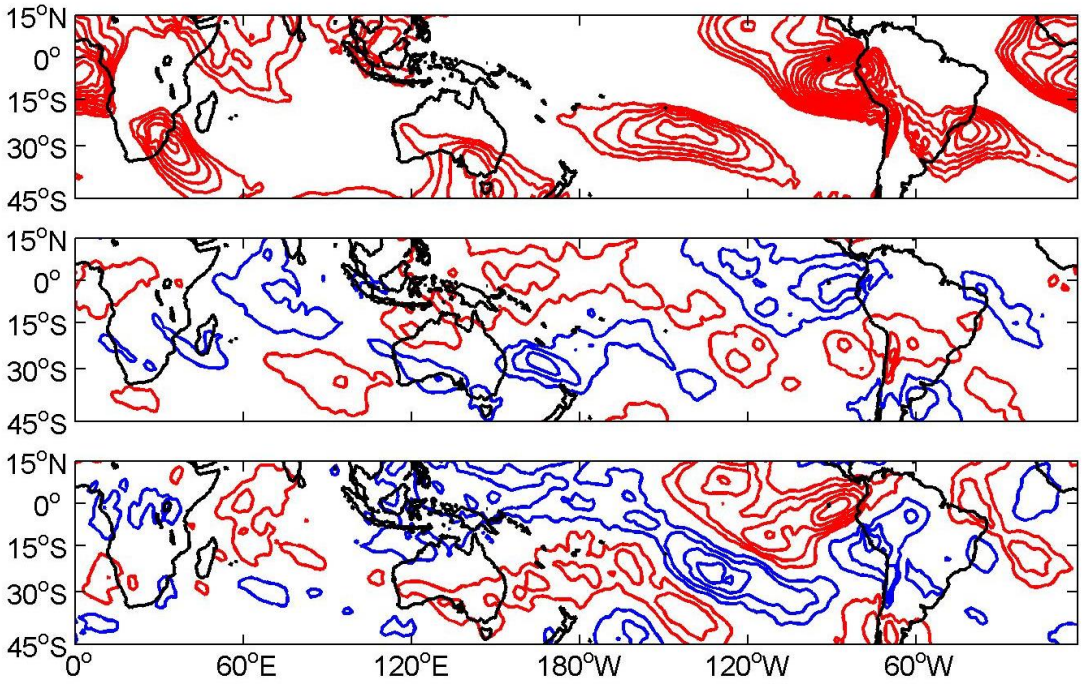

Figure 5.5: Top panel displays climatological values of summer (October to March) negative zonal stretching deformation at 1 x 10^{-6} s^{-1}. Middle panel shows summertime zonal stretching deformation anomalies during El Niño years (1982/83, 1987/88, 1991/92, 1993/94, 1994/95, 1997/98, 2002/03, 2006/07 and 2009/10). Bottom panels shows summertime anomalies during La Niña years (1988/89, 1998/99, 1999/00, 2000/01, 2007/08, 2008/2009, 2010/11).

During El Niño summers, there is a deepening of negative zonal stretching deformation over the South American continent from 15ºS to 30ºS and over the adjacent Atlantic Ocean south of 30ºS and centered at 30ºW. The spatial distribution of these anomalies is in agreement with the southward-shifted SACZ observed from 1979 to 1999, especially because the stronger El Niños were observed before 1999 (1982/83, 1987/88 and 1997/98). La Niña conditions, on the other hand, show stronger negative zonal stretching deformation to the north of the climatological values, with weak positive anomalies to the south-southwest. This pattern possibly indicates conditions closer to average and, hence, the leveling off of rainfall anomalies during the more recent period. It is important to note that most La Niñas took place after 1999, possibly related to the shift in the Pacific Ocean interdecadal cycle.

Conclusions

Recent floods and landslides resulting from strong summertime rainfall in Brazil have raised the question of whether these extreme events were related to long-term trends or cycles in precipitation, particularly those associated with the SACZ. Previous studies showed an increase in mean annual rainfall tied to a summertime increase in frequency of and intensity during the last decades of the twentieth century [Liebmann et al., 2004; Haylock et al., 2006]. Nevertheless, there is no scientific consensus on the origin of these trends and no information about their persistence throughout the first decade of the present century.

Seasonal trends during the last 30 years reveal that the significant tendency for wetter summer conditions to the south of the climatological SACZ occurs during a period of increasingly more active eastern Pacific El Niños from 1979 to 1999. These trends did not persist afterward possibly due to a migration of dominant ENSO-related positive SST anomalies from the eastern to the central Pacific [Kim et al., 2009]. There is evidence that central Pacific warm events produce different spatial patterns in rainfall anomalies over

South America when compared to eastern Pacific El Niños. For instance, the 2002-2003 central Pacific El Niño exhibited a weaker low-level jet east of the Andes and teleconnections that induced less moisture transport to the subtropics when compared to the strong El Niño of 1997-1998 [Silva and Ambrizzi, 2006; Hill et al., 2009]. Furthermore, the 2002-2003 event may have been associated with weaker subsidence over the Amazon [Hill et al., 2011]. Thus, the increasing tendency of more central Pacific El Niños and their distinct impacts over the atmospheric circulation that causes rainfall anomalies over South America can explain the increase in precipitation over the region between 10^{o}S and 20^{o}S observed after 1999.

Liebmann et al. [2004] speculated that a weakening in the South Atlantic subtropical high pressure could abate and drive the southward shift of the SACZ, explaining observed trends in summer rainfall over Brazil from 1976 to 1999. On the other hand, Haylock et al. [2006] identified a relationship between summer rainfall in Brazil and a tendency for more negative Southern Oscillation Index from 1960 to 2000. Reanalysis and SST data support the second hypothesis. Concurrent upward trends in eastern Pacific SST and SLP off Chile reflect a tendency toward more El Niño-like conditions from 1979 to 1999. These changes in the Pacific basin are able to modulate extratropical waves and the alternation between wet and dry conditions over the SACZ region and the South American subtropics east of the Andes. Moreover, this modulation appears to result in increased submonthly variability associated with synoptic activity that favors precipitation over the subtropics.

The progressive increase in submonthly variability associated with the first summer EOF is accompanied by a decrease in spectral power in the low-frequency edge of the intraseasonal band, which corresponds to periods longer than 30 days. This low-frequency band is thought to be associated with the MJO [Nógues-Paegle et al., 2000]. During austral summer, MJO activity was almost uniform from the 1960s to mid-1990s with a decline afterward [Jones and Carvalho, 2006]. Thus, it seems unlikely that the

observed trends in South American rainfall until 1999 can be explained by changes in MJO activity, even though the MJO is also able to modulate the extratropical wave trains linking the Pacific and the SACZ region in a similar way as ENSO [Grimm and Silva Dias, 1995]. In the previous chapter, it was argued that the MJO is important for the SACZ formation, but that high-frequency extratropical transients were fundamental for intense convergence zones over eastern Brazil.

Robertson and Mechoso [2000] argued that interannual variability of the SACZ seems to be largely independent of ENSO. However, Carvalho et al. [2004] and Grimm [2003] showed that ENSO-related variations are important to convective variability in the SACZ and the summer monsoon. On decadal time scales, there is evidence that the PDO acts to enhance ENSO teleconnections toward South America when both cycles are in a warm phase [Kayano and Andreoli 2007]. This association is similar to PDO impacts on ENSO teleconnections in the Northern Hemisphere [e.g. Gershunov and Barnett, 1998]. The PDO presented a well-recognized shift from a negative to a positive phase in 1976-1977 and there is some debate about a PDO phase reversal that took place between 1999 and 2002 [Peterson and Schwing 2003; Bond et al. 2003]. Nonetheless, the lack of consistency of a PDO regime after 1999 may be the cause for the leveling off of rainfall trends near the SACZ due to a change or a weakening of PSA teleconnection patterns.

It is important to note that Pezza et al. [2007] observed more intense cyclones and anticyclones over the southern Brazilian coast during the positive PDO phase and a decrease intensity of the systems afterwards. Negative zonal stretching deformation anomalies during El Niño summers support this idea, considering that the most intense El Niños occurred before 1999 and that El Niños cause an intensification of the negative zonal stretching deformation in the vicinity of the SACZ region. The SACZ spectra, however, indicates that submonthly activity continues to be more important during the 2000-2011 decade compared to the 1979-1999 period, even though only small significant changes in precipitation are observed after 1999. One possible explanation is that the

relaxation of teleconnection patterns in the more recent period, evidenced by the lack of significant upper-level trends and change in the extratropical wave-like pattern, led to a reduction in the depth of synoptic systems propagating through the region. This effect would result in a suppression of rainfall anomalies and trends over southern Brazil. Again, negative zonal stretching deformation anomalies are in line with this idea once most of La Niña events since 1979 took place after 1999 and La Niñas are associated with a weaker negative stretching deformation in the SACZ region. However, a more careful analysis is needed to confirm this speculation.

Precipitation over southern Brazil, Uruguay, and northern Argentina is projected to present more intense or frequent extremes in the future associated with climate change [Marengo et al., 2009]. The amount of water vapor in the atmosphere increases as the climate warms, possibly leading to increased moisture transport from the Amazon basin to the south. Soares and Marengo [2009] argued that the intensification of rainfall extremes over southeastern South America is related to more frequent and intense episodes of the South American low-level jet occurring within global warming scenarios. This hypothesis would be consistent with increasing southward moisture transport. The results presented here, however, suggest that long-term increase in seasonal rainfall associated with a weaker SACZ during the last decades of the twentieth century is strongly tied to synoptic systems activity rather than to the intensification of the low-level jet. The leveling off of precipitation trends after 1999 indicates that, at least for seasonal averages, long-term fluctuations of the climate are more important than continuous linear trends in the last 30 years and projections of future precipitation over the continent should take such variations into account.

CHAPTER 6

CONCLUSION

This thesis aimed to contribute to the understanding of the behavior of the SACZ on a diverse range of time scales in order to pursue an extended-range weather forecast over heavily populated metropolitan areas in Brazil. The hypothesis tested is that the SACZ exhibits strong intraseasonal variations influenced by large-scale modes of variability that would allow enhanced predictability beyond the current numerical weather prediction horizon of around five days. Such predictability is paramount to avoid economic and human losses during SACZ extreme rainfall events, which seem to become more frequent recently.

The most important climate oscillation associated with extended predictability worldwide is the MJO. Waliser et al. [2003] points out that the MJO has been associated with active and breaks of Asian and Australian monsoons, winter rainfall variability over the United States and summertime precipitation over Mexico and South America, favorable conditions to tropical storms and hurricanes in the Atlantic and the Pacific, and even with variations of ENSO. However, the scientific community has adopted a somewhat loose concept of the MJO that are reflected in the indices used to track MJO convection or circulation anomalies across the globe and or in the statistical correlations with weather patterns elsewhere. Therefore, the first task of this thesis was to investigate the main modes of tropical intraseasonal variability and their evolution in order to define the MJO's impact over South American precipitation more adequately.

Chapter 2 presented a simple analysis of the distinct patterns of tropical intraseasonal evolution of convection over the Indian and West Pacific Oceans. It is

demonstrated that nearly half of all October-March intraseasonal events over the warm pools do not exhibit steady eastward propagation across the Maritime Continent. The concern with intraseasonal eastward propagation of tropical convection and related anomalies is justified by the importance of these signals to the convective development to the east of the Andes.

Carvalho et al. [2004] and Jones et al. [2004] showed that the SACZ region tends to experience more extremes in precipitation during an MJO convective break over the eastern Indian Ocean and Maritime Continent. In this case, the relationship is based on statistical correlations. Nonetheless, Souza and Ambrizzi [2006] argue that when the MJO active phase effectively arrives over South America an enhanced convective band spreads from northwest to southeast over eastern Brazil, resembling a slightly northward-shifted SACZ coupled with the ITCZ. The active phase Souza and Ambrizzi refer to is the eastward propagating tropical signal. However, the results presented on chapter 2 suggest that the convective anomalies east of the dateline during the MJO cycle are not necessarily associated with strong intraseasonal events and, therefore, the use of traditional MJO tracking indices are not very useful to extend the limits of prediction of the SACZ. This becomes clear in the intraseasonal composites presented on chapter 3 for different MJO-SACZ events. Although the composites showed the same relationship between the MJO break over the warm pools and South American convection, the convective anomalies east of the break (ahead of the positive-pressure Kelvin wave) are not tied to a previous strong intraseasonal event as defined by the amplitude of the two main tropical EOF patterns of convection. High RMM index amplitudes over the Western Hemisphere and Africa (phase 8 and 1) do not necessarily mean that the MJO active phase is over Africa. More strictly, it is very common that the RMM index exceeding one standard deviation in phases 8 or 1 cannot be related to any kind of strong intraseasonal convection over the Indian or West Pacific Oceans as defined by the main EOF modes.

It is worth noting that the results here do not challenge the notion that upper-level divergent anomalies triggered by strong intraseasonal convection over the eastern Indian Ocean propagating eastward are able to facilitate or excite convective development east of the Andes. The interpretation here is that this is not always the case, especially if one is concerned with extreme intraseasonal convection over the SACZ region. In fact, most of intense SACZ events identified here occurred after weak intraseasonal variations over the Eastern Hemisphere. Weak intraseasonal events, called MJO-independent to stress their independence from MJO events as defined on chapter 2, have small convective anomalies but the large-scale wave associated with these anomalies is sufficiently strong to carry the signal eastwards both through the tropics and the extratropics. The composite cycle of SACZ events independent of the MJO shows that 10 days before maximum SACZ convection there is no significant anomalies over the global tropics near the surface (Figure 4.3). Hence, one may speculate that the eastward propagation of the active phase occurs in the upper-levels. However, even if one considers all strong SACZ events, the propagation in the upper-levels is not continuous and stumbles before the anomalies are blocked by the Andes (Figure 6.1, 6.2, and 6.3).

In addition, a category of intense SACZ events lags the MJO by a few days but there are no significant negative pressure anomalies over the Atlantic prior to the SACZ development. Also, no significant negative OLR anomalies are observed in the Atlantic ITCZ, demonstrating that an intense SACZ can be triggered even when the tropical precursors seem to be less important. These SACZ events are apparently more influenced by extratropical disturbances modulated by large-scale waves in the tropics.

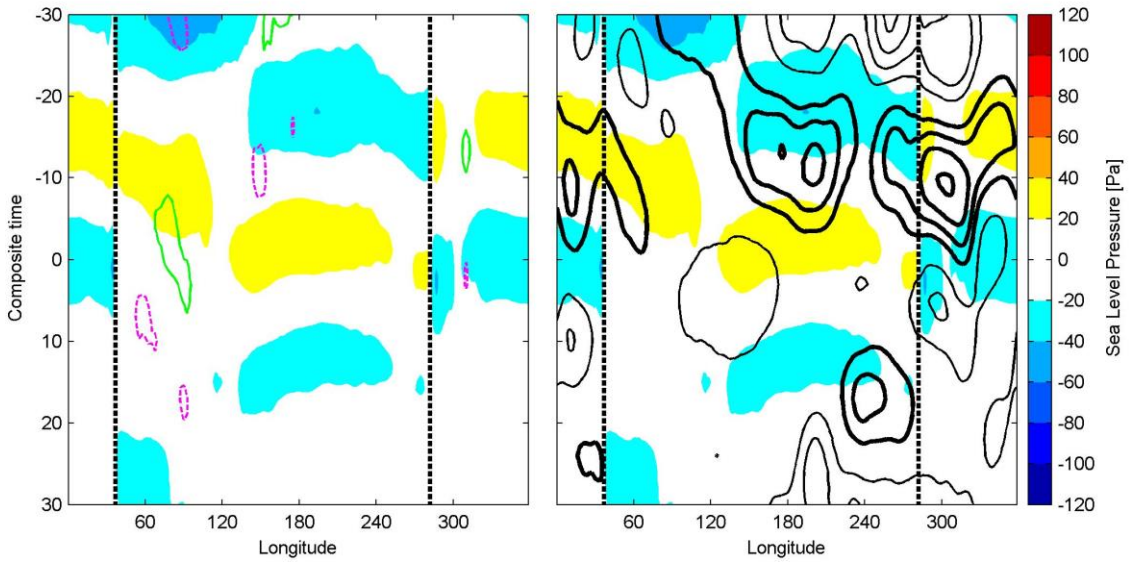

Figure 6.1: Composite time-longitude diagrams averaged at the between 5ºN and 5ºS relative to independent SACZ events identified on chapter 3. The left hand side plot displays the same pressure shadings with green (magenta) contours representing positive (negative) OLR anomalies at 5 W m^{-2} intervals (zero contour is omitted). The right hand side plot displays band-passed (20-90 days) sea level pressure anomalies (shadings in Pa) and thick (thin) contours indicate positive (negative 200 hPa geopotential anomalies at 15 m^2 s^2 (zero contour is omitted). Dashed vertical lines indicate the mean longitude of the East African Highlands and the Andes.

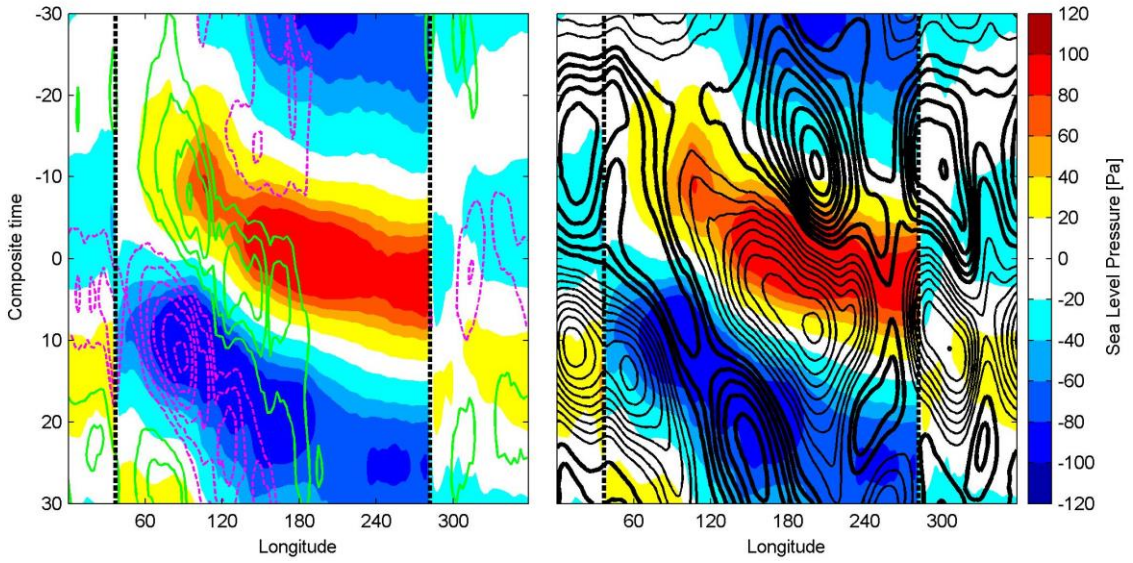

Figure 6.2: Same as Figure 6.1 but for SACZ preceding MJO events.

Several studies focused on extratropical Rossby waves excited by tropical and subtropical heating [e.g. Hoskins and Karoly, 1981; Karoly, 1983]. In the Southern Hemisphere summer, stationary long waves (wavenumbers 1 to 3) are able to propagate meridionally north of 60ºS [Berbery et al., 1992]. Wave modes linking the Pacific to

South America (PSA modes) along rays of constant group speed as defined by Hoskins and Karoly [1981], sometimes associated with the MJO and ENSO, acquire meridional propagation east of 150^{o}E [Grimm and Silva Dias, 1995; Mo and Higgins, 1998; Renwick and Revell, 1999].

Renwick and Revell [1999] suggest that the divergent winds driven by tropical convection on intraseasonal time scales act as a moving source of Rossby waves as they propagate eastward over the Pacific and waves are generated wherever the meridional component of the divergent wind intersects regions of strong meridional gradient of vorticity. West of 150^{o}E, tropical upper-level easterly winds tend to prevent meridional propagation of Rossby waves, but east of the dateline, upper-level westerlies are conducive to wave propagation [Webster and Holton, 1982; Webster and Chang, 1997]. Waves generated by such mechanisms are associated with excessive rainfall over southern Brazil and breaks in SACZ activity on interannual time scales [Grimm et al., 1998], even though divergent forcing near the SPCZ region is able to enhance the SACZ around 5 days later [Grimm and Silva Dias, 1995]. Results presented on chapter 3 indicate that the strongest convective anomalies near the SPCZ before the SACZ convective maximum are observed when the MJO precedes the SACZ (Figure 4.8a), with the organization of a wave train propagating towards South America (Figure 4.4 r). This result, combined with the lack of significant anomalies in the tropical Atlantic immediately before the SACZ maximum, highlights the importance of extratropical wave propagation for most of the intense SACZ analyzed here.

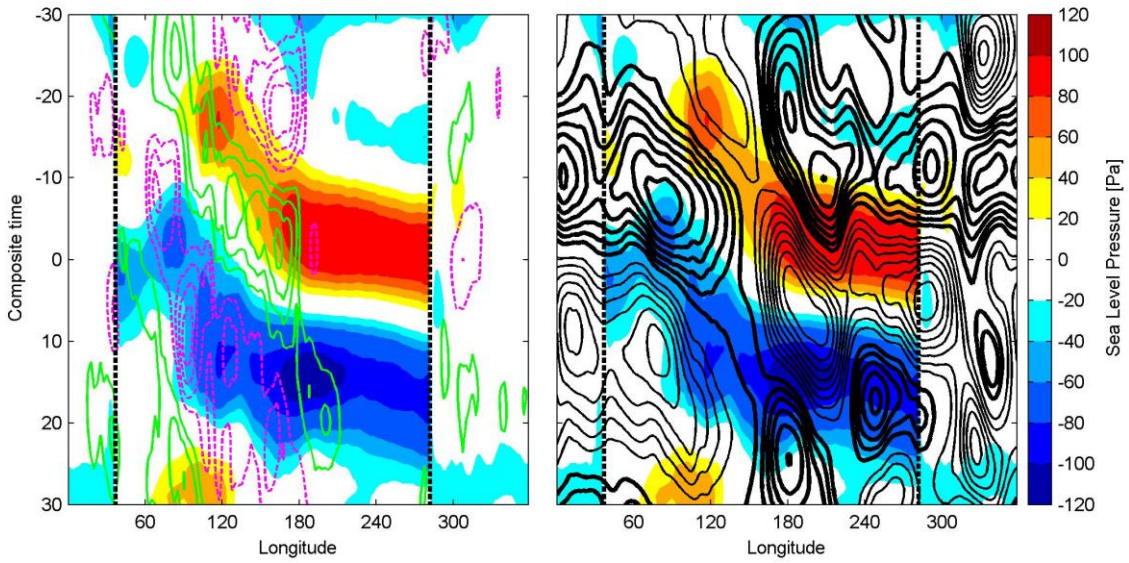

Figure 6.3: Same as Figure 6.3 but for MJO preceding SACZ events.

Other SACZ cycles show smaller anomalies in the vicinity of the SPCZ but the anomalies over the tropical Atlantic are significant prior to the SACZ (Figures 4.3 and 4.5). They also present the wave train organization linking the Pacific to South America (Figure 4.4), although no significant convective anomaly is present over the tropical Pacific. Webster and Chang [1988] argue that wave energy accumulates over the tropical eastern Pacific from where it emanates and effectively force Rossby waves in the extratropics. Figures 6.1 to 6.3 does show a band of positive 200 hPa geopotential anomalies leading positive pressure anomalies with higher amplitudes just east of the dateline. Over the eastern Pacific, positive geopotential anomalies seem to emanate towards the extratropics, acting as Rossby wave source for the extratropical wave trains observed in Figure 4.4. Therefore, it appears that the occurrence of these events is a combination of tropical and extratropical intraseasonal anomalies meeting east of the Andes. These intraseasonal anomalies are not necessarily associated with the MJO or other modes of strong intraseasonal convection once wave accumulation and emanation can foster further propagation of the anomalies especially through the extratropics.

It is argued on chapter 2 that the strength and duration of an MJO convective break is a better predictor for the next MJO active phase than circumnavigating anomalies associated with the previous convective cycle. Results on chapter 3 also point out that intraseasonal convective breaks over the Indian and Pacific Oceans are also significant and robust precursors of strong SACZ events. The most important categories of intense SACZ are observed after the eastward propagation of a Kelvin wave of positive pressure anomalies across the tropical Pacific. Merging tables 3.1 and 4.1, 24 out of 52 MJO events were preceded by a strong convective break and an intense SACZ, suggesting SACZ intraseasonal activity may be important for MJO development and eastward propagation. So far, it was not possible to determine the reasons why intraseasonal convective breaks last long enough or intensify in order to produce SST anomalies within the Maritime Continent that fuels the eastward propagation of the MJO.

Another interesting aspect of the intraseasonal variations of the SACZ highlighted on chapter 3 is the apparent role of wave accumulation over the Atlantic Ocean in intensifying and extending convective activity southeastward. The accumulation of wave energy is fostered by the existence of a region of climatological negative zonal stretching deformation generated by the establishment of the Bolivian High, in part by mature summertime convection over the Amazon. The same mechanism of wave accumulation are observed in the SPCZ [Widlansky et al., 2010] and, in the SACZ, it is significant for all SACZ cases, especially for MJO-independent cases when tropical anomalies over the Atlantic are not significant. As high-frequency synoptic disturbances propagate northeastward across the SACZ climatological domain, their longitudinal extent and phase speed decrease while convection is strengthened. The characteristics of these disturbances seem to be affected by the intensity of the intraseasonal anomalies. Deeper upper-level anomalies during SACZ preceding MJO events (Figure 4.4l,m) are more effective to reduce zonal winds at the exit of the South American subtropical jet and result in longitudinally shorter and slower systems. Matthews and Kiladis [1999]

suggested that as the winds at the jet exit decrease, short waves propagating along the jet may leak from the weakened waveguide. From a predictability perspective, monitoring the position and zonal winds associated with the subtropical jet over South America may be a key predictor of intense SACZ events. The downside of this approach is that wave accumulation still depends on the propagation of synoptic systems, assumed to be less predictable on medium temporal range.

The analysis of intraseasonal teleconnections presented here focused on the austral summer season. However, PSA modes associated with intraseasonal convection over the tropical Pacific Ocean also propagate during austral winter [Mo and Higgins, 1998]. Marengo et al. [2002] identified 2-30-day quasi-stationary Rossby waves originated in the western Pacific associated with cold surges in tropical and subtropical South America. Some of these cold air incursions were able to reach very low latitudes [Myers, 1964] and are of particular interest for agricultural activities. Thus, teleconnections between tropical intraseasonal oscillations during the northern summer can also be useful for attempts to extend the range and increase the skill of weather forecast in South America.

As it was mentioned before, PSA modes are very common both on intraseasonal and interannual timescales. Interannual variations are usually linked to ENSO and SACZ long-term variability is strongly tied to Pacific Ocean SST anomalies from interannual to interdecadal scales. Precipitation trends observed over South America during the last decades of the last century are apparently driven by more effective teleconnections resulting from El Niño events occurring during a warm PDO phase. These teleconnections drive wet anomalies over subtropics and dry anomalies to the north. A warming trend over the adjacent Atlantic seems to be a result of the weaker and southward-shifted SACZ. When the PDO shifts (or loses its robustness) after the mid-1990s, rainfall trends tend to level off. Evidences are presented to suggest that much of the precipitation trends over South America from 1979 to 2011 are linked to a

redistribution of energy from intraseasonal to higher frequencies highlighting once again the importance of extratropical teleconnections and heating anomalies over the Eastern Hemisphere. These changes are apparently not associated with MJO variations. Some projections of future rainfall conditions over the continent associated with global warming tend to reproduce the patterns observed during the latter half of the last century. However, the way global warming will influence SST anomaly patterns over the Pacific seem to be a fundamental aspect for such projections.

REFERENCES

Adler, R. F., G. J. Huffman, A. Chang, R. Ferraro, P. Xie, J. Janowiak, B. Rudolf, U. Schneider, S. Curtis, D. Bolvin, A, Gruber, J. Susskind, and P. Arkin [2003], The Version 2 Global Precipitation Climatology Project (GPCP) Monthly Precipitation Analysis (1979-Present). *J. Hydrometeor*., 4, 1147-1167.

Agudelo, P. A., J. A. Curry, C. D. Hoyos, and P. J. Webster [2006], Transition between suppressed and active phases of intraseasonal oscillations in the Indo-Pacific warm pool, *J. Clim.*, 19, 5519-5530.

Almeida, R. A. F., P. Nobre, R. J. Haarsma, and E. J. D. Campos [2007], Negative ocean-atmosphere feedback in the South Atlantic Convergence Zone, *Geophys. Res. Lett.*, 34, L18809.

Barros, V. R., M. Gonzalez, B. Liebmann, and I. Camilloni [2000], Influence of the South Atlantic Convergence Zone and South Atlantic Surface Temperature on Interannual Summer Variability in Southeastern South America, *Theor. Appl. Climatol.*, 67, 123-133.

Berbery, E.H., and J. Nogués-Paegle [1993], Intraseasonal interactions between the tropics and extratropics in the Southern Hemisphere, *J. Atmos. Sci.*, 50, 1950-1965.

Berbery, E.H., J. Nogués-Paegle, and J. D. Horel [1992], Wavelike Southern Hemisphere extratropical teleconnections, *J. Atmos. Sci.*, 49, 155-177.

Blackmon, M. L., Y. H. Lee, and J. M. Wallace [1984], Horizontal structure of 500 mb height fluctuations with long, intermediate and short time scales, *J. Atmos. Sci.*, 41, 961-979.

Bond, N. A., J. E. Overland, M. Spillane, and P. Stabeno [2003], Recent shifts in the state of the North Pacific, Geophys. Res. Lett., 30, doi: 10.1029/2003/GL018597.

Carvalho, L. M. V., C. Jones, and B. Liebmann [2002], Extreme precipitation events in southeastern South America and large-scale convective patterns in the South Atlantic Convergence Zone, *J. Clim.*, 15, 2377-2394.

Carvalho, L. M. V., C. Jones, and B. Liebmann [2004], The South Atlantic Convergence Zone: intensity, form, persistence, and relationships with intraseasonal to interannual activity and extreme rainfall, *J. Clim.*, 17, 88-108.

Cavalcanti, I, F. A., and M. T. Kayano [1999], High-frequency patterns of the atmospheric circulation over the Southern Hemisphere and South America, *Meteor. Atmos. Phys*., 69, 179-193.

Chang, C. P. [1977], Viscous internal gravity waves and low-frequency oscillations in the tropics, *J. Atmos. Sci.*, 34, 901-910.

Chang, H. R., and P. J. Webster [1995], Energy accumulation and emanation at low latitudes: forward and backward accumulation, *J. Atmos. Sci.*, 52, 2384-2403.

Chatterjee, P., and B. N. Goswami [2006], Structure, genesis, and scale selection of the tropical quasi-biweekly mode, *Quart. J. Roy. Meteor. Soc.*, 130, 1171-1194.

Chaves, R. R., and P. Nobre [2004], Interactions between sea surface temperature over the South Atlantic Ocean and the South Atlantic Convergence Zone, *Geophys. Res. Lett*., 31, L03204.

Chen, M., W. Shi, P. Xie, V.B.S. Silva, V.E. Kousky, R.W. Higgins, and J.E. Janowiak [2008], Assessing objective techniques for gauge-based analyses of global daily precipitation, *J. Geophys. Res.*, 113, D04110, doi: 10.1029/2007JD009132.

Collins, M., S. I. An, W. Cai, A. Ganachaud, E. Guilyardi, F. F. Jin, M. Jochum, M. Lengaigne, A. Timmermann, G. Vecchi, and A. Wittenberg [2013], The impact of global warming on the tropical Pacific Ocean and El Niño, *Nature Geosci.*, 3, 391-397.

Cunningham, C. A. C., and I. F. A. Cavalcanti [2006], Intraseasonal modes of variability affecting the South Atlantic Convergence Zone, *Int. J. Clim.*, 26 (9), 1165-1180.

Curry, J. A., A. Bentamy, M. A. Bourasa, D. Bourras, E. F. Bradley, M. Brunke, S. Castro, S. H. Hou, C. A. Clayson, W. J. Emery, L. Eymard, C. W. Fairall, M. Kubota, B. Lin, W. Perrie, R. A. Reeder, I. A. Renfrew, W. B. Rossow, J. Schulz, S. R. Smith, P. J. Webster, G. A. Wick, and X. Zeng [2004], SEAFLUX, *Bull. Amer. Meteor. Soc.*, 85 (3), 409-424.

Dee, D. P., S. M. Uppala, A. J. Simmons, P. Berrisford, P. Poli, S. Kobayashi, U. Andrae, M. A. Balmaseda, G. Balsamo, P. Bauer, P. Bechtold, A. C. M. Beljaars, L. van de Berg, J. Bidlot, N. Bormann, C. Delsol, R. Dragani, M. Fuentes, A. J. Geer, L. Haimberger, S. B. Healy, H. Hersbach, E. V. Hólm, L. Isaksen, P. Kållberg, M. Köhler, M. Matricardi, A. P. McNally, B. M. Monge-Sanz, J.-J. Morcrette, B.-K. Park, C. Peubey, P. de Rosnay, C. Tavolato, J.-N. Thépaut, and F. Vitart [2011], The ERA-Interim

reanalysis: configuration and performance of the data assimilation system, *Quart. J. Royal Metor. Soc*., 137 (656), 553-597.

Doyle, M. E., and V. R. Barros [2002], Midsummer low-level circulation and precipitation in subtropical South America and related sea surface temperature anomalies in the South Atlantic, *J. Clim*., 15, 3394-3410.

Duchon, C. E. [1979], Lanczos filter in one and two dimensions, *J. Appl. Meteor*., 18, 1016-1022.

Figueroa, S. N., P. Satyamurty, and P. L. Silva Dias [1995], Simulations of the summer circulation over the South American region with an Eta Coordinate Model, *J. Atmos. Sci.*, 52, 1573-1584.

Fu, R., B. Zhu, and R. E. Dickinson [1999], How do atmosphere and land surface influence seasonal changes of convection in the tropical Amazon?, *J. Clim.*, 12, 1306-1321.

Gan, M. A., and V. B. Rao [1991], Surface cyclogenesis over South America, *Mon. Wea. Rev*., 119, 1293-1302.

Gan, M. A., V. E. Kousky, and C. F. Ropolewski [2004], The South America Monsoon Circulation and its relationship to rainfall over West-Central Brazil, *J. Clim.*, 17, 47-66.

Garreaud, R. D., and J. M. Wallace [1997], The diurnal march of convective cloudiness over the Americas, *Mon. Wea. Rev.*, 125, 3157-3171.

Garreaud, R. D., and J. M. Wallace [1999], Summertime incursions of midlatitudes air into subtropical and tropical South America, *Mon. Wea. Rev.*, 126, 2713-2733.

Genta, J. L., G. Perez-Irribaren, and C. R. Mechoso [1998], A recent increasing trend in the streamflow of rivers in southeastern South America, *J. Clim*., 11, 2858-2862.

Gershunov, A., and T. P. Barnett [1998], Interdecadal modulation of ENSO teleconnections, *Bull. Amer. Meteor. Soc.*, 79, 2715-2725.

Ghil, M., and K. Mo [1991], Intraseasonal oscillations in the global atmosphere. Part II: Southern Hemisphere, *J. Atmos. Sci.*, 48, 780-790.

Gill, A. E. [1980], Some simple solutions for heat-induced tropical circulation, *Quart. J. Roy. Meteor. Soc.*, 106, 447-462.

Grimm, A. M. [2003], The El Niño impact on the summer monsoon in Brazil: regional processes versus remote influences, *J. Clim.*, 16, 263-280.

Grimm, A. M. [2004], How do La Niña events disturb the summer monsoon system in Brazil?, *Clim. Dyn*., 22, 123-138.

Grimm, A. M., and P.L. Silva Dias [1995], Analysis of tropical-extratropical interactions with influence functions of a barotropic model, *J. Atmos. Sci.*, 52, 3538-3555.

Grimm, A. M., and T. Ambrizzi [2009], Teleconnections into South America from the tropics and extratropics on interannual and intraseasonal time scales, *Past climate variability in South America and surrounding regions*, *Developments in Paleoenvironmental Research*, 14, 159-191.

Grimm, A. M., and M. T. Zilli [2009], Interannual variability and seasonal evolution of summer monsoon rainfall in South America, *J. Clim*., 22, 2257-2275.

Grimm, A. M., S. E. T. Ferraz, and J. Gomes [1998], Precipitation anomalies in southern Brazil associated with El Niño and La Niña events, *J. Clim*., 11, 2863-2880.

Grimm, A. M., J. Pal, and F. Giorgi [2007], Connection between spring conditions and peak summer monsoon rainfall in South America: role of soil moisture, surface temperature, and topography in eastern Brazil, *J. Clim*., 13, 759-776.

Haddad, E. A., and E. Teixeira [2013], Economic impacts of natural disasters in megacities: the case of floods in São Paulo, Brazil, *Núcleo de Economia Regional e Urbana da Universidade de São Paulo (NEREUS)*, 4, 1-20.

Hastenrath, S., and L. Greischar [1993], The monsoonal heat budget of the hydrosphere-atmosphere system in the Indian Ocean sector, *J. Geophys. Res.*, 98, 6869-6881.

Haylock, M. R., T. C. Peterson, L. M. Alves, T. Ambrizzi, Y. M. T. Anunciação, J. Baez, V. R. Barros, M. A. Berlato, M. Bidegain, G. Coronel, V. Corradi, V. J. Garcia, A. M. Grimm, D. Karoly, J. A. Marengo, M. B. Marino, D. F. Moncunill, D. Nechet, J. Quintana, E. Rebello, M. Rusticucci, J. L. Santos, I Trebejo, and L. A. Vincent [2006], Trends in total and extreme South American rainfall in 1960-2000 and links with sea surface temperature, *J. Clim*., 19, 1490-1512.

Hendon, H. H., and M. L. Salby [1994], The life cycle of the Madden-Julian oscillation, *J. Atmos. Sci.*, 51, 2207-2219.

Hill, K. J., A. S. Taschetto, and M. H. England [2009], South American Rainfall Impacts Associated with Inter-El Niño Variations, *Geophys. Res. Lett*., 36, doi: 10.1029/2009GL040164.

Hill, K. J., A. S. Taschetto, and M. H. England [2011], Sensitivity of South American Summer Rainfall to Tropical Pacific Ocean SST Anomalies, *Geophys. Res. Lett*., 38, doi: 10.1029/2010GL045571.

Hirata, F. E., P. J. Webster, and V. E. Toma [2013], Distinct manifestations of austral summer tropical intraseasonal oscillations, *Geophys. Res. Lett.*, 40, doi: 10.1002/grl.50632.

Horel, J. D., A. N. Hahmann, and J. E. Gleiser [1989], An Investigation of the Annual Cycle of Convective Activity over the Tropical Americas, *J. Clim*., 2, 1388-1403.

Hoskins, B. J., and D. J. Karoly [1981], Steady linear response of a spherical atmosphere to thermal and orographic forcing, *J. Atmos. Sci.*, 38, 1179-1196.

Hoyos, C. D., and P. J. Webster [2007], The Role of Intraseasonal Variability in the Nature of Asian Monsoon Precipitation. J. Climate, 20, 4402-4424.

Hsu, H.-H., B. J. Hoskins, and F.-F. Jin [1990], The 1985/86 intraseasonal oscillation and the role of the extratropics, *J. Atmos. Sci.*, 47, 823-839.

Jones, C., and L. M. V. Carvalho [2002], Active and Break Phases in the South American Monsoon System, *J. Clim.*, 15, 905-914.

Jones, C., and L. M. V. Carvalho [2006], Changes in the Activity of the Madden-Julian Oscillation during 1958-2004, *J. Clim*., 19, 6353-6370.

Jones, C., D. E. Waliser, K. M. Lau, and W. Stern [2004], Global occurrences of extreme precipitation and the Madden-Julian Oscillation: observations and predictability, *J. Clim.*, 17, 4575-4589.

Karoly, D. J. [1983], Rossby wave propagation in a barotropic atmosphere, *Dyn. Atmos. Oceans*, 7, 11-125.

Kayano, M. T., and R. V. Andreoli [2007], Relations of South American summer rainfall interannual variations with Pacific Decadal Oscillation, *Int. J. Clim.*, 27, 531-540.

Kikuchi, K., and Y. N. Takayabu [2003], Equatorial circumnavigation of moisture signal associated with the Madden-Julian Oscillation during boreal winter, 81, 851-869.

Kikuchi, K., and B. Wang [2009], Global perspective of the quasi-biweekly oscillation, *J. Clim.*, 22, 1340-1359.

Kim, H-.M., P. J. Webster, and J. A. Curry [2009], Impact of shifting patterns of Pacific Ocean warming on the North Atlantic tropical cyclones, *Science*, 325, 77.

Kessler, W. S. [2001], EOF representation of the Madden-Julian oscillation and its connection to ENSO, *J. Clim.*, 14, 3055-3061.

Kodama, Y. M. [1992], Large-Scale Common Features of Subtropical Precipitation Zones (the Baiu Frontal Zone, the SPCZ, and the SACZ). Part I: Characteristics of Subtropical Frontal Zones, *J. Meteor. Soc. Japan*, 70, 813-835.

Knutson, T. R., and K. M. Weickmann [1987], 30-60 day atmospheric oscillations: composite life cycles of convection and circulation anomalies, *Mon. Wea. Rev.*, 115, 1407-1436.

Lawrence, D., and P. J. Webster [2001], Interannual variations of the intraseasonal oscillation in the South Asian monsoon region, *J. Clim.*, 14, 2910-2922.

Lenters, J. D., and K. H. Cook [1995], Simulation and diagnosis of the regional summertime precipitation climatology of South America, *J. Clim.*, 8, 2988-3005.

Lenters, J.D., and K.H. Cook [1997], On the origin of the Bolivian High and related circulation features of the South American climate, *J. Atmos. Sci.*, 54, 656-678.

Lenters, J. D., and K. H. Cook [1999], Summertime precipitation variability over South America: role of the large-scale circulation, *Mon. Wea. Rev.*, 127, 409-431.

Liebmann, B., and J. A. Marengo [2004], Interannual Variability of the Rainy Season and Rainfall in the Brazilian Amazon Basin, *J. Clim.*, 14, 4308-4318.

Liebmann, B., and C.A. Smith [1996], Description of a complete (interpolated) outgoing longwave radiation dataset. *Bul. Amer. Meteor. Soc.*, 77, 1275-1277.

Liebmann, B., G. N. Kiladis, J. A. Marengo, T. Ambrizzi, and J. D. Glick [1999], Submonthly convective variability over South America and the South Atlantic Convergence Zone, *J. Clim.*, 12, 1877-1891.

Liebmann, B., C. S. Vera, L. M. V. Carvalho, I. A. Camilloni, M. P. Hoerling, D. Allured, V. R. Barros, J. Báez, and M. Bidegain [2004], An Observed Trend in Central South American Precipitation, *J. Clim.*, 17, 4357-4367.

Liebmann, B., G. N. Kiladis, L. M. V. Carvalho, C. Jones, C. S. Vera, I. Bladé, and D. Allured [2009], Origin of convectively coupled Kelvin waves over South America, *J. Clim*., 22, 300-315.

Livezey, R. E., and W. Y. Chen [1983], Statistical Significance and its Determination by Monte Carlo Techniques, *Mon. Wea. Rev*., 111, 46-59.

Lorenz, E N. [1963], Deterministic nonperiodic flow, *J. Atmos. Sci.*, 20, 130-141.

Loschnigg, J., and P. J. Webster [2000], A coupled ocean-atmosphere system of SST regulation for the Indian Ocean, *J. Clim.*, 13, 3342-3360.

Madden, R. A., and P. R. Julian [1971], Detection of a 40-50 day oscillation in the zonal wind in the tropical Pacific, *J. Atmos. Sci.*, 28, 702-708.

Madden, R. A., and P. R. Julian [1972], Description of global scale circulation cells in the tropics with a 40-50 day period. *J. Atmos. Sci.*, 29, 1109-1123.

Madden, R. A., and P. R. Julian [1994], Observations of the 40-50-day tropical oscillation – a review, *Mon. Wea. Rev.*, 122, 814-837.

Mantua, N. J., S. R. Hare, Y. Zhang, J. M. Wallace, and R. C. Francis [1997], A Pacific interdecadal climate oscillation with impacts on salmon production, *Bull. Amer. Meteor. Soc*., 78, 1069-1079.

Marengo, J. A. [2004], Interdecadal variability and trends of rainfall across the Amazon basin, *Theor. Appl. Climatol*., 78, 79-96.

Marengo, J. A., J. Tomasella, and C. R. Uvo [1998], Trends in streamflow and rainfall in tropical South America: Amazonia, eastern Brazil, and northwestern Peru, *J. Geophys. Res*., 103D, 1775-1783.

Marengo, J. A., T. Ambrizzi, G. Kiladis, and B. Liebmann [2002], Upper-air wave trains over the Pacific Ocean and wintertime cold surges in tropical-subtropical South America leading to freezes in southern and southeastern Brazil, *Theor. Appl. Climatol*., 73, 223-242.

Marengo, J. A., B. Liebmann, V. E. Kousky, N. P. Filizola, and I. C. Wainer [2001], Onset and end of the rainy season in the Brazilian Amazon basin, *J. Clim.*, 14, 833-852.

Marengo, J. A., R. Jones, L. M. Alvez, and M. C. Valverde [2009], Future change of temperature and precipitation extremes in South America as derived from the PRECIS regional climate modeling system, *Int. J. Clim.*, 29, 2241-2255.

Marengo, J. A., M. Rusticucci, O. Penalba and M. Renom [2010], An intercomparison of observed and simulated extreme rainfall and temperature events during the last half of the twentieth century: part 2: historical trends, *Clim. Change*, 98, 509-529.

Matsuno, T. [1966], Quasi-geostrophic motions in the equatorial area, *J. Meteor. Soc. Japan*, 44, 25-42.

Mao, J., and J. C. L. Chan [2005], Intraseasonal variability of the South China Sea summer monsoon, *J. Clim.*, 18, 2388-2402.

Matthews, A. J. [2000], Propagation mechanisms for the Madden-Julian Oscillation, *Quart. J. Roy. Meteor. Soc.*, 126, 2637-2651.

Matthews, A. J. [2009], Primary and successive events in the Madden-Julian Oscillation, *Quart. J. Roy. Meteor. Soc.*, 134, 439-453.

Matthews, A. J., and G. N. Kiladis [1999], The tropical-extratropical interaction between high-frequency transients and the Madden-Julian Oscillation, *Mon, Wea. Rev.*, 127, 661-677.

Matthews, A. J., J. M. Slingo, B. J. Hoskins, and P. M. Inness [1999], Fast and slow Kelvin waves in the Madden-Julian oscillation of a GCM, *Quart. J. Roy. Meteor. Soc.*, 125, 1473-1498.

Matthews, A. J., B. J. Hoskins, J. M. Slingo, and M. Blackburn [2006], Development of convection along the SPCZ within a Madden-Julian Oscillation, *Quart. J. Roy. Meteor. Soc.*, 122, 669-688.

Milliff, R. F., and R. A. Madden [1996], The existence and vertical structure of fast, eastward-moving disturbances in the equatorial troposphere, *J. Atmos. Sci.*,53, 586-597.

Mo, K. C., and R. W. Higgins [1998], The Pacific-South American modes and tropical convection during the Southern Hemisphere winter, *Mon. Wea. Rev.*, 126, 1581-1596.

Mo, K. C., and J. Nogués-Paegle [2001], The Pacific-South American modes and their downstream effects, *Int. J. Climatol*., 21, 1211-1229.

Montecinos, A., A. Diaz, and P. Aceituno [2000], Seasonal diagnostic and predictability of rainfall in subtropical South America based on Tropical Pacific SST, *J. Clim*., 13, 746-758.

Mori, M., and M. Watanabe [2008], The growth and triggering mechanisms of the PNA: a MJO-PNA coherence, *J. Meteor. Soc. Japan*, 86, 213-236.

Myers, V. A. [1964], A cold front invasion of southern Vanezuela, *Mon. Wea. Rev.*, 92, 513-521.

Nieto-Ferreira, R., T. M. Rickenbach, and E. A. Wright [2011], The role of cold fronts in the onset of the South American monsoon, *Quart. J. Royal Meteor. Soc*., 137 [657), 908-922.

Nogués-Paegle, J., and K. C. Mo [1997], Alternating wet and dry conditions over South America during summer, *Mon. Wea. Rev.*, 125, 279-291.

Nogués-Paegle, J., L. A. Byerle, and K. C. Mo [2000], Intraseasonal modulation of South America summer precipitation, *Mon. Wea. Rev*., 128, 837-850.

North, G. R., T. L. Bell, and R. F. Cahalan [1992], Sampling errors in the estimation of empirical orthogonal functions, *Mon. Wea. Rev*., 110, 699-706.

Parker, D. E. [1973], Equatorial Kelvin waves at 100 millibars, *Quart. J. Roy. Meteor. Soc.*, 99, 116-129.

Peterson, W. T., and F. B. Schwing [2003], A new climate regime in northeast Pacific ecosystems, *Geophys. Res. Lett.*, 30, doi: 10.1029/2003GL017528.

Pezza, A. B., I. Simmonds, and J. A. Renwick [2007], Southern Hemisphere cyclones and anticyclones: recent trends and links with decadal variability in the Pacific Ocean, *Int. J. Clim.*, 27, 1403-1419.

Ray, P., and C. Zhang [2010], A case study of the mechanics of extratropical influence on the initiation of the Madden-Julian Oscillation, *J. Atmos. Sci.*, 67, 515-528.

Renwick, J. A., and M. J. Revell [1999], Blocking over the South Pacific and Rossby wave propagation, *Mon. Wea. Rev.*, 127, 2233-2247.

Reynolds, R. W., T. M. Smith, C. Liu, D. B. Chelton, K. S. Casey, and M. G. Schlax [2007], Daily high-resolution blended analyses for sea surface temperature, *J. Clim.*, 20, 5473-5496.

Robertson, A. W., and C. R. Mechoso [1998], Interannual and decadal cycles in river flows of southeastern South America, *J. Clim*., 11, 2570-2581.

Robertson, A. W., and C. R. Mechoso [2000], Interannual and interdecadal variability of the South Atlantic Convergence Zone, *Mon. Wea. Rev*., 128, 2947-2957.

Raia, A., and I. F. A. Cavalcanti [2008], The life cycle of the South American monsoon system, *J. Clim.*, 21, 6227-6246.

Ramage, C. S. [1971], Monsoon meteorology, *Academic Press*, NY, 296 p.

Rao, G. V., and S. Erdogan [1989], The atmospheric heat source over the Bolivian plateau for a mean January, *Bound. Lay. Meteor*., 46,13-33.

Roundy, P. E., and W. M. Frank [2004], Effects of low-frequency wave interactions on intraseasonal oscillations, *J. Atmos. Sci.*, 61, 3025-3040.

Rusticucci, M., and O. Penalba, [2000], Interdecadal changes in the precipitation seasonal cycle over southern South America and their relationship with sea surface temperature, *Clim. Res*., 16, 1-15.

Seluchi, M. E., and J. A. Marengo [2000], Tropical-midlatitude exchange of air masses during summer and winter in South America: climatic aspects and examples of intense events, *Int. J. Climatol*., 20, 1167-1190.

Silva, G. M., and T. Ambrizzi [2006], Inter-El Niño variability and its impact on the South American low-level jet east of the Andes during austral summer: two case studies, *Adv. Geosci*., 6, 283-286.

Silva Dias, P. L., W. H. Schubert, and M. DeMaria [1983], Large-scale response of the tropical atmosphere to transient convection, *J. Atmos. Sci.*, 40, 2689-2707.

Silva Dias, M. A. F., J. Dias, L. M. V. Carvalho, E. D. Freitas, and P. L. Silva Dias [2013], Changes in extreme daily rainfall for Sao Paulo, Brazil, *Clim. Change*, 116, 705-722.

Siqueira, J. R., and L. A. T. Machado [2004], influence of the frontal systems on the day-to-day convection variability over South America, *J. Clim.*, 17, 1754-1766.

Smith, T. M., R. W. Reynolds, T. C. Peterson, and J. Lawrimore [2008], Improvements to NOAA's historical merged land-ocean surface temperature analysis (1880-2006), *J. Clim.*, 21, 2283-2296.

Soares, W. R., and J. A. Marengo [2009], Assessment of moisture fluxes east of the Andes in South America in a global warming scenario, *Int. J. Clim.*, 29, 1395-1414.

Souza, E. B., and T. Ambrizzi [2006], Modulation of the intraseasonal rainfall over tropical Brazil by the Madden-Julian Oscillation, *Int. J. Climatol.*, 26, 1759-1776.

Stephens, G. L., P. J. Webster, R. H. Johnson, R. Engelen, and T. L'Ecuyer [2004], Observational evidence for the mutual regulation of the tropical

hydrological cycle and tropical sea surface temperatures, *J. Clim.*, 17, 2213-2224.

Straub, K. [2013], MJO initiation in the real-time multivariate MJO index. *J. Clim.*, 26, 1130-1151.

Straub, K. H., and G. N. Kiladis [2003], Interactions between the boreal summer intraseasonal oscillation and higher-frequency tropical wave activity, *Mon. Wea. Rev.*, 131, 945-960.

Torrence, C., and G. P. Compo [1998], A practical guide to wavelet analysis, *Bull. Amer. Meteor. Soc.*, 79, 61-78.

Torrence, C., and P. J. Webster [1999], Interdecadal changes in the ENSO-monsoon system, *J. Clim*., 12, 2679-2690.

Torres, R. R., D. m. Lapola, J. A. Marengo and M. A. Lombardo [2012], Socio-climatic hotspots in Brazil, *Clim. Change*, 115, 597-609.

Venagas, S. A., L. A. Mysak, and D. N. Straub [1996], Evidence for interannual and interdecadal climate variability in the South Atlantic, *Geophys. Res. Lett.*, 23, 2673-2676.

Vialard, J., K. Drushka, H. Bellenger, M. Lengaigne, S. Pouls, and J. P. Duvel [2012], Understanding Madden-Julian-induced sea surface temperature variations in the North Western Australian basin., *Clim. Dyn.*, doi: 10.1007/s00382-012-1541-7.

Yamagata, T., and Y. Hayashi [1984], A simple diagnostic model for the 30-50 day oscillation in the tropics, *J. Meteor. Soc. Japan*, 62, 709-717.

Wallace, J. M., and D. S. Gutzler [1981], Teleconnections in the geopotential height field during the Northern Hemisphere winter, *Mon. Wea. Rev.*, 109, 784-812.

Waliser, D. E., K. M. Lau, W. Stern, and C. Jones [2003], Potential predictability of the Madden-Julian Oscillation, *Bull. Amer. Meteor. Soc.*, 84, 33-50.

Wang, B., and H. Rui [1990], Synoptic climatology of transient tropical intraseasonal convection anomalies: 1975-1985, *Meteor. Atmos. Phys.*, 44, 43-61.

Wang, B., P. J. Webster, and H. Teng [2005], Antecedents and self-induction of active-break south Asian monsoon unraveled by satellites, *Geophys. Res. Lett.*, L04704, doi:10.1029/2004GL020996.

Wang, B., P. J. Webster, K. Kikuchi, T. Yasunari, and Y. Qi [2006], Boreal summer quasi-monthly oscillation in the global tropics, *Clim. Dyn.*, 27, 661-675.

Webster, P. J. [1972], Response of the tropical atmosphere to local steady forcing, *Mon. Wea. Rev.*, 100, 518-541.

Webster, P. J., and J. R. Holton [1982], Wave propagation through a zonally varying basic flow: the influences of mid-latitude forcing in the equatorial regions, *J. Atmos. Sci.*, 39, 722-733.

Webster, P. J., and H. R. Chang [1988], Energy Accumulation and emanation regions at low latitudes: impacts of a zonally varying basic state, *J. Atmos. Sci.*, 45, 803-829.

Webster, P. J., and H. R. Chang [1997], Atmospheric wave propagation in heterogeneous flows: basic flow controls on tropical-extratropical interaction and equatorial wave modification. *Dyn. Atmos. Oceans*, 27, 722-733.

Webster, P. J., and J. Fasullo [2003], Monsoon: dynamical theory, *Encyclopedia of Atmospheric Sciences*, 3, 1370-1391.

Webster, P. J., and C. D. Hoyos [2004], Prediction of monsoon rainfall and river discharge on 15-30 day time scales, *Bull. Amer. Meteor. Soc.*, 85, 1745-1765.

Webster, P. J., and S. Yang [1992], Monsoon and ENSO: selectively interactive systems, *Quart. J. Roy. Meteor. Soc.*, 73, 1377-1416.

Webster, P. J., V. O. Magaña, T. N. Palmer, J. Shukla, R. A. Tomas, M. Yanai and T. Yasunari [1998], Monsoons: processes, predictability and the prospects for prediction, *J. Geosphys. Res.*, 103, 14451-14510.

Webster, P. J., C. Clark, G. Cherikova, J. Fasullo, W. Han, J. Loschnigg and K Sahami [2002], The monsoon as a self-regulating coupled ocean-atmosphere system, *Meteorology at the Millenium*, International Geophysical Series, 93, 198-219.

Wentz, F.J. [1997], A well-calibrated ocean algorithm for Special Sensor Microwave/Imager, *J. Geophys. Res.*, 102, 8703-8718.

Widlansky, M. J., P. J. Webster, and C. D. Hoyos [2010], On the location and orientation of the South Pacific Convergence Zone, *Clim. Dyn*., 36, 561-578.

Wheeler, M. C., and H. H. Hendon [2004], An all-season real-time multivariate MJO index: development of an index for monitoring and prediction, *Mon. Wea. Rev*., 132 (8), 1917-1932.

Wheeler, M. C., and G. N. Kiladis [1999], Convectively coupled equatorial waves: analysis of clouds and temperature in the wavenumber-frequency domain, *J. Atmos. Sci.*, 56, 374-399.

Wheeler, M., G. N. Kiladis, and P. J. Webster [2000], Large-scale dynamical fields associated with convectively coupled equatorial waves, *J. Atmos. Sci.*, 57, 613-640.

Woolnough, S. J., J. M. Slingo, and B. J. Hoskins [2000], The relationship between convection and sea surface temperature on intraseasonal timescales, *J. Clim.*, 13, 2086-2104.

Zhang, C. [2005], Madden-Julian Oscillation, *Rev. Geophys.*, 43, doi:10.1029/2004RG000158.

Zhou, J. and K. M. Lau [1998], Does a monsoon climate exist over South America?, *J. Clim.*, 11, 1020-1040.

VITA

FERNANDO ENDO HIRATA

HIRATA was born in São Paulo, Brazil and got a major in Journalism in 2001. Received a B. S. in Oceanography in 2006 and a M. S. in Physical Oceanography in early 2008 before moving to Georgia Tech to pursue a doctorate in Climate Dynamics at EAS.